

Spring 2015

Optimizing the neural response to electrical stimulation and exploring new applications of neurostimulation

Kurt Yuqin Qing
Purdue University

Follow this and additional works at: https://docs.lib.purdue.edu/open_access_dissertations



Part of the [Biomedical Engineering and Bioengineering Commons](#), and the [Neuroscience and Neurobiology Commons](#)

Recommended Citation

Qing, Kurt Yuqin, "Optimizing the neural response to electrical stimulation and exploring new applications of neurostimulation" (2015). *Open Access Dissertations*. 538.

https://docs.lib.purdue.edu/open_access_dissertations/538

**PURDUE UNIVERSITY
GRADUATE SCHOOL
Thesis/Dissertation Acceptance**

This is to certify that the thesis/dissertation prepared

By Kurt Y Qing

Entitled

Optimizing the Neural Response to Electrical Stimulation and Exploring New Applications of Neurostimulation

For the degree of Doctor of Philosophy



Is approved by the final examining committee:

Pedro Irazoqui

Chair

John Jefferys

Edward Bartlett

Riyi Shi

Robert Worth

To the best of my knowledge and as understood by the student in the Thesis/Dissertation Agreement, Publication Delay, and Certification Disclaimer (Graduate School Form 32), this thesis/dissertation adheres to the provisions of Purdue University's "Policy of Integrity in Research" and the use of copyright material.

Approved by Major Professor(s): Pedro Irazoqui

Approved by: George R Wodicka

Head of the Departmental Graduate Program

4/24/2015

Date

OPTIMIZING THE NEURAL RESPONSE TO ELECTRICAL STIMULATION AND
EXPLORING NEW APPLICATIONS OF NEUROSTIMULATION

A Dissertation

Submitted to the Faculty

of

Purdue University

by

Kurt Y Qing

In Partial Fulfillment of the

Requirements for the Degree

of

Doctor of Philosophy

May 2015

Purdue University

West Lafayette, Indiana

For my family

ACKNOWLEDGEMENTS

First, I would like to acknowledge all the people who have served on my thesis committee: current Drs. Pedro Irazoqui, Edward Bartlett, Riyi Shi, Robert Worth, and John Jefferys; past: Drs. Kevin Otto and Zachary Rodd. It was a pleasure and an honor to have worked with you all, and thank you for all the advice and suggestions that you have already provided and will provide in the future. I especially thank Dr. Irazoqui, who in the beginning supported my entry into the PhD program and since then has provided incredible opportunities to me over the years and always pushed me to accomplish more.

I would like to also highlight all the help that Dr. Worth gave me with the clinical side of my training. Seeing the actual surgical procedures and the patients living with their implanted stimulators provided a clearer view of the bigger picture of what my work seeks to do. Talking with the surgeons, neurologists, and the patients themselves was also an interesting and important learning experience.

To my current and former lab mates, thank you for all the sharing, helping, and supporting. Omar Abdel-Latief, thank you for helping me get started. To Henry Mei, our early experiments were grueling but also taught me a lot. To Gabriel Albors and Henry Zhang, thank you for all the technical and administrative support. To Steven Lee and Rebecca Bercich, thank you two for sharing your expertise, and working with you was always enjoyable. To Ashir Shah, Oren Gall, Young-Joon Kim, and Hansraj Bhamra,

thank you for helping me with the ASIC design. To Daniel Pederson and Zhi Wang, thank you for bring your skills to our lab and sharing with everyone. To Muhammad Arafat and Jack Williams, thank you for your help with my experiments. A special big thank-you goes to Dr. Matthew Ward. Without you leading the initial charge, my work would be near impossible. And working together with you was both fun and productive. To everyone, it has been a great, unforgettable experience. I wish you all luck with your current and future pursuits.

Last but not least, I would like to thank the staff of Biomedical Engineering and the veterinary staff. Your support made my experiments possible.

TABLE OF CONTENTS

	Page
LIST OF TABLES	viii
LIST OF FIGURES	ix
ABSTRACT	xi
CHAPTER 1. INTRODUCTION TO ELECTRICAL STIMULATION	1
1.1 <u>Medical Uses of Electrical Stimulation</u>	1
1.2 <u>Historical Advances in Stimulation Paradigms</u>	2
1.3 <u>Core Principles of Electrical Stimulation</u>	5
1.3.1 The Electrode-Tissue Interface	5
1.3.2 Strength-Duration Relationships	7
1.3.3 Current-Distance Relationship	10
1.3.4 Electrical Properties of the Neuron	11
1.3.5 Cathodic versus Anodic Stimulation	12
1.3.6 Monophasic versus Biphasic Stimulation	13
1.3.7 Current- versus Voltage-Controlled Stimulation	13
1.4 <u>Modern Stimulation Paradigms</u>	15
1.5 <u>Overview of Dissertation</u>	16
CHAPTER 2. DBS TO TREAT ALCOHOL USE DISORDER	19
2.1 <u>Introduction to Alcohol Use Disorder</u>	19
2.2 <u>Experimental Design and Methods</u>	20
2.2.1 Animals and Surgery	20
2.2.2 Experimental Setup	22
2.2.3 Experimental Design and Data Analysis	22
2.3 <u>The Effect of DBS on Alcohol Intake</u>	24

	Page
2.4 <u>Discussion</u>	25
2.5 <u>Developing a Better Method for Stimulus Waveform Design</u>	26
2.6 <u>Notes</u>	27
CHAPTER 3. BURST-MODULATED STIMULUS WAVEFORMS	28
3.1 <u>Introduction to Vagus Nerve Stimulation and Its Challenges</u>	28
3.2 <u>Mechanism of Electrical Nerve Stimulation</u>	30
3.3 <u>Effects of VNS</u>	32
3.4 <u>Existing Methods for Selective Stimulation</u>	36
3.4.1 Selective Conduction Block.....	36
3.4.2 Fiber-Selective Electrodes	37
3.4.3 Fiber-Selective Stimulus Waveforms	38
3.5 <u>Introducing Burst-Modulated Stimulus Waveforms</u>	41
3.6 <u>Methods for Characterizing Burst-Modulated Waveforms</u>	43
3.6.1 Animals and Surgery.....	43
3.6.2 Custom Electrode Design and Fabrication	44
3.6.3 Experimental Setup.....	45
3.6.4 Neural Activation Data Analysis	46
3.7 <u>Differences between Pulse and Pulsons</u>	51
3.8 <u>Proposed Mechanism of Action for Burst-Modulated Waveforms</u>	58
3.9 <u>Implementation of Burst-Modulated Waveforms</u>	59
3.10 <u>Conclusion</u>	60
3.11 <u>Notes</u>	61
CHAPTER 4. ACTIVATION CONTROLLED VNS	62
4.1 <u>Introduction to Activation Control</u>	62
4.2 <u>Vagus Nerve and Heart Disease</u>	63
4.3 <u>Epilepsy, Vagus Nerve, and Heart Disease</u>	65
4.4 <u>VNS for Treating Autonomic Dysfunction</u>	67
4.5 <u>The Benefits of Activation Control</u>	68
4.6 <u>Methods for Testing Activation Control</u>	70

	Page
4.7 <u>ECG Data Analysis</u>	72
4.8 <u>The Effects of Stimulus Parameters on the Vagal Response and Heart Rate</u>	73
4.9 <u>The Vagal-Heart Rate Relationship</u>	77
4.10 <u>The Effects of Right-Side VNS on Heart Function</u>	83
4.11 <u>Notes</u>	86
CHAPTER 5. CONCLUSION	87
5.1 <u>Objective, Individualized Stimulation Dosing</u>	87
5.2 <u>Refining DBS Parameters</u>	89
5.3 <u>Ideas for Future VNS Work</u>	91
REFERENCES	94
VITA.....	112
PUBLICATIONS.....	114

LIST OF TABLES

Table	Page
Table 1. Nerve fiber classification and function	32
Table 2. Stimulus pulse characteristics compared to the rectangular pulse	39
Table 3. SAS output for multiple regression of Q₅₀A and burst modulation parameters	54
Table 4. SAS output table for multiple regression of Q₅₀C	54
Table 5. SAS output table for multiple regression of A fiber activation at Q₅₀C.	56

LIST OF FIGURES

Figure	Page
Figure 1 The Randles equivalent circuit model for the electrode-tissue interface.	6
Figure 2 Strength-duration curves.	9
Figure 3 Simplified Hodgkin-Huxley model.	11
Figure 4 Example pulse train.	16
Figure 5 Ethanol (EtOH) intake in the 100μA group.	24
Figure 6 Ethanol (EtOH) intake in the 200μA group.	25
Figure 7 The Cyberonics VNS device.	30
Figure 8 The vagus nerve anatomy and composition.	33
Figure 9 Rectangular pulse and burst-modulated waveforms.	42
Figure 10 Cuff electrode for VNS experiments.	45
Figure 11 Instrumentation for VNS experiments.	47
Figure 12 Example processed nerve responses during stimulation trials.	49
Figure 13 Fiber recruitment curves for selected pulse waveforms.	50
Figure 14 Example CNAP response for $I_{pIx} = 1\text{ms}$.	52
Figure 15 Q_{50A}, Q_{50C}, and level of A fiber activation at Q_{50C} for all waveforms. ...	53
Figure 16 CNAP responses to burst-modulated waveforms.	57
Figure 17 Animal with nerve cuffs and ECG electrodes attached.	71
Figure 18 ECG data analysis.	73

Figure	Page
Figure 19 Example nerve responses at varying current amplitudes.....	74
Figure 20 Fiber recruitment profiles for selected waveforms.	75
Figure 21 CNAP and corresponding heart rate.	76
Figure 22 Example trial resulting in arrhythmia.....	78
Figure 23 Right vagal CNAP and heart rate data from all animals.	79
Figure 24 Combined normalized data from all animals.....	81
Figure 25 Example B fiber-heart rate relationships with waveforms marked.	82
Figure 26 Ultrasound image processing.....	83
Figure 27 R166 vagal CNAP magnitudes and heart rate.....	84
Figure 28 R166 B fiber-left ventricle function relationship.....	85

ABSTRACT

Qing, Kurt Y. Ph.D., Purdue University, May 2015. Optimizing the Neural Response to Electrical Stimulation and Exploring New Applications of Neurostimulation. Major Professor: Pedro Irazoqui.

Electrical stimulation has been successful in treating patients who suffer from neurologic and neuropsychiatric disorders that are resistant to standard treatments. For deep brain stimulation (DBS), its official approved use has been limited to mainly motor disorders, such as Parkinson's disease and essential tremor. Alcohol use disorder, and addictive disorders in general, is a prevalent condition that is difficult to treat long-term. To determine whether DBS can reduce alcohol drinking in animals, voluntary alcohol consumption of alcohol-preferring rats before, during, and after stimulation of the nucleus accumbens shell were compared. Intake levels in the low stimulus intensity group (n=3, 100 μ A current) decreased by as much as 43% during stimulation, but the effect did not persist. In the high stimulus intensity group (n=4, 200 μ A current), alcohol intake decreased as much as 59%, and the effect was sustained. These results demonstrate the potent, reversible effects of DBS.

Left vagus nerve stimulation (VNS) is approved for treating epilepsy and depression. However, the standard method of determining stimulus parameters is imprecise, and the patient responses are highly variable. I developed a method of designing custom stimulus

waveforms and assessing the nerve response to optimize stimulation selectivity and efficiency. VNS experiments were performed in rats aiming to increase the selectivity of slow nerve fibers while assessing activation efficiency. When producing 50% of maximal activation of slow fibers, customized stimuli were able to activate as low as 12.8% of fast fibers, while the lowest for standard rectangular waveforms was 35.0% (n=4-6 animals). However, the stimulus with the highest selectivity requires 19.6nC of charge per stimulus phase, while the rectangular stimulus required only 13.2nC.

Right VNS is currently under clinical investigation for preventing sudden unexpected death in epilepsy and for treating heart failure. Activation of the right vagal parasympathetic fibers led to waveform-independent reductions in heart rate, ejection ratio, and stroke volume. Customized stimulus design with response feedback produces reproducible and predictable patterns of nerve activation and physiological effects, which will lead to more consistent patient responses.

CHAPTER 1. INTRODUCTION TO ELECTRICAL STIMULATION

1.1 Medical Uses of Electrical Stimulation

Many neurologic and neuropsychiatric disorders have no cure. Even for disorders that have established behavioral and pharmacological treatments, a significant amount of patients respond poorly and inconsistently. Parkinson's disease¹⁻³, epilepsy^{4,5}, neuropathic pain^{6,7}, alcoholism⁸⁻¹⁰, and depression^{11,12} are a few examples. Some conditions, such as neurological blindness and deafness, have no pharmacological treatments. These disorders and disabilities can be debilitating and pose high burdens on healthcare and society^{13,14}.

Electrical stimulation offers a safe and effective treatment for these conditions. Neuroprosthetics, with cochlear implants, vagal nerve stimulators (VNS), and deep brain stimulators (DBS) being the prominent examples, are now well known and common treatment options. Cochlear implants have been very successful in restoring hearing. However, because cochlear stimulation tends to be in a field by itself, it will not be discussed in detail. VNS has been FDA-approved for use in epilepsy and depression¹⁵, and DBS has been approved for treating Parkinson's disease, essential tremor, and dystonia¹⁶. In addition, there are strong indications for other applications of VNS and DBS^{15,16}, where many more patients can receive much needed therapeutic benefits.

To deliver effective treatments, the electrical stimulus must be both therapeutically efficacious and safe. For both VNS and DBS, overall efficacy has been solidly established, but patient response is highly variable. Also, modern stimulators are still plagued by side effects and complications, which are largely due to lack of selectivity and somewhat due to limited battery life, respectively¹⁶⁻¹⁹. Side effects differ among patients as well and can limit efficacy. Therefore, increasing the selectivity of stimulation and prolonging battery life can increase the effectiveness of treatment.

As our understanding of the field improves, and as efforts continue to solve the major challenges, the technology has been evolving steadily, and the scope is becoming increasingly vast. The major aims of my thesis work were 1) to explore new areas to apply electrical stimulation and 2) to improve the current stimulation paradigm by introducing a new method of designing stimulus waveforms and analyzing the effects. In this first chapter, I review the key advances in the field of electrical stimulation and describe the current paradigm. This introduction chapter establishes the foundation and rationale for the experiments that follow.

1.2 Historical Advances in Stimulation Paradigms

To improve electrical stimulation therapy, refining stimulus design is the key. With more than two centuries of laboratory research and clinical studies, there exists abundant knowledge regarding how neural tissue responds to different stimuli.

Guillaume Duchenne, in his book A Treatise on Localized Electrization²⁰, attributed the first documented therapeutic uses of electricity to Kruger d'Helmstadt in 1744. These initial attempts utilized static electricity, the only available form of

electricity at the time, and involved devices such as Leyden jars, which stored and discharged static charge. This method is poorly controlled, has questionable efficacy, and can be dangerous. Fortunately, over time, both technique and understanding of electrical stimulation improved dramatically.

First came direct current (DC) stimuli, mostly resulting from the Galvani-Volta debates at the end of the 18th century²⁰⁻²². Then in early 1800's, due to the birth of electromagnetism, alternating currents (AC) became available. The constant push and pull of electrical charge made it superior to DC stimuli²⁰, but the push-pull also led to a lack of charge buildup in tissue, and efficacy is still low²³. Indeed, even among modern waveforms, the biphasic charge-balanced pulse without delay, which resembles an AC waveform, is comparatively not so efficacious²⁴⁻²⁶.

Batteries (voltaic cells) alone can only produce DC stimuli, but with a switch for completing and breaking the circuit, experimenters were able to produce interrupted DC waveforms. Using such waveforms, Emil du Bois-Reymond found that the response is much higher than DC and AC waveforms²². Circa 1850, he established the “general law of excitation of nerves”, which states that nerve activation is due to changes in current amplitude and not the exact amplitude²².

At about the same time, Eduard Pflüger introduced his “law of contraction”²⁷. In addition to supporting du Bois-Reymond's law of excitation, Pflüger's experiments also resulted in two important findings. The first is that excitation originates at the cathode, not the anode, upon making the circuit (this point will be discussed further in Subsection 1.3.5). Pflüger's second finding is that when breaking the circuit, excitation can occur at

the anode. This “anode break excitation” has since been well-characterized^{28,29} and is regarded as an unintended effect that is to be avoided^{30,31,32}.

At the start of the 20th century, the monumental works of Georges Weiss and Louis Lapicque formed the foundation of modern electrical stimulation (their findings are discussed in Subsection 1.3.2)^{23,33–35}. Their experiments contributed to a new paradigm that is still the standard today—pulsatile stimulation, where waveforms are constructed using brief pulses with defined parameters, such as pulse width and amplitude. Compared to interrupted DC waveforms, pulse waveforms have a much lower duty cycle but are still effective at activating excitable tissue.

As a safer variant of simple pulsatile waveforms (monophasic), John Lilly and colleagues presented the biphasic pulse waveform (sometimes referred to as the Lilly waveform)³⁶. Termed “zero net flow” by Lilly, these biphasic waveforms are now widely used, though monophasic pulses are commonly used as well. A comparison is provided in Subsection 1.3.6.

After Lilly’s modification, there have been no major advances in stimulation paradigms. Not much has changed since the time of Weiss and Lapicque, over a century ago. However, the collective understanding of the mechanisms of electrical stimulation and the relationships between the stimulus and physiological response has increased substantially. The next section will synthesize key early discoveries reviewed above and some of the major concepts established more recently. These principles are important for understanding the modern stimulation paradigm and for exploring new paradigms.

1.3 Core Principles of Electrical Stimulation

1.3.1 The Electrode-Tissue Interface

Electrical stimulation acts by driving currents through tissue, which includes neurons, glia, and extracellular matrix. Delivering current into target tissue requires the use of electrodes. The study of electrodes is a vast field in itself, so only basic principles relevant to stimulus design will be discussed here. A thorough analysis of the electrochemistry of electrodes can be found in the well-known book by Bard and Faulkner³⁷. An article by Stuart Cogan³⁸ also offers a good review of electrode properties and design.

Many electrode designs and configurations exist, including monopolar, bipolar, cuff, concentric, tripolar, etc. For simplicity, the analysis here will focus on the monopolar configuration, in which a single electrode serves as the working electrode while a second electrode serves as both the counter and reference. In this case, if this second electrode is implanted in distant tissue that is not of interest, its effects can essentially be ignored.

When a voltage is applied across the working and counter electrodes, it drives a current between the electrodes and through tissue. With an ideal non-polarizable electrode, the stimulus current readily drives faradaic reactions at the electrode-tissue interface—electrons will be transferred across the interface via oxidation-reduction^{32,37,38}. Significant faradaic reactions can damage both electrode and tissue.

In contrast, with an ideal polarizable electrode, electrons cannot cross the interface. Instead, the applied current will cause charged molecules and ions to form what

is termed the “double layer” at the interface, which behaves like a capacitor³⁷. A more detailed description of the double layer can be found in Chapters 1, 10, and 13 of the Bard-Faulkner book³⁷.

The electrochemical behavior of the stimulating electrode, target tissue, and the interface can be approximated as an electrical equivalent circuit. While many circuit models exist, this document will focus on the famous Randles model³⁹, shown in **Figure 1**. This model also applies to the counter and reference electrodes.

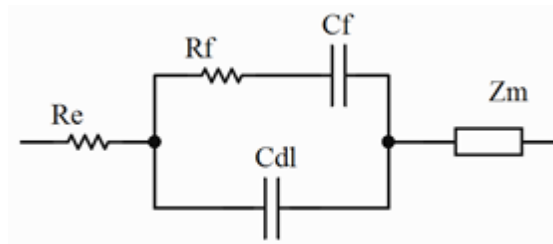


Figure 1 The Randles equivalent circuit model for the electrode-tissue interface. Please see text for description and explanation. The figure is created based on Randles’s original work³⁹.

Re is the resistance of the electrode material; the impedance due to **Re** tends to be negligible relative to that of other components. **Zm** denotes the passive impedance of the medium, which is a conductive solution or tissue. In a solution, **Zm** is purely resistive, but in tissue, **Zm** is complex. The **Rf** and **Cf** terms represent, respectively, the resistive and capacitive behavior of faradaic charge transfer at the interface. These two terms collectively form the faradaic impedance, **Zf**. **Cdl** represents the double layer capacitance.

Each component of this circuit model is associated with a physical phenomenon and can be used to infer characteristics of the electrode and tissue. **Zf** and **Cdl** are particularly important. For example, a highly polarizable electrode with high **Zf** and large **Cdl** is great for stimulation. The significance of a large **Cdl** is that, given a voltage, more

charge can be injected into the double layer. A high Zf allows the electrode to sustain higher voltages without undergoing significant faradaic reaction. Zm is also important. For chronic implants, Zm typically increases over time, which is attributed to tissue encapsulation. Tissue encapsulation is an innate response and adversely affects treatment⁴⁰⁻⁴³.

To determine these circuit components for a particular system, electrochemical impedance spectroscopy (EIS) is commonly performed^{38,41,44,45}. EIS builds the voltage-current relationship of the system by measuring the impedance to sinusoidal voltage signals over a large range of frequencies. The impedance data then can be used to construct a circuit model with quantified component values. EIS theory is discussed in detail in Chapter 10 of the Bard-Faulkner book³⁷ and by Andrzej Lasia⁴⁶.

The properties of the electrode-tissue interface create major limits for stimulus design and the device. For example, smaller stimulating electrodes can be more region-specific but have smaller Cdl . A small Cdl results in higher impedance, which increases the stimulator voltage required to deliver the same therapeutic level of current and the overall power consumption.

1.3.2 Strength-Duration Relationships

Georges Weiss developed instruments to generate brief, voltage-controlled rectangular pulses, of which both the pulse width and voltage amplitude can be precisely adjusted. Using this pulsatile stimulation, he built a mathematical model that relates nerve responses to stimulus parameters. In 1901, he proposed the following formula:

$$Q = a + bt \qquad \text{Equation 1}$$

where “**t**” is the pulse width (duration) and “**Q**” the product of the threshold voltage amplitude for nerve activation and pulse width^{33,34}. “**a**” and “**b**” are merely empirical constants used to fit the data to a linear regression model. Today, “**Q**” is defined as the product of threshold current and pulse width, which for rectangular pulses, is the charge injected by the pulse.

In a follow-up article in 1909¹, Louis Lapicque expanded upon Weiss’s model and defined the terms “rheobase” (“rhéobase” in French) and “chronaxie”³⁵. The rheobase is the theoretical minimum pulse voltage required to activate a nerve using an infinite pulse width. The chronaxie is the pulse width required to activate a nerve when using a pulse voltage twice the rheobase. Again, today, these concepts are described using current amplitudes.

The relationships described by Weiss and Lapicque are now known as the strength-duration relationships (**Figure 2**). The strength-duration equations, written below, relate the threshold current (**I_{th}**), threshold charge (**Q_{th}**), and threshold energy (**E_{th}**) required for nerve activation to pulse width (**t**), rheobase (**I_r**), and chronaxie (**t_c**)^{34,47,48}. For energy, a constant resistance (**R**) is assumed.

$$I_{th} = I_r \left(\frac{t_c}{t} + 1 \right) \quad \text{Equation 2}$$

$$Q_{th} = I_{th} * t = I_r t_c + I_r t \quad \text{Equation 3}$$

$$E_{th} = I_{th}^2 * R * t = I_r^2 R t \left(\frac{t_c}{t} + 1 \right)^2 \quad \text{Equation 4}$$

¹ This article is actually located in Comptes Rendus Soc Bio. The article is sometimes wrongly cited as Comptes Rendus Acad. Sci. Lapicque did publish an article in the same year there, but it was not the one where he introduced the concepts of rheobase and chronaxie.

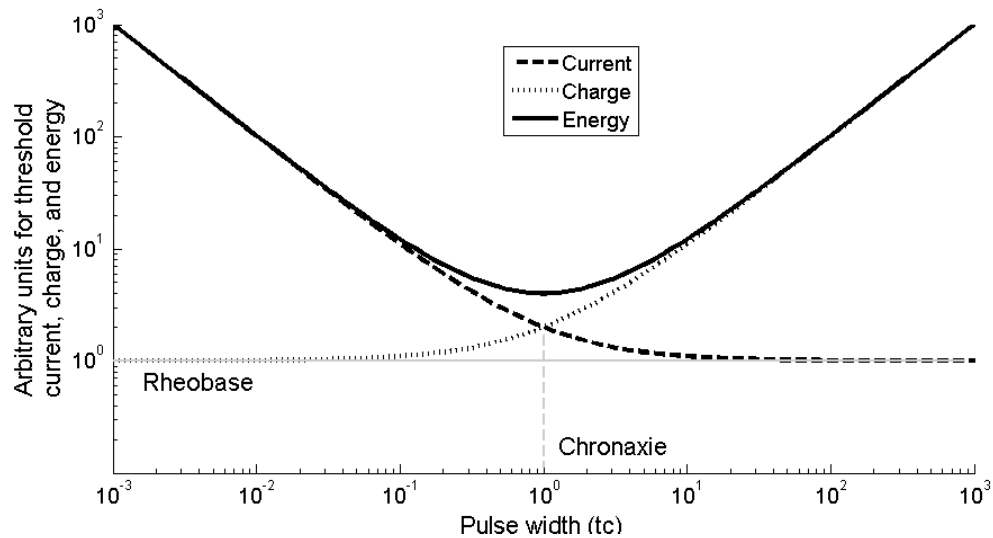


Figure 2 Strength-duration curves. The black dashed line illustrates *Equation 2*. The black dotted line illustrates *Equation 3*. The black solid line illustrates *Equation 4*. The rheobase current is set to an arbitrary value of 1, and so is the chronaxie. All values on the axes are therefore relative to the rheobase (gray solid line) and chronaxie (gray dashed line). For *Equation 4*, R is also set to 1.

These equations do not perfectly fit empirical data but are close approximations; reported r^2 is usually $> 0.99^{48-50}$. It is important to note that, for pulse shapes other than rectangular, the current-duration relationship still holds true, but the average, not the peak, current should be used for analysis³⁴. Also, it is interesting to note that, though Weiss and Lapicque used voltage-controlled stimuli in their experiments, they presented their models in terms of **I** and **Q**.

The strength-duration equations and curves illustrate clearly the importance of pulse width in determining efficacy:

1. The longer the pulse width is, the lower the threshold current is.
2. The shorter the pulse width is, the less the threshold charge is.
3. At the chronaxie, the lowest energy is needed.

While strength-duration relationships were first created for studying nerve activation, these principles certainly can be applied to brain stimulation as well. Charles Gallistel and colleagues published a series of articles in the 1970s that characterized the relationship between stimulus pulse width and the charge required to elicit reward-seeking behavior in rats⁵¹⁻⁵³. Though the data tend to deviate more from the models, the general relationship does hold true. Other laboratory^{54,55} and clinical^{56,57} studies also agree with this finding.

1.3.3 Current-Distance Relationship

When driving currents using electrodes, a voltage profile that is dependent on tissue impedance develops in tissue (good illustrations of such voltage profiles can be found in ⁵⁸⁻⁶¹). Therefore, a relationship exists between threshold current and distance of a neuron from the electrode, which takes on a parabolic shape, with threshold current increasing with increasing distance⁶². The existence of such a relationship is easy to appreciate, and the concept is rather intuitive. Thus, the details of the current-distance relationship will not be discussed further here. A 1996 article by Edward Tehovnik⁶³ offers a good review of this principle.

This relationship is very important in brain stimulation, where, less so for nerves, tissue organization and function vary highly with respect to space. So, when stimulating a specific region, much of the neural tissue near the electrode will be activated, leading to the therapeutic effect. However, a portion of the tissue surrounding the target region will be activated as well, leading to side effects. Ensuring adequate stimulation of the target region while minimizing activation of the neighboring tissue is very difficult.

1.3.4 Electrical Properties of the Neuron

Neurons respond to electrical stimuli by changing their membrane properties. Activating a neuron is simply inducing an action potential. The renowned Hodgkin-Huxley study²⁸ essentially created an equivalent circuit that describes the behavior of neuron membranes to an applied current (see **Figure 3** for a simplified model).

The mechanism of the action potential lies in the dynamics of the channel conductances. The membrane voltage is a function of the Nernst potentials and conductances of the many types of ion channels^{28,64}. The Nernst potentials are fairly constant, but the conductance of each channel type varies differently with membrane voltage and time. If the resting membrane is depolarized past the threshold voltage, due to a natural or artificial stimulus, changes in conductances are initiated, resulting in the action potential²⁸.

Though the Hodgkin-Huxley model was built for the isolated axon, similar models can be built for the neurons of the central nervous system. These models can be used to study and predict how different axon fiber populations^{58,65-67} and different compartments of the neuron, such as dendrites and somata⁶⁸⁻⁷⁰, respond to electrical stimuli.

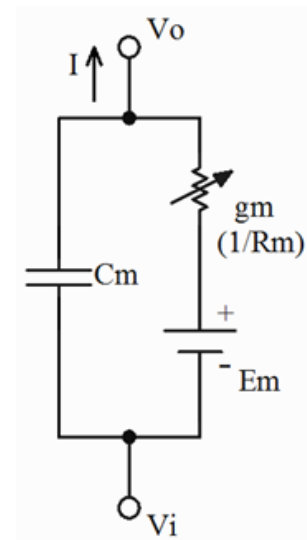


Figure 3 Simplified Hodgkin-Huxley model. V_o and V_i denote the potentials on the outside and inside of the membrane, respectively. C_m models the membrane's capacitive behavior. E_m represents the membrane voltage, and g_m is the membrane conductance lumped from all the channels (note $g = 1/\text{resistance}$). By modern convention, $E_m = V_i - V_o$, and the current I is positive flowing from inside to outside. Modified from Hodgkin and Huxley²⁸.

1.3.5 Cathodic versus Anodic Stimulation

Based on the Hodgkin-Huxley model and its conventions, the membrane is negatively polarized at rest, meaning there is an excess of negative charge on the inside. If an outward current is induced, it will depolarize the membrane, and vice-versa^{28,71}. To produce an outward current, the working electrode is driven to a negative potential, termed cathodic stimulation. Negative charge then accumulates near the extracellular side of the membrane, leading to depolarization, which subsequently can initiate an action potential. Note that in electrical stimulation, the intracellular compartment is not directly manipulated.

On the other hand, when the working electrode is driven to a positive potential— anodic stimulation—positively charged ions will accumulate, leading to hyperpolarization. However, anodic stimulation can still elicit action potentials in nerves or axons via the creation of what Merrill *et al.* referred to as a “virtual cathode”³², which is a relative cathodic field that surrounds the applied anodic field^{58,71,72}. These virtual cathodes are weaker in amplitude than a directly applied cathodic field, and so the expected efficacy is lower as well.

Indeed, for neuronal activation, modeling^{58,65,66} and empirical evidence^{73,74} both suggest that cathodic pulses are more efficacious⁷⁵. For DBS, results from laboratory⁵⁴ and clinical studies⁷⁶ also support the use of cathodic pulses.

For cortical stimulation, when using penetrating electrodes, like those used in DBS studies, cathodic stimulation is also more efficacious^{62,77,78}. However, when using surface electrodes to stimulate the cortex, researchers have shown that anodic stimulation can be more efficacious in regions with high corticofugal output^{75,79,80}. Due to the

current-distance relationship, it is difficult to activate deeper axon-rich layers with cathodic pulses from the surface. In this case, to target the axon-rich layers, anodic stimulation can be used to create virtual cathodes deeper in the cortical tissue.

1.3.6 Monophasic versus Biphasic Stimulation

As mentioned earlier, biphasic waveforms are used mostly for safety reasons. By principle discussed previously, biphasic waveforms usually are cathode leading. The initial cathodic pulse is intended to depolarize the neurons, eliciting action potentials. The charge injected by the cathodic pulse is then reversed by the anodic pulse that follows, so that there is no potential buildup that could lead to faradaic reactions. Cathode leading has been shown to yield lower threshold currents in nerve stimulation²⁵ and cortical stimulation⁷⁸.

Though there is disagreement^{81,82}, overwhelming evidence suggests that biphasic stimuli are indeed safer^{15,80}. The tradeoff, however, is that biphasic waveforms are less efficacious, with the delay between cathodic and anodic pulses being an important factor²⁴⁻²⁶.

1.3.7 Current- versus Voltage-Controlled Stimulation

Whereas all articles up to Weiss's and Lapicque's time described using voltage-controlled stimuli, as early as Penfield's homunculus experiments, experimenters began to report that current-controlled stimuli tend to be more consistent and effective^{85,86}. Today, overall, current-control is the standard. In this paper, "current-control" refers to applying a current of defined amplitude between the working and counter electrodes, and

“voltage-control” refers to applying a defined voltage across the working and counter electrodes.

The major disadvantage of using voltage-controlled stimuli is that only the voltage between the working and counter electrodes is controlled³². At the pulse onset, when the capacitive components of the electrode and tissue are not charged, the current is high, but as they charge, the current will decrease. In addition, because the electrode and tissue impedances are both variable over space and with time, the voltage profile through the tissue is inconsistent.

Based on these observations, from an efficacy perspective, voltage-control offers poor reproducibility³². Indeed, modeling has shown that, with voltage-controlled stimuli, the volume of tissue activation and the voltage profile are highly dependent on electrode and tissue capacitances⁸⁷. In a recent investigation, Lempka *et al.* have shown that voltage-controlled stimulation causes significantly larger variability in the voltage recorded from recording electrodes near the DBS electrode⁸⁸. And from a safety perspective, though the voltage is set, electrode potentials can drift over time with repeated stimuli, especially with high frequency pulses, which leads to undesirable faradaic reactions^{32,81,82}.

Voltage-control is mainly seen in DBS, where the voltage amplitude requires constant readjustment⁸⁹⁻⁹². Recently, this DBS paradigm has been called into question⁹³. Laboratory experiments^{88,94} and randomized clinical trials⁹⁵ have shown that current-controlled DBS yields more consistent results, and voltage-controlled DBS may soon become obsolete.

1.4 Modern Stimulation Paradigms

The standard modern stimulus waveform is composed of a train of repeating pulse waveforms. Important parameters regarding each pulse are listed below:

- Pulse shape – examples include rectangular, triangle, and sinusoid
- Amplitude (AMP) – amplitude of the pulse, either voltage or current
- Pulse width (PW) – the duration (a time value) of each pulse

Though many pulse shapes have been proposed and studied⁹⁶⁻⁹⁹, the rectangle is still the most common shape used in research and clinical settings. Used since the time of Weiss and Lapicque, it is popular due to its ease in implementation and mathematical simplicity.

A pulse train then can be formed using single pulses—monophasic—or biphasic pulse waveforms. Important biphasic pulse parameters are:

- Cathodic amplitude – amplitude (either voltage or current) of the cathodic pulse
- Anodic amplitude – amplitude of the anodic pulse
- Interphase delay – the delay (a time value) between cathodic and anodic phases; this value could be 0 and usually is not longer than the interpulse interval
- Interpulse interval – the time between the end of the first pulse and the beginning of the following pulse

Biphasic waveforms can lead with either the cathodic or anodic phase. In addition, the pulse widths and amplitudes of each phase can be intentionally mismatched. And finally, the pulse train has the following important parameters:

- Pulse period – the time between the beginning of two successive pulses

- Pulse repetition frequency – this is equal to $1/\text{period}$ and is commonly referred to as the stimulation frequency

Figure 4 illustrates a pulse train, with parameters annotated, constructed from biphasic, charge balanced, pulse waveforms with interphase delay.

In certain applications, more complex features are introduced into the stimulus waveform in the form of amplitude (AM) and/or frequency modulation (FM) of the parameters. In AM, the amplitude parameters of the individual pulses within the train are varied; in FM, the time parameters are varied. In auditory stimulation and cochlear implants, the advantages of AM and FM are well-established^{100,101}. Similar work is being conducted for DBS^{102,103}.

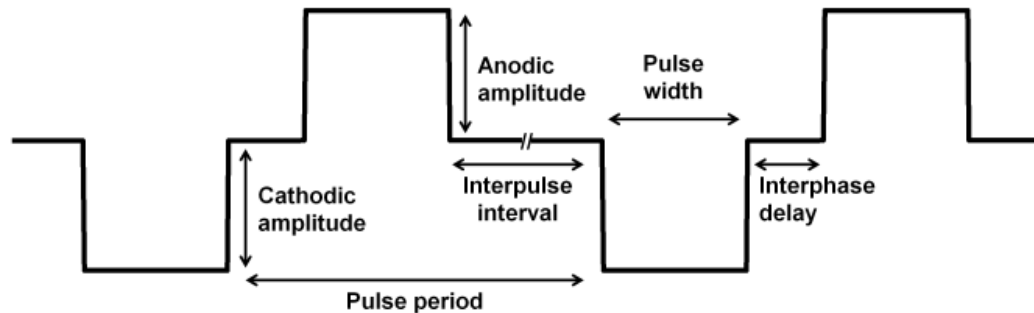


Figure 4 Example pulse train. The waveform above is a biphasic, charge balanced, rectangular pulse train. Key parameters are annotated.

1.5 Overview of Dissertation

The contents of this introduction chapter so far have described the current state of the broad field of electrical stimulation. CHAPTER 1 only serves as a general review of the established theory and principles. The next three chapters all deal with specific

applications of electrical stimulation in medical science and practice. Each of these chapters contains a further review of relevant background information and key findings.

CHAPTER 2 explores the effects of electrical stimulation on alcoholism, a condition that affects many and has proven to be difficult to treat with conventional methods. The neural circuitry of reward and addiction has been studied for many decades, and by stimulating the appropriate parts of that circuit, it is theoretically possible to modify addiction behavior. Others have attempted to reduce alcohol consumption in animal studies but have not produced convincing results^{104,105}. Through collaboration with Dr. Zachary Rodd's group in Indianapolis, I was able to show that DBS of the nucleus accumbens shell reduced alcohol drinking in rats. These results have important implications for treating alcoholism and addiction.

CHAPTER 3 introduces a novel method of designing and studying stimulus waveforms that has potential to increase the effectiveness of stimulation therapy. This work originated from the DBS work described in CHAPTER 2. When applied to nerve stimulation, the vagus nerve in particular, this novel method seems capable of producing patterns of nerve fiber activation different from the conventional method, which simply involves delivering rectangular pulse waveforms. The different activation patterns signify that the efficiency and selectivity of nerve stimulation can be fine-tuned with careful adjustments of the stimulus based on response feedback.

In CHAPTER 4, the work in CHAPTER 3 is expanded. In addition to demonstrating how the stimulus can be manipulated to vary the nerve activation pattern, I show that the differences in the resulting nerve response profiles have a significant impact on the physiological response as well. Actually, the nerve response has a

consistent relationship with the ultimate physiological response. As a result, a stimulation paradigm that allows improved control of the nerve response also provides better control of the physiological response.

CHAPTER 5 concludes all of the work detailed in this dissertation. This final chapter reviews the key concepts and summarizes the important results. And finally, there is a discussion of the significance of the results and ways to expand this work.

CHAPTER 2. DBS TO TREAT ALCOHOL USE DISORDER

2.1 Introduction to Alcohol Use Disorder

Alcohol use disorder (AUD) – alcohol abuse and dependence – is a highly prevalent condition with serious health and societal impacts^{14,106,107}. An estimated 30% of the U.S. population will suffer from AUD during their lifetime¹⁰⁶, and in the world, about 125 million people suffer from AUD¹⁴. Patients with AUD have 1.8 to 9.5 times higher mortality rates than the general population, and death from accidents, particularly motor vehicle collisions, is common^{108–110}. Existing treatments can be effective but only temporarily so, because about 50% of patients become noncompliant or relapse in just one month^{8,9,111–113}.

Deep brain stimulation (DBS) offers a promising alternative to conventional AUD treatments¹⁶ and may provide reliable treatment with sustained long-term effectiveness. Recent clinical studies and reports have shown that DBS can reduce alcohol intake and craving^{114–116} as well as other addictive behavior, such as cigarette smoking, drug use, and overeating^{117–119}. Animal studies suggest the same^{104,105,120–123}. However, there are still concerns about beginning large-scale clinical trials. The major criticism is that there is not enough evidence on long-term efficacy and safety in animals to justify such an invasive and risky intervention^{124–127}.

There is actually not much animal data on the effects of DBS on alcohol consumption in general^{124–127}. One study showed that DBS can reduce alcohol intake but relied on a saccharin fading procedure to induce alcohol drinking¹⁰⁵. Another study used P-rats, which voluntarily drink alcohol, but the study yielded inconclusive results due to very low levels of alcohol intake¹⁰⁴. The P rats are a unique breed of rats with characteristic alcohol preference and intense alcohol drinking behavior^{128,129}, which make them a good model for studying alcoholism^{130,129}.

This chapter presents a set of experiments characterizing the effects of DBS on voluntary ethanol consumption in the P rats. These experiments were aimed to provide more efficacy data from animal studies. The results of this work contributed to the increasing amount of evidence that supports the use of electrical stimulation in treating AUD and related disorders.

2.2 Experimental Design and Methods

These experiments were designed and conducted in collaboration with Dr. Zachary Rodd's research group in Indianapolis. The animal experimentation took place in Indianapolis.

2.2.1 Animals and Surgery

Adult female alcohol-preferring (P) rats weighing 200 to 350 gm from the 78th generation were used in this experiment. Female rats were used because they maintain body weight and head size better than male rats for more accurate stereotactic placements. Rats were double-housed upon arrival to the lab and maintained on a 12-hr reverse light-

dark cycle (lights off at 9:00 AM). Food and water were freely available throughout the experiment except in the test cage. Animals used in this study were maintained in facilities fully accredited by the Association for the Assessment and Accreditation of Laboratory Animal Care. All research protocols were approved by the institutional animal care and use committee and are in accordance with the guidelines of the Institutional Care and Use Committee of the National Institute on Drug Abuse, NIH, and the Guide for the Care and Use of Laboratory Animals (National Research Council, 1996).

A twisted pair of Platinum electrodes (Plastics One, Inc.) was implanted into the left nucleus accumbens shell (AcbSh) of each animal. The AcbSh is a major center in the reward/addiction circuitry^{131,132}. Unilateral implantation was performed instead of bilateral, mainly to simplify the surgery and experimentation. Left sided implantation was chosen based on a previous human study, which demonstrated abnormal neural activity in the left AcbSh only (i.e. no change in right AcbSh) in response to drug-related cues¹¹⁵. Target coordinates for the AcbSh were 1.6 mm anterior to bregma, 2.4 mm lateral to the midline, and 8.5 mm ventral from the surface of the skull at a 10-degree angle to the vertical.

Each electrode terminated in two female sockets that were connected to a multi-channel electrode pedestal, which was secured firmly using cranioplasty (OrthoJet) layered around the device and over three stainless steel screws fastened to the skull. After surgery, rats were individually housed and allowed to recover for at least 2 days before resuming testing.

2.2.2 Experimental Setup

The DBS system consisted of an “animal proof” stainless-steel-shielded cable that attached the implanted electrode pedestal and to an electrical commutator (all from Plastics One, Inc.), which allowed free movement within the cage. The commutator was mounted over the top of the testing cage, which is 30 x 30 x 26 cm (*w x h x d*) in size. A waveform generator (Agilent 33522A) was used to design the stimulus waveform, and a custom-made current pump was used to convert the voltage waveform to a constant current waveform (more detail on the current pump can be found in Section 3.6). The stimulus parameters were as follows: biphasic, rectangular pulses with no interphasic delay, pulse frequency 150 Hz, pulse width 100 μ sec, and current intensities of 100 μ A ($n=3$) or 200 μ A ($n= 4$).

The implanted electrodes were checked periodically by performing electrochemical impedance spectroscopy with a Gamry Reference 600 Potentiostat (detailed methods can be found in Section 3.6). The functionality of the DBS system was tested before each stimulation session by checking the stimulator output via a digital multimeter (Agilent 34410A) in series with the stimulator and electrodes. All measurements were done outside the 60-min testing session and did not interfere with behavior testing.

2.2.3 Experimental Design and Data Analysis

In the testing cage, 15% non-flavored ethanol (EtOH) and water were freely available, via two separate 15 mL graduated tubes. Rats were placed in the training box with access to the fluids for one hour a day (limited access) each day for 4 weeks to

establish consistent alcohol intake behavior. Alcohol-preferring P rats are natural drinkers and do not typically require food/water restrictions, or sucrose fading procedures to acquire stable daily alcohol intake in a free choice limited access setting^{128,129}. Once chronic drinking levels were established and stable over several days, rats underwent surgery for DBS lead placement. After a recovery period of 2 days, the rats resumed the daily 1-hour sessions in the training box.

During the first postoperative week, the rats were tethered to the DBS system but did not receive any active stimulation. This period allowed each rat to acclimate to the new sensation of the cable and reach a new post-implant baseline of alcohol intake. In the second postoperative week, once rats re-established alcohol drinking behavior, DBS was delivered to the rats in the training box for 5 minutes prior to and during the entire 60 minute drinking session.

DBS therapy occurred each day during the 1-hour session for 5 days at 100 μ A in 3 rats and for 6 days at 200 μ A in 4 rats. A technical issue in the 100- μ A group caused the DBS to not be delivered on Day 1, but this was not identified until after the completion of the experiment, leaving just five days of active DBS data for analysis. All 7 rats underwent an additional 3 daily post-DBS sessions, during which they were tethered but not stimulated to assess for any post-treatment effects. At the completion of the experiment, rats were euthanized by CO₂ inhalation. Brains were then removed, and histology was examined for accurate placement of electrodes to confirm proper implantation.

The analysis for the DBS data was simplified since there were not enough values to fulfill the degrees of freedom requirement to perform a mixed factor ANOVA.

Therefore, paired t-tests were performed comparing baseline EtOH consumption to intake during test session. To adjust for multiple comparisons, the p value of significance was lowered to $p < 0.01$.

2.3 The Effect of DBS on Alcohol Intake

DBS delivered at 100 μA temporarily reduced EtOH consumption (see **Figure 5**) with 35% and 43% decreases on Days 2 and 3 (p values < 0.002) but no effect on Days 1, 4, and 5. DBS delivered at 200 μA consistently reduced EtOH consumption, with a 35%, 42%, 53%, and 59% decrease on Days 3, 4, 5, and 6, respectively (p values < 0.0018 ; **Figure 6**). There was no effect of DBS on water intake, indicating that the stimulation did not affect overall fluid intake or interfere with normal animal behavior. Baseline intake levels in both groups would have resulted in blood ethanol concentrations ranging from 75-125 mg%; these levels are much higher than what others reported¹⁰⁴.

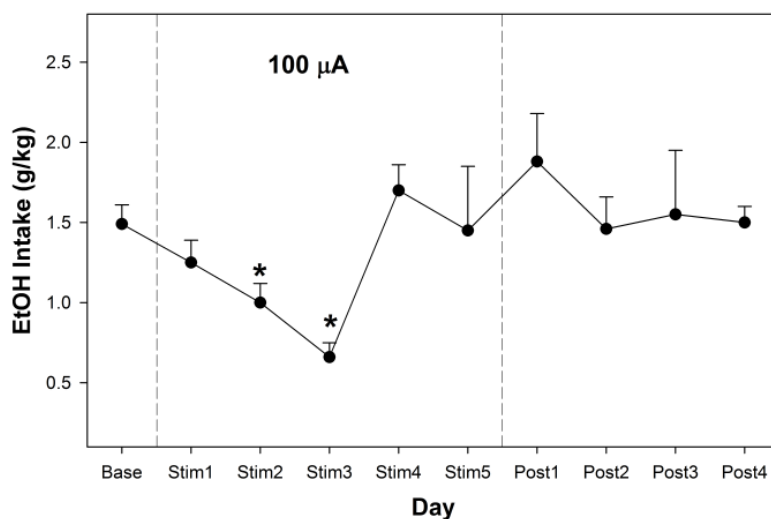


Figure 5 Ethanol (EtOH) intake in the 100 μA group. The average EtOH intake per 1-hour session is plotted over time. Data were collected each day during DBS delivery (Stim1–Stim5) and for 4 days after the last day of DBS delivery (Post1–Post4). Baseline is estimated by averaging the intake for 3 days before stimulation. Data were obtained from a total of 3 rats.

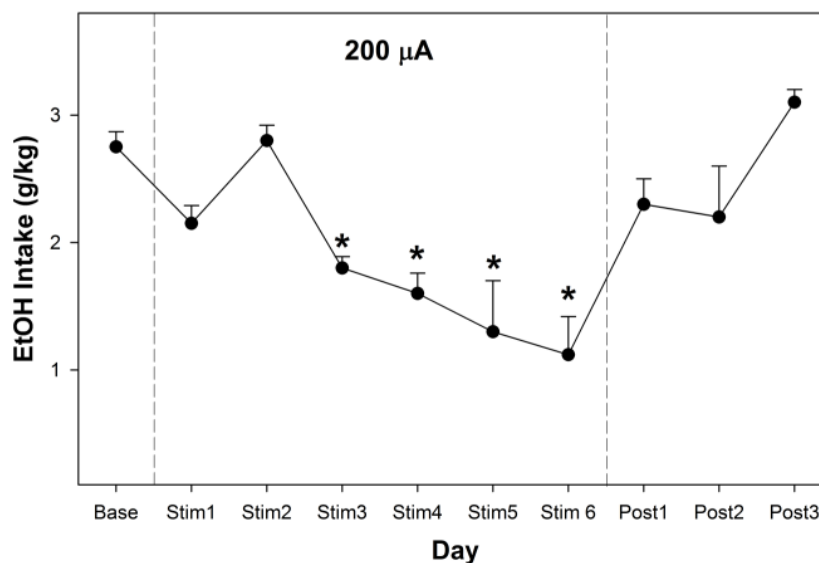


Figure 6 Ethanol (EtOH) intake in the 200 μ A group. The average EtOH intake per 1-hour session is plotted over time. Data were collected each day during DBS delivery (Stim1–Stim6) and for 3 days after the last day of DBS delivery (Post1–Post3). Baseline is estimated by averaging the intake for 3 days before stimulation. Data were obtained from a total of 4 rats.

At 100 μ A, there seems to be only a transient decrease in alcohol intake in the subjects. However, at 200 μ A, the effect is more sustained. Also, the effect seems to be reversible, with intake rebounding to baseline levels after the stimulation either is no longer effective or is turned off.

2.4 Discussion

DBS of the AcbSh seemed to be capable of reducing alcohol drinking in alcohol preferring P rats. Considering that the overall amount of stimulation is fairly low, only about 1 hr per day, and that only unilateral stimulation was delivered, the observed significant effect on alcohol drinking behavior is highly promising. DBS may just provide the type of lasting treatment that is specific, adjustable, and less dependent on patient compliance.

However, as can be seen in the difference between the 100 and 200 μA test groups, the stimulus parameters can dictate the success of the therapy. The two amplitudes, 100 and 200 μA , were chosen somewhat arbitrarily when designing the experiment, with prior studies in mind^{104,105}. Though the final behavioral effect can be measured, the exact neural response to the stimulation is unknown.

With only physiological or behavioral data as feedback and no neural response data, it is difficult to determine the stimulus parameters to ensure that the patient or subject is receiving appropriate stimulation. Too little stimulation can result in lack of therapy or loss of therapy over time, as seen in the 100 μA group. Too much stimulation may result in harmful side effects. Dosing for each individual is a major challenge in the field of electrical stimulation today.

2.5 Developing a Better Method for Stimulus Waveform Design

The next two chapters present a new way to design and assess stimulus waveforms. The work builds on the thesis of Dr. Matthew Ward¹³³, who provided a stimulation system to characterize and analyze the neural responses to different stimuli. This system, termed Autonomous Neural Control (ANC), allows users to empirically determine how neurons will respond to stimulation. The neural response then can be matched to the physiological or behavioral response. This way, determining the stimulus parameters can be objective, involving less guesswork.

So far, ANC is best developed for nerve stimulation, with particular focus on the vagus nerve due to the many applications of vagus nerve stimulation therapy. When stimulating the nerve, the response is relatively simple, because the nerve is a neatly

organized, essentially parallel bundle of axons, whereas the brain is a vast network.

Though the nerve response can be more easily captured and quantified, the vagus nerve is by no means simple. Stimulating the vagus nerve can cause many different effects, and these effects can be matched to the nerve response. Therefore, vagus nerve stimulation provides a good platform for testing methods to optimize stimulus parameters.

2.6 Notes

With permission from Journal of Neurosurgery, some portions of the texts and several figures in this chapter were reproduced and adapted from the published article Wilden *et. al.*¹³⁴, which is the fruit of the collaboration with Dr. Rodd's group and contains my original work.

CHAPTER 3. BURST-MODULATED STIMULUS WAVEFORMS

3.1 Introduction to Vagus Nerve Stimulation and Its Challenges

Electrical stimulation of the vagus nerve is an FDA-approved treatment for certain types of epilepsy that are resistant to conventional treatments. Vagus nerve stimulation (VNS) is also approved for treatment-resistant major depression, and it is under investigation for treating other disorders¹⁵. In epilepsy, up to 24% of patients cannot adequately control their seizures with medication^{4,5}, and among patients being treated for depression, as many as 50% experience recurrent major depressive episodes¹³⁵. Some of these patients, who do not respond to pharmaceutical therapy, do respond positively to VNS. Response rate to VNS is about 25-45% in patients with drug-resistant epilepsy¹⁷ and about 30-40% in patients with drug-resistant depression¹³⁶. Though the anti-depression effect is highly significant, the contents of this chapter will focus mostly on VNS in epilepsy, the major reasons being that VNS in epilepsy has been studied in more detail and that the effects are more quantifiable.

A significant amount of patients benefit from VNS, but there are many patients who do not respond well. Clinical studies generally conclude that patient response rates increase with time, and tolerability to the stimulation increases as well¹³⁷⁻¹⁴⁰. However, a closer look at the clinical VNS data will show that, patients who initially responded to therapy will continue to respond, and those who did not respond tend to remain

unresponsive. Ultimately, the patients who do not respond tend to stop treatment. For example, in a key clinical trial by DeGiorgio *et. al.*¹³⁷, 164 patients completed the study, and out of those, 68 patients were responders, with “response” defined as 50% reduction in the number seizures. Of the 98 remaining patients, 22 discontinued therapy, and the mean seizure reduction in this group is only 7%. A retrospective study by Labar¹³⁸ found that patients receiving higher levels of stimulation are actually less responsive, and that patients with more severe epilepsy tend to be less responsive.

Currently, the method for determining VNS parameters—the method of dosing—is not an exact process. Patients pay multiple clinical visits and have their care providers manually adjust the stimulation parameters. The intensity is increased slowly and set to a point slightly lower than the maximum level that the patient can tolerate. If symptom relief is not enough, then the physician will attempt to increase the stimulation level without exceeding the maximal tolerable level¹⁴¹. Adjustment is mostly based on the patient’s perception and the physician’s intuition (there is a safety limit as well that is somewhat arbitrary). It is not surprising, then, that patients who do not respond well to VNS are the ones to receive higher and higher levels of stimulation, and that if a patient does not respond initially, it will be difficult to improve the effects in that patient.

Increasing the overall response rate and reducing the variability among patients are major challenges. After reviewing the background of VNS, this chapter will propose a strategy aiming to improve the effectiveness of VNS. This strategy is based on existing knowledge in the field as well as data collected through original experiments, and it is devised with the goal of allowing simple, quick translation into the clinical setting.

3.2 Mechanism of Electrical Nerve Stimulation

In VNS, electrical charge is applied to the nerve to depolarize the axons within the vagus nerve, evoking action potentials. Generally, electrical charge is delivered through a set of cuff electrodes that wrap around the nerve. The charge is supplied by a stimulus generator, which is powered by a battery. The electrodes, stimulator, and battery are all implanted inside the body (see **Figure 7**). When a stimulus is applied across the electrodes that are placed near the nerve, charges move and distribute in the space surrounding the electrodes and the nerve. In this type of extracellular stimulation (as opposed to intracellular stimulation techniques that require accessing the intracellular space), axons will generate action potentials if their membranes are depolarized sufficiently by the movement of charges.

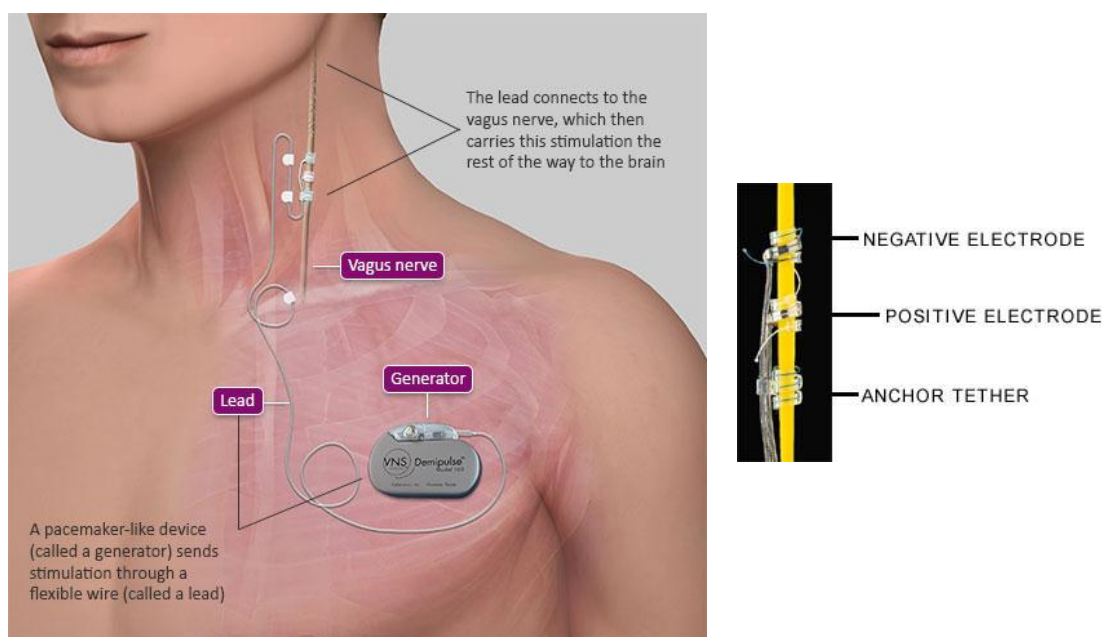


Figure 7 The Cyberonics VNS device. **Left)** An illustration of the VNS implant, composed of the electrode cuffs, connecting leads, and the stimulus generator housed with a battery. **Right)** Close up of the electrode cuffs. Reprinted with permission from Cyberonics, Inc.

Though it affects all axons within the nerve, the stimulus has a stronger effect on the axons nearer to the nerve periphery and closer to the electrodes. However, since there is not enough evidence to suggest that the axons within the vagus nerve are spatially distributed in a consistent, predictable manner, VNS is not specific for axons with respect to the axon's target and function.

Aside from target and function, there are factors that do influence how individual axons respond. In the vagus nerve, as in the entire peripheral nervous system, some axons are myelinated by Schwann cells. The axon together with its myelin sheath, Schwann cells, and endoneurium are referred to as a nerve fiber; the term fiber pertains to even the unmyelinated axon with its endoneurium. In the vagus nerve, 70-90% of all nerve fibers are unmyelinated, and the rest are myelinated to different degrees^{142,143}. The axons with larger diameters tend to have more myelination¹⁴⁴, and the larger, more myelinated fibers conduct action potentials at faster velocities¹⁴⁵⁻¹⁴⁷. Nerve fibers are historically grouped by their conduction velocities as summarized in **Table 1** (compiled from multiple sources^{15,142,146,148,149}).

With typical electrical stimuli, fast-conducting fibers have lower activation thresholds^{24,58,97,150-152}—the lowest stimulus intensity that can elicit an action potential. The smaller, slow-conducting fibers of the nerve are harder to activate^{50,153,154}. Therefore, though all the axons are affected during stimulation, generally more of the larger, faster fibers will respond to each stimulus. As such, electrical stimulation is intrinsically selective for larger fibers, a characteristic that is important for understanding the effects of VNS.

Table 1. Nerve fiber classification and function

	A fibers	B fibers	C fibers
Diameter (micron)	5 – 10	2 – 5	< 2
Myelination	Thick	Thin	None
Conduction velocity (m/s) *	> 10	1.5-20	< 6
Direction	Efferent & afferent	Efferent	Afferent
Main function	Somatic motor, fast pain, epicritic sensation, proprioception	Vasomotor, visceromotor (autonomic)	Nociceptive and visceral sensory
Relative activation threshold	Low	Medium	High

* Large overlap in conduction velocity range is due to discrepancies, which may arise from differences in recording setups, animal models, and methods of calculation.

3.3 Effects of VNS

The vagus nerve (cranial nerve X) is a large collection of axons that innervates tissues and organs spanning from the face/head region down to the colon. The axons that innervate skeletal muscles for swallowing and speech originate from the nucleus ambiguus in the medulla. The soma in the nucleus ambiguus also send efferents to the heart, which, together with the efferents to the respiratory and abdominal organs from the dorsal motor nucleus (also in medulla) of the vagus, constitute the major parasympathetic pathway of the body. In addition to efferents, the vagus nerve contains many sensory afferents that synapse in nuclei also found in the medulla. A small portion of the vagus

nerve relays general sensation to the spinal trigeminal nucleus. More importantly, vagal afferents are responsible for monitoring the cardiovascular and respiratory systems, digestive, and other abdominal organs. These pseudounipolar axons synapse in the nucleus tractus solitarius (NTS)¹⁵⁵. **Figure 8** illustrates key components of the functional anatomy of the vagus nerve.

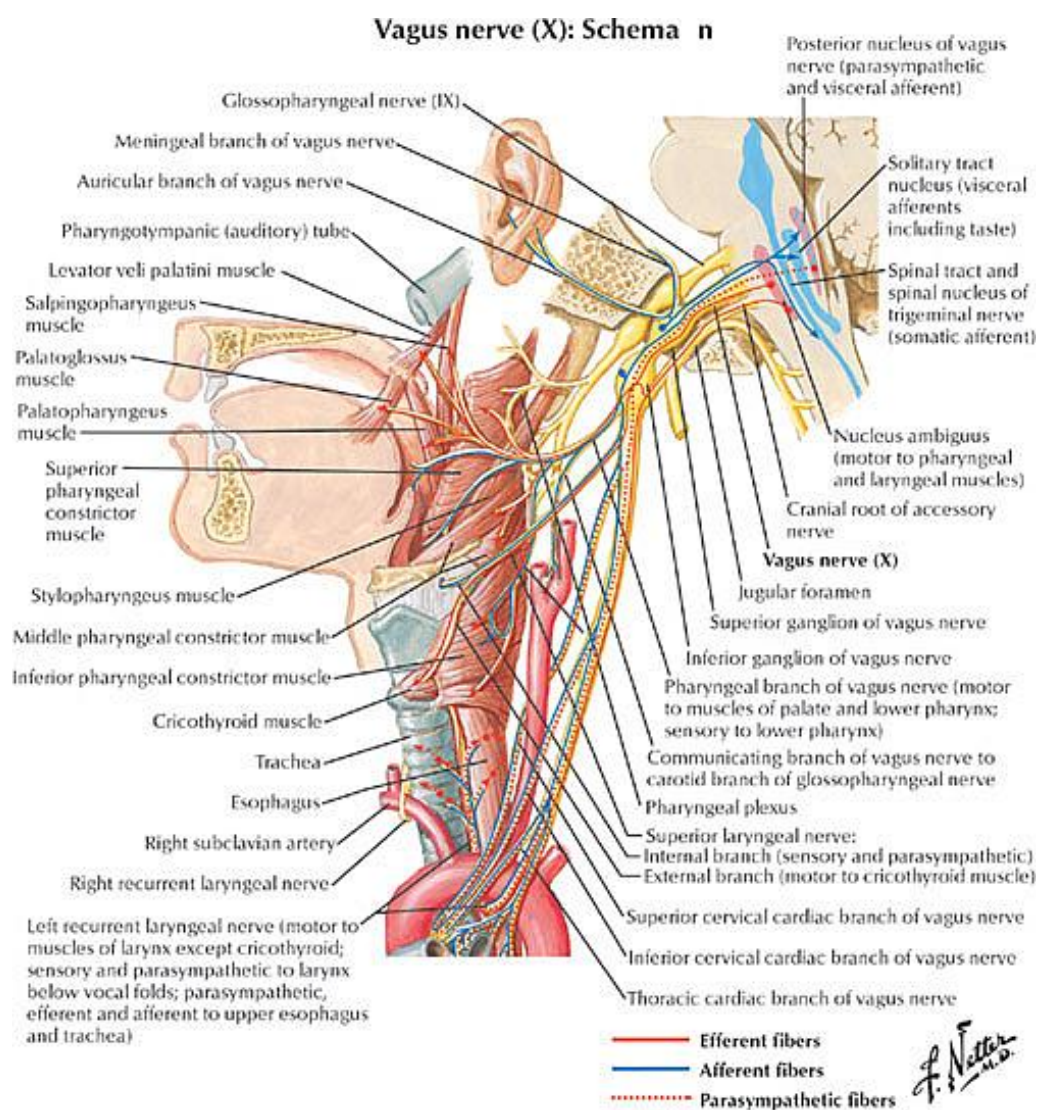


Figure 8 The vagus nerve anatomy and composition. Only the proximal portion, down to the thoracic region, of the vagus nerve is shown. Nearby nerves are illustrated as well. The figure is reproduced from an open source review article¹⁷⁶.

Due to the complex nature of the vagus nerve and the nonspecific nature of electrical stimuli, VNS can create a wide range of effects in the body, some of which are on the heart and are of particular importance. Stimulating cardiac portions of the vagus nerve on either the left or the right side will activate the parasympathetic efferents to the heart, producing negative chronotropic (decreased heart rate), inotropic (decreased contractile force), and dromotropic (decreased conduction) effects. The left and right vagus nerves both innervate the heart, but they are not symmetric¹⁵⁶. Stimulating the right vagus has strong negative effects on heart rate and contractile force, and though stimulating the left vagus has stronger negative effects on the atrioventricular nodal conduction¹⁵⁶⁻¹⁵⁸, this dromotropic effect is less of a clinical concern than the bradycardia and low cardiac output caused by stimulating the right vagus. Therefore, in patients with epilepsy, VNS implants are typically only implanted on the left side, so that harmful cardiac effects are avoided.

Heart-related effects aside, the other effects of VNS can also have clinical impact on patients; these effects are mostly side effects. Ignoring the surgery- and device-related complications (such as infection, scarring, etc.), side effects manifest in the nervous system (pain, paresthesia, headache, dizziness, etc.), respiratory system (dyspnea, pharyngitis), and in the digestive system (dysphagia, nausea, vomiting). The most common ones are coughing and hoarseness/voice alterations^{136,140,141,159,160}, which correspond to the stimulation of the motor efferents to the larynx. Since the motor efferents, which are the fast conducting fibers, generally are the easiest to activate, it is not surprising that VNS leads to strong motor-related side effects. Though the side effects improve over time, the severity of side effects and how well each patient tolerates the

side effects are important factors when determining the proper stimulus intensity, because tolerability limits the stimulus intensity.

The observed side effects are consistent with the activation of vagal A and B fibers, but how VNS leads to the observed therapeutic effects is less clear. Considering the composition of the vagus nerves, which is dominated by small, slow-conducting axons^{142,143}—afferent C fibers—many have suggested that the central effects (e.g. antiepileptic, antidepressant) of VNS are caused by activating the afferent pathway^{15,148,161,162}. Because VNS can cause activation of the neurons in the NTS and thus influence many structures in the brain associated with the NTS, this conclusion is the most intuitive. In a particular study by Zabara¹⁶², the stimulus was still effective in suppressing motor seizures even after the vagus nerve was transected distal to the stimulating electrodes. However, there is no evidence that directly links therapeutic effect to C fiber activation. For example, vagotomy alone may have anticonvulsive effects.

Some studies have argued that C fibers are not involved at all in the mechanism of VNS, and that efferent fibers (most likely B fibers) are more important for therapy (at least for epilepsy)^{163–165}. In the key study backing this argument, Krahl *et al.* used capsaicin, an excitotoxin more selective for C fibers, to destroy C fibers and eliminate C fiber activation. They then found that VNS is still effective in seizure suppression¹⁶⁴. However, this study failed to provide electrophysiological data that C fibers were indeed destroyed. Also, the method used to achieve fiber-selective stimulation is not suitable for patient use, and so the experiment cannot be translated into the clinical setting.

Overall, neither the Krahl *et al.* study nor any other study has produced definitive evidence to link certain fiber group to the therapy. It may be that the therapeutic effects

of VNS are due to activation of a combination of nerve fiber groups. To assess how different fiber activation patterns changes the effects of VNS, it is necessary first to have methods to alter the fiber selectivity of the stimulus.

3.4 Existing Methods for Selective Stimulation

3.4.1 Selective Conduction Block

It is possible to block conduction in fiber populations without chemicals. In a 2004 article, Bhadra & Kilgore thoroughly summarized the method of blocking with direct current, which involves holding a nerve segment at a depolarized or hyperpolarized state with an extra set of blocking electrodes proximal and distal to the stimulating electrodes¹⁶⁶. This technique is more effective at blocking larger fibers, as well as fibers near the surface. Similarly, the set of blocking electrodes can generate alternating current waveforms to block conduction^{167,168}, and again, larger fibers are more susceptible. These electrical block methods, though less damaging to the nerve, still are not much different from the chemical methods. In addition, the blocking stimuli can be very energy costly, which is a non-trivial concern for battery-powered implants.

Overall, conduction block is not an appropriate strategy for altering fiber selectivity VNS treatment, because, as mentioned before, blocking conduction in vagal fibers and silencing their activity will have large system-wide effects and may interact with or confound the therapeutic effects of VNS. Conduction block is also not a practical strategy in the clinical setting for the following reasons:

- The extra blocking electrodes would require more space and further complicate surgery
- The blocking waveform would greatly increase the energy consumption
- The impaired conduction would lead to a different set of side effects

Therefore, it is better to control the fiber selectivity of VNS without modifying properties of the nerve.

3.4.2 Fiber-Selective Electrodes

Different electrode designs can produce different patterns of fiber activation without conduction block. Using a penetrating microelectrode array, Branner *et. al.* were able to access nerve bundles and fascicles¹⁶⁹. Using a multi-contact electrode cuff that flattens the nerve, Tyler & Durand were able to achieve selectivity without penetrating the nerve¹⁷⁰. Though effective, these electrodes are more invasive than the cuff and are not in use clinically. In addition, with these electrodes, to selectively activate target nerve bundles and fiber populations requires mapping different portions of the nerve to the different contact sites. Implementing this system requires a level of data processing and computation that is difficult to implement in an implantable device.

It is also important to note that these electrodes offer only spatial selectivity. The multiple contacts can be used independently to activate portions of the nerve, but there is still no control over which types of fibers are activated. Fiber group selectivity can be achieved only if the individual contacts are making contact with separate fiber groups. However, in the vagus nerve, there is no specific spatial organization. The bundles of fibers going to the different end targets all contain their own mix of fiber groups^{142,143,149}.

3.4.3 Fiber-Selective Stimulus Waveforms

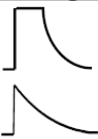
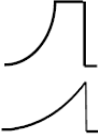



Achieving different patterns of fiber activation with different stimulus waveform designs is perhaps the best strategy. Though it may not be the most selective, this strategy does not create any additional disruption or damage to the nerve and does not raise much safety or feasibility concerns for future integration into VNS implants. Different stimulus waveforms can be implemented with standard cuff electrodes and without additional instrumentation. Finally, without conduction block, the nerve behaves in a more natural manner.

In the past, stimulus waveforms with various pulse shapes have demonstrated adjustable fiber selectivity. Quasi-trapezoidal and quasi-triangular pulses that have a steep rising edge and a slow decay over millisecond scale can be designed to be selective for small fibers^{30,171–173}. The reverse quasi-trapezoidal or quasi-triangular pulse (a slow rise with steep falling edge) can also be selective for small fibers, but it is less so than the normal quasi-trapezoidal pulse, and it requires more charge per phase for nerve activation¹⁷³. Other non-rectangular pulse shapes have been investigated as well and have been shown to be more efficient for neurostimulation^{96,99}, and they may also be selective for different fiber groups. **Table 2** contains an illustration of these pulse shapes.

However, all the non-rectangular pulse waveforms suffer from a common flaw—they are difficult to implement in an implantable device. Rectangular pulses can be generated simply by switching the stimulus on and off, but non-rectangular pulses require the processing unit to create the digital waveform and convert it to an analog stimulus, a process that is much more energy costly.

Rectangular pulse waveforms can be cleverly designed to be selective for certain fibers. Grill & Mortimer have shown that the activation threshold of different fiber groups can be altered by applying hyperpolarizing or depolarizing prepulses to condition the axon membrane, before delivering the stimulus pulse^{97,150}. These pulse shapes tend to be stepwise ramping rectangles (see **Table 2** for illustration).

Table 2. Stimulus pulse characteristics compared to the rectangular pulse

Pulse shape	Maximal efficiency for small fibers*	Maximal selectivity for small fibers	Notes
Quasi-trapezoidal/quasi-triangular 	--	+++	The stimulus itself requires more current/charge; the pulse generator would also require more energy to generate these waveforms
Reverse quasi-trapezoidal/quasi-triangular 	---	+	Same as non-reversed
Gaussian 	+	Unknown	The stimulus itself is more efficient, but it incurs the higher pulse generator energy cost.
Hyperpolarizing prepulse 	--	--	Intended for targeting large fibers. Degree of selectivity slightly adjustable at the cost of efficiency.
Depolarizing prepulse 	-	++	Degree of selectivity slightly adjustable at the cost of efficiency.

* Note that efficiency generally decreases with increasing selectivity for these waveforms.

Hyperpolarizing prepulses, which causes the inactivation gates of the voltage-sensitive sodium channels to open, increase the excitability of nerve fibers. Conversely, depolarizing prepulses, by closing the inactivation gates, decrease excitability and increase activation threshold. Because large fibers respond more to electrical stimuli^{24,58,97,150–152}, which applies to the prepulse as well, the prepulses affect the activation threshold of large fibers more, and the stimulus can be designed to be more or less selective for large fibers. Though this type of stimulus waveform is not as effective as quasi-trapezoidal waveforms in eliminating the larger fiber response¹⁷³, it is more easily implemented with a stimulator, and it has the extra ability to increase the selectivity for large, fast fibers.

Second, because the prepulses are low-intensity stimuli, they only affect fibers near the surface; deeper fibers have normal activation thresholds^{97,150}. When aiming to activate large portions of the nerve, a stronger pulse must be delivered to recruit deeper fibers, and so a stronger prepulse must be also delivered to condition the deeper fibers. However, increasing the prepulse duration would decrease the change in activation threshold¹⁵⁰, while increasing the amplitude may cause the prepulse to be suprathreshold. Therefore, the prepulse strategy is only valid for lower nerve activation levels.

Finally, despite using long pulses with low amplitudes, the prepulses are still capable of activating large, fast fibers. As reported by Vuckovic *et. al.*, a 0.31mA, 0.8ms depolarizing prepulse did not activate any fibers in the pig vagus nerve, but a 0.4mA, 0.8ms prepulse did activate a portion of the A_β fibers¹⁷³, the fastest subgroup of A fibers. The 4mA, 0.2ms stimulating pulse that followed the suprathreshold 0.4mA, 0.8ms prepulse then elicited a lower A_β response about 1ms after the first A_β response, while the

nerve response to the subthreshold 0.31mA, 0.8ms prepulse plus the 4mA, 0.2ms stimulating pulse is about the same as the response with a rectangular pulse. In fact, it seems that it is because portions of the A_{β} fibers were activated by the prepulse and thus refractory that the stimulating pulse activates fewer fibers. In essence, when prepulses are applied to condition the fiber groups to a stimulus pulse, the large fibers may fire two sets of action potentials for every one set of small fiber action potentials. As a result, it is difficult to maintain the frequency of the stimulation and ensure consistent nerve response when changing the prepulse parameters.

With electrical stimulation, overall selectivity is low, and even minor shifts in selectivity may lead to significant effects. **Table 2** provides a summary of the characteristics of the relevant stimulus waveforms. It compares the efficiency of the waveforms at activating nerve fibers and the fiber selectivity, using the rectangular pulse as the standard.

3.5 Introducing Burst-Modulated Stimulus Waveforms

Because of the flaws in the existing fiber-selective stimulation strategies, I developed a different method of designing stimulus waveforms, termed burst modulation. In contrast to standard rectangular pulse waveforms, which are created by repeating rectangular pulses with defined pulse width (PW) and amplitude (AMP, could be voltage or current), burst-modulated waveforms are created by repeating bursts of much narrower pulses, termed “pulsons”. Pulsons can be rectangular in shape as well, so that they can be generated in the same simple on-off, switch-like manner. An example of burst-modulated waveforms is illustrated in **Figure 9**.

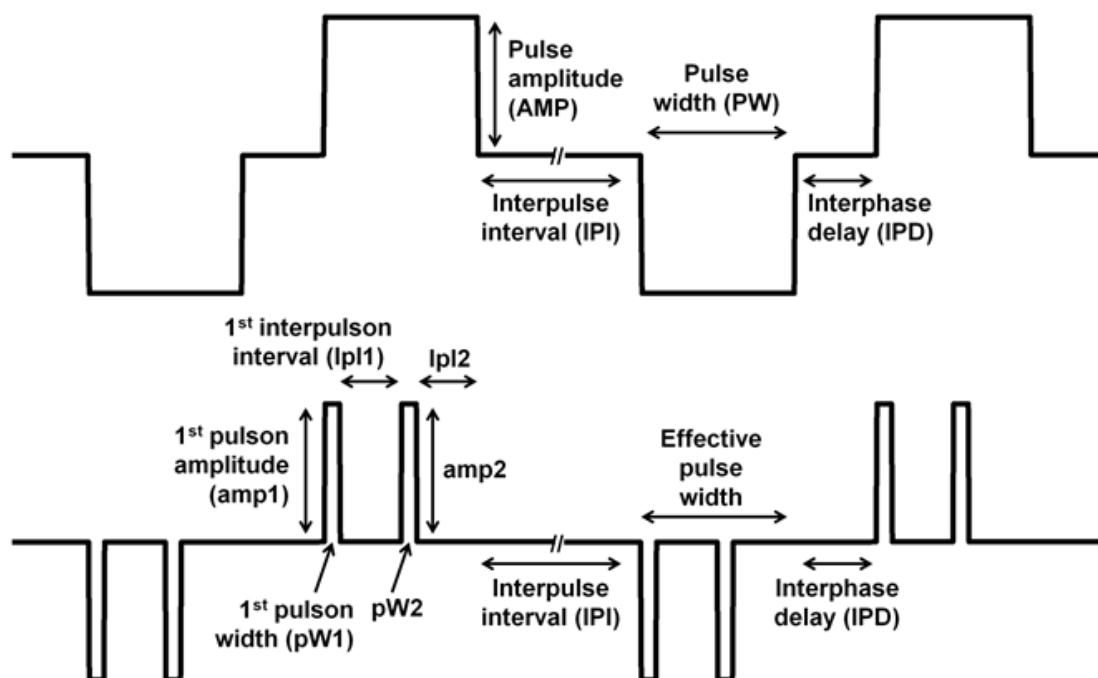


Figure 9 Rectangular pulse and burst-modulated waveforms. A comparison of the standard rectangular pulse waveform and a 2-pulson burst waveform, with stimulus parameters annotated. Both are biphasic, cathode-leading, charge-balanced waveforms with the same repetition frequency. In this example, I_{pl2} exists to simplify calculations and comparisons. Reprinted © 2015 IEEE.

When a pulse is to be delivered, the stimulator generates a burst of pulsons in place of a single rectangular pulse. In burst modulation, only the pulse shape is replaced; other stimulus parameters such as stimulation frequency and train duration are not modified. For a burst of pulsons, each pulson has a defined pulson width (pW_x , x denoting the pulson number in the burst) and amplitude (amp_x). The interpulson interval (I_{plx}) defines the interval between successive pulsons. Number of pulsons (N_{op}) refers to the number of pulsons within the burst. There are also two derived parameters that are useful for characterizing these waveforms: effective PW and burst duty cycle. These terms and definitions are based on those for the standard rectangular pulse.

The parameters, i.e. Nop , amp_x , pW_x , and IpI_x , can all be changed independently in a free-form manner that allows the creation of complex waveforms. To simplify experimentation and analysis, all pulsons in the burst can be set to be identical (e.g. $pW1 = pW2 = pW_x$). Even with identical pulsons, the stimulus waveform has many more degrees of freedom that can be manipulated. Please see Qing *et. al.*¹⁷⁴ for more details.

3.6 Methods for Characterizing Burst-Modulated Waveforms

3.6.1 Animals and Surgery

Several experiments were performed to test burst-modulated waveforms against rectangular pulse waveforms. The experiments involved electrical stimulation of the left vagus nerve in rats under anesthesia. All procedures were approved by the Institutional Animal Care and Use Committee (IACUC) and adhered to the guidelines set for in the *NIH Guide for the Care and Use of Laboratory Animals (Eighth Edition)*.

For each experiment, a female, Long-Evans rat (275-350g) was anesthetized with isoflurane (induction: 5% in 2L/min O₂; maintenance: 0.5- 2%). Butorphanol (1.5mg/kg per 4 hours of surgery) was injected subcutaneously for analgesia. A midline incision was then made in the ventral cervical region. By dissecting between the infrahyoid muscles and the sternocleidomastoid, the left carotid sheath was exposed. The left cervical vagus nerve is inside the sheath and was isolated from the carotid artery.

Two two-lead cuff electrodes were wrapped around the nerve, with the distal one for stimulation and the proximal for recording. The stimulating electrode was placed below the omohyoid muscle (which was kept intact), around C-6 vertebra level; the

recording electrode was placed above the omohyoid, slightly below the carotid bifurcation, around C-4 level. The typical electrode separation was 7.0mm (range 6.0-8.0mm, measuring error ± 0.25 mm).

Initially, the only rationale for having the stimulation electrode more distal/caudal and the recording electrode more proximal/rostral is so that the nerve response travelling to the brain is recorded. Because an action potential generated in the middle of an axon will conduct both ways, swapping the cuff positions yields the same result. However, because the vagus nerve may branch in the cervical region, stimulating the distal end will ensure that all stimulated axons are cuffed by the more proximal recording electrodes.

3.6.2 Custom Electrode Design and Fabrication

The electrodes were made in house with braided Pt10Ir microwires (an alloy with 90% platinum and 10% iridium), 0.006 inch total diameter (supplied by Fort Wayne Metals), and a silicone material for the cuff (see **Figure 10** for more details on the cuff). The microwires were only exposed inside the cuff, with an estimated contact area of 0.011cm^2 for each microwire. For each cuff, the microwires were spaced 1mm apart (center-to-center). The lead-to-lead impedance values of two of these electrodes were measured to be 0.95 and $0.98\text{k}\Omega$ at 1kHz, and the charge storage capacity values were 4.2 and $3.7\text{mC}/\text{cm}^2$.

These capacity values are rather high compared to what others reported³², the reason being that the geometric area was estimated without accounting for the braiding. Impedance spectroscopy and cyclic voltammetry measurements were performed in

phosphate buffered saline with a Gamry Reference 600, as detailed in a study by Ward *et al.*¹⁷⁵, except a 50mV/sec step was used instead of 1V/sec for cyclic voltammetry.

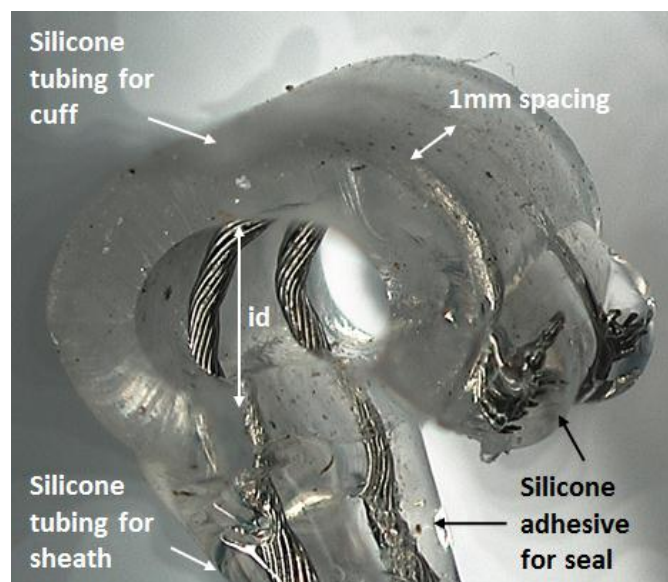


Figure 10 Cuff electrode for VNS experiments. The electrode leads are made of braided platinum-iridium microwires (90% Pt, 10% Ir) with total outer diameter of 0.006 inch. The cuff material is made with a silicone tubing with an inside diameter of 0.635mm (AM Systems 806700). The microwires are sheathed in silicone tubing (inner diameter, id = 0.304mm, AM Systems 806100). Exposed lead segments are threaded through the cuff, and then silicone adhesive (Nusil MED2-4420 or MED2-4213) is applied to seal the joints and insulate exposed lead segments outside the cuff lumen. The leads are spaced 1mm apart. Generally the cuffs are made such that the lumen opens up to allow the nerve to enter the lumen. The opening then can be closed by wrapping suture around the outside wall of the cuff, between the two leads. Reprinted © 2015 IEEE.

3.6.3 Experimental Setup

For each trial of stimulation, a 1-second train of 20 pulses or 20 pulson-bursts was delivered (VNS is commonly set to be 20Hz in both research and clinical settings^{136,141,148,162,176}), and the nerve response was recorded. All stimuli were charge-balanced, cathode-leading, alternating monophasic waveforms. The alternating

monophasic waveform, where the anodic charge-balancing phase was applied at half the period after the cathodic phase, allows artifact cancellation¹⁷⁷.

The stimulus waveforms were first generated using MATLAB. A data acquisition system (DAQ, National Instruments, USB-635x) converted the digital waveform into an analog voltage signal. A custom-made Howland current pump (with $\pm 10\text{V}$ power supply) then converted the voltage signal into a current waveform and passed the stimulus to the distal cuff. The nerve response at the proximal cuff was amplified and conditioned using a Grass P511 preamplifier, with 1Hz – 10kHz passband, 1000 – 2000x gain, and a 60Hz notch filter. Through the same DAQ, the conditioned signal was digitized initially at 50kHz. The sampling rate was lowered to 25kHz in later experiments, with no noticeable differences in signal quality. This experimental setup (see **Figure 11**) is modified from that in Ward *et. al.*¹⁷⁷.

3.6.4 Neural Activation Data Analysis

When the stimulus was above threshold, each pulson-burst with effective PW shorter than the refractory period elicited only a single compound nerve action potential (CNAP) (see **Figure 12**). In our experiments, the averaged CNAP signal typically consisted of two large, distinct peaks. The faster peak (conduction velocity falling in the range of 10-27m/s) was designated as the A fiber response, and the second, slower peak was designated as the C fiber response (range 2.5-3.3m/s, see **Table 1** and references^{145,148}). Conduction velocity was calculated by dividing the electrode separation distance by the peak latency^{145,154}. The height of each peak was designated as the response magnitude for the corresponding fiber groups. In some animals, the CNAP

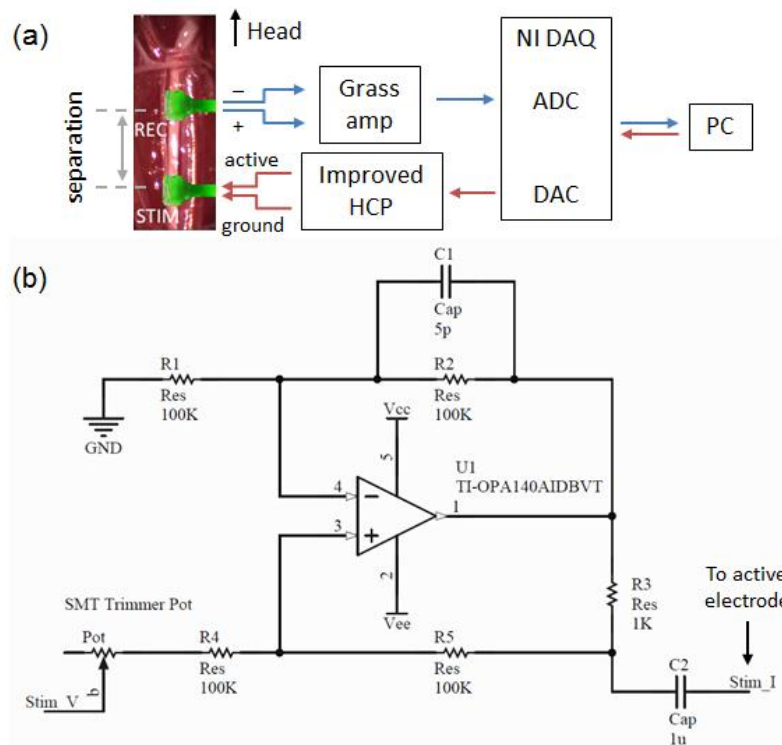


Figure 11 Instrumentation for VNS experiments. (a) Hardware setup for simultaneous left vagus nerve stimulation and recording. The stimulation cuff is distal to the head; the recording cuff is proximal. The more distal lead of the stimulation cuff is always grounded, while the more proximal lead is the active electrode. The active electrode is driven both cathodically and anodically during stimulation. The more distal lead of the recording cuff is always the positive differential input into the Grass amplifier, and the proximal lead is always the negative input. With this configuration, the stimulus artifacts for the cathodic and anodic phases are always equal and opposite in magnitude. During a trial, the computer (PC) software generates a digital waveform that is converted to an analog voltage waveform via the DAC on the National Instruments DAQ. The voltage waveform is then converted into a current waveform through the improved Howland current pump. At the start of the stimulus, the software also triggers the DAQ's ADC to sample the conditioned signal from the Grass amplifier. (b) Circuit schematic of the custom improved Howland current pump. The op amp OPA140 is powered by $\pm 10V$. Stim_V is the voltage waveform input, and Stim_I is the current waveform output, with R3 (1k Ω in this case) setting the gain. A blocking capacitor is placed at the output to prevent DC leak. The settling time for the pump is about 3 μ s when loaded with an electrode cuff and passing 1mA. Reprinted © 2015 IEEE.

peaks have a larger negative component, in which case the negative peak height is taken as the response magnitude. Other fiber populations and subpopulations did not produce prominent and consistent peaks and were excluded from analysis.

For each waveform, the fiber response magnitudes were measured at varying stimulus intensities (sample responses in **Figure 12**). For both A and C fibers, the relationships between the stimulus intensity and fiber response magnitudes were characterized using sigmoidal recruitment curves (see **Figure 13**, similar methods have been used elsewhere^{169,178}). The function used to model the sigmoidal recruitment curves is:

$$V(Q) = V_{\min} + \frac{V_{\max}}{1 + \exp[rate * (Q_{50} - Q)]}, \quad \text{Equation 5,}$$

where V , the response magnitude in μV , is a function of Q the stimulus charge per phase, with units in nC ; V_{\min} and V_{\max} are the asymptotes; Q_{50} is the charge per phase value at the inflection; and $rate$ is a constant that describes the steepness of the curve and relates to the rate of fiber recruitment. Curve fitting was done using MATLAB.

V_{\min} and V_{\max} correspond to the minimal and maximal response magnitude, respectively. Rather than assuming it is 0, V_{\min} is determined by delivering zero-amplitude stimuli. With no charge injection, the resulting nerve recording captures only noise and baseline nerve activity, and the root mean squared voltage (V_{rms}) of this recording is set to be the V_{\min} . For stimuli with non-zero amplitudes, CNAP peaks in the A and C fibers latency ranges that have peak heights lying outside the 95% confidence interval of the noise/baseline peak heights are considered above threshold. All sub-threshold CNAP peaks are set to be V_{\min} .

Response magnitudes were then normalized by first subtracting V_{\min} and then dividing by V_{\max} , yielding recruitment curves based on activation levels (illustrated in **Figure 13**). Fiber activation describes the fraction of maximal response of the fiber

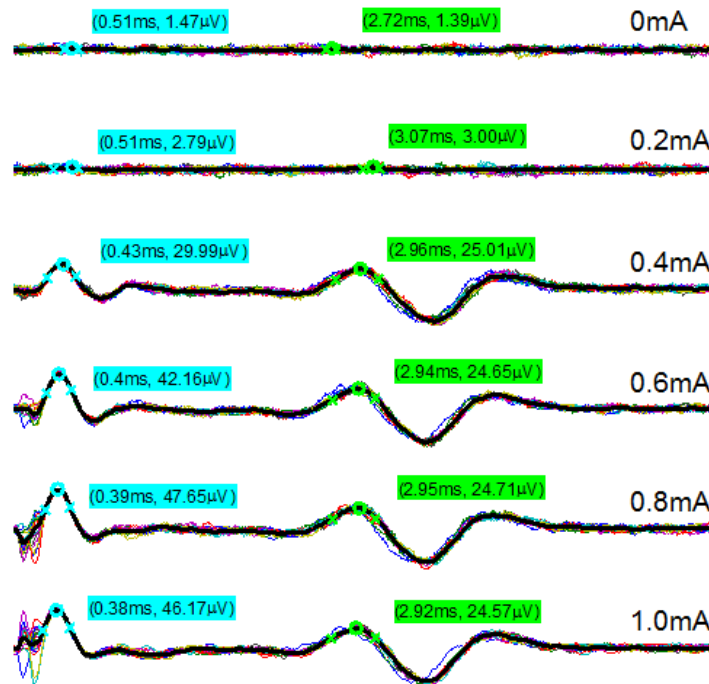


Figure 12 Example processed nerve responses during stimulation trials. The stimulus waveform (Nop 2, pWx 20 μ s, IpIx 80 μ s) was delivered at varying current amplitudes in random order. For each trial, a 1-second, 20Hz train was delivered. After the artifact was eliminated¹⁷⁷, the individual CNAP responses for each stimulus (thin traces) were averaged (thick trace, n=20 stimuli). All traces are shown from time 0 to 6ms. The top trace corresponds to an amplitude of 0, the bottom 1mA, and the traces in between are arranged in increments of 0.2mA. Peak latencies and heights (o's) and widths at half peak height (x's) were extracted from the averaged signal. Within each trial, the individual heights of the fiber peaks did not exhibit any order effect or deviation from a normal distribution, *e.g.* the peak height did not decrease with subsequent stimuli. The peaks labeled for the 0mA trial are due to noise and baseline activity. These peaks are not actual response peaks from the nerve and are ignored. Reprinted © 2015 IEEE.

population that is elicited by a stimulus, and using fiber activation instead of response magnitude accounts for variability in V_{\max} across animals.

There also seemed to be variability in V_{\max} across waveforms within the same animal, and the fiber recruitment models suggest that some waveforms were capable of reaching higher V_{\max} than that of the continuous pulse (as shown in **Figure 13**). As a result, magnitudes were all normalized to the V_{\max} of the continuous pulse. For example,

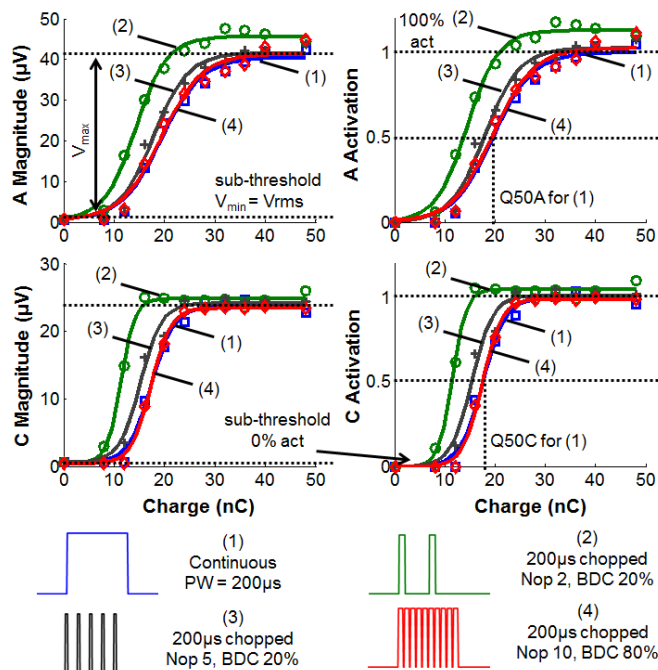


Figure 13 Fiber recruitment curves for selected pulse waveforms. Left plots, the response magnitudes for A and C fibers were extracted from CNAP responses and plotted against the stimulus charge per phase value. Each data point represents a single trial of 20 pulses/pulson-bursts. The data points follow a sigmoidal curve (R^2 generally > 0.9). All data shown are from the same nerve, same animal. V_{max} is the estimated maximal response achievable with a certain waveform and can differ with each waveform. Peak magnitudes from sub-threshold stimuli are assigned the V_{rms} of the noise floor. **Right plots**, response magnitudes are normalized to the V_{max} of the continuous pulse, after subtracting V_{rms} , for each respective fiber group. Q_{50} values are calculated from these normalized activation levels. The legend only shows the anodic phase of the waveform. All waveforms in the experiment are alternating monophasic. “Chopped” refers to a simple way to generate burst-modulated waveforms by dividing a rectangular pulse evenly with a certain burst duty cycle (BDC). Reprinted © 2015 IEEE.

the Q_{50} of a waveform is the charge required to activate 50% of the maximal response achievable with the continuous pulse.

The charge per phase values, rather than current amplitudes, is used to characterize stimulus intensities for recruitment curves. Amplitudes can be used to model recruitment curves as well, but when using waveforms with different pulse shapes or, in this case, burst-modulated waveforms, the amplitude is insufficient for describing the

pattern of charge injection. Moreover, the stimulus charge per phase is more closely tied to energy consumption and battery life in implants.

Because the fiber recruitment rates can differ, as can be seen in **Figure 13**, both the efficiency and selectivity of a waveform are dependent on the fiber activation level. For example, the waveform with the lowest Q_{50C} is the most efficient at activating C fibers to 50%, but it may not be the most efficient one at 75%. Fiber recruitment curves give a more complete representation of the nerve's response than strength-duration or charge-duration relationships. Recruitment curves can also describe strength-duration or charge-duration relationships (Mollet *et. al.*¹⁷⁸ demonstrated how fiber recruitment curves can be used to construct strength-duration curves).

Statistical analyses of nerve response data for comparing the waveforms were performed using SAS 9.3.

3.7 Differences between Pulse and Pulsons

To find the relationship between each burst modulation parameter and efficiency, different free-form waveforms at varying intensities were delivered in random order. Because the results from the chopped pulse experiments suggest that the 2-pulson/20 μ s pWx (chopping a 200 μ s pulse with 2 pulsons at 20% yields 20 μ s per pulson) combination behaves most differently from the continuous pulse, the 2-pulson/20 μ s pWx waveform was selected as the starting point. Fixing the Nop at 2, the pWx was set at 20, 30, and then 40 μ s. Then fixing the pWx at 20 μ s, the Nop was set at 2, 3, and 4. At each Nop-pWx combination, the IpIx was set to 0, 10, 20, 40, 100, and 200 μ s (note, waveforms with IpIx = 0 are equivalent to continuous pulse waveforms, where essentially, Nop = 1).

Pulson-bursts longer than 1ms (longer than the refractory period) are excluded from analysis because multiple action potentials were elicited (example in **Figure 14**).

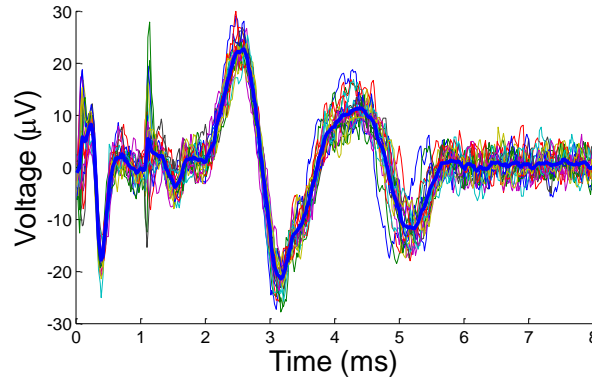


Figure 14 Example CNAP response for $I_{pIx} = 1\text{ms}$. The type of data is the same as shown in **Figure 12**. The waveform used was a 2-pulson burst with $pWx = 20\mu\text{s}$ and $I_{pIx} = 1\text{ms}$. For this particular trial, the stimulus artifacts were not cancelled completely. The sharp artifact near 0 and 1ms mark where the pulsons were delivered. Immediately following each artifact is an A fiber response, which is then followed by a second one smaller in magnitude than the first (due to the relative refractory period). The C fiber response peaks from the two pulsons overlap with each other. Reprinted © 2015 IEEE.

The Q_{50A} and Q_{50C} for all waveforms and animals are summarized in **Figure 15**.

To assess how burst modulation parameters affect efficiency, the effects of Nop , pWx , and I_{pIx} on Q_{50A} and Q_{50C} are tested using multiple linear regression, in the form:

$$Q_{50} = \beta_{Nop}Nop + \beta_{pWx}pWx + \beta_{IpIx}IpIx + \delta_{animal}D_{animal} + \varepsilon$$

Equation 6

where Q_{50} (Q_{50A} or Q_{50C}) is the response variable; Nop , pWx , and I_{pIx} are the predictors, with their corresponding β 's being the regression coefficients; D_{animal} is the dummy variable matrix for the animals, and δ_{animal} is the corresponding coefficients; and ε is the error term. Regression analysis establishes a quantitative relationship between each burst modulation parameter and fiber recruitment characteristics, allowing prediction and interpolation of fiber recruitment based on a continuum of parameter values.

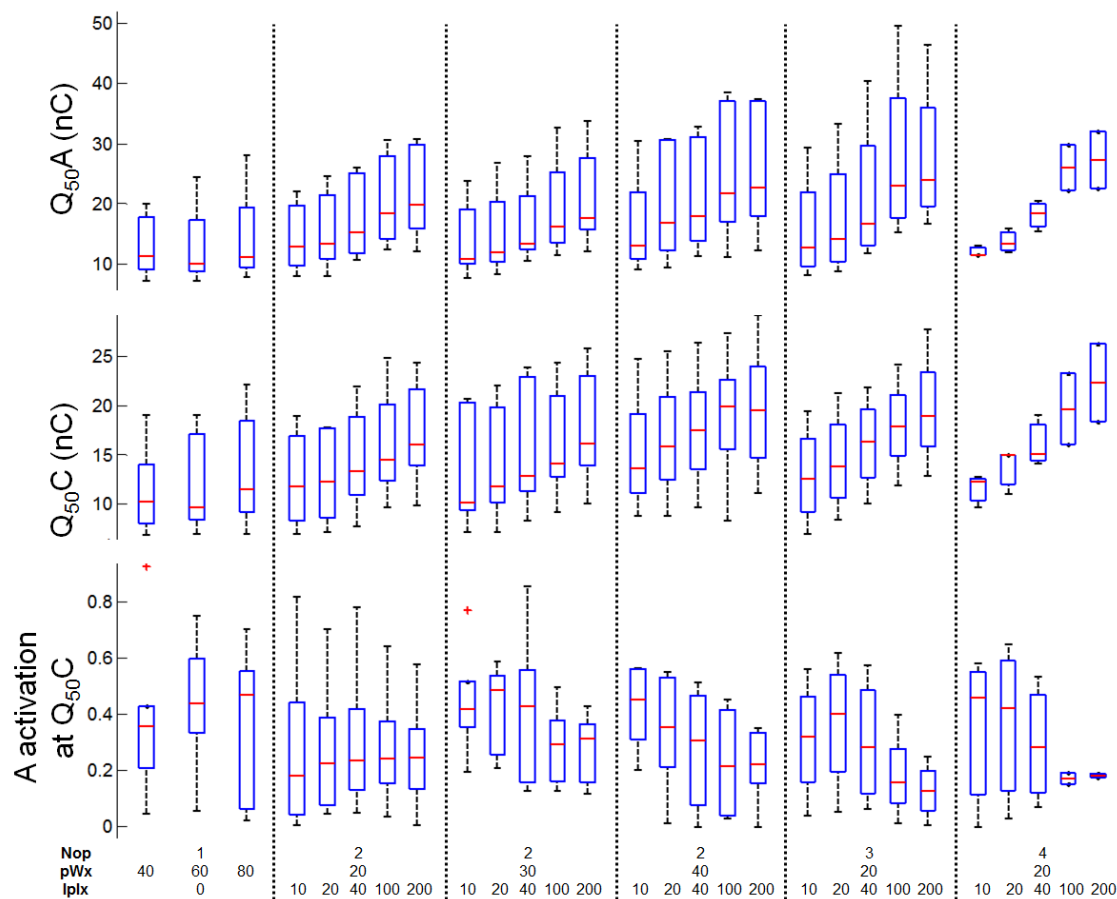


Figure 15 Q_{50A} , Q_{50C} , and level of A fiber activation at Q_{50C} for all waveforms. Q_{50} values and A fiber activation levels were calculated from recruitment curves for both A and C fibers. The Nop, pWx, and IpIx parameters are annotated below the box and whiskers, the units for pWx and IpIx being μs . Waveforms with IpIx = 0 were treated as continuous waveforms with PW equal the report Nop multiplied by the pWx. $n = 3-6$ animals for each waveform (low variability for some waveforms is due to having $n = 3$ animals). Note, data distribution is not always normal. Reprinted © 2015 IEEE.

The regression results (**Table 3** & **Table 4**) suggest that both Q_{50A} and Q_{50C} increase with increasing Nop, pWx, and IpIx (the p-values for all three coefficients were < 0.0001 for Q_{50A} and Q_{50C} ; residual diagnostics confirmed the regression assumptions). That is, the charge per phase required to reach 50% A and C fiber activation increases with increasing Nop, pWx, and IpIx. Among these three parameters, Nop had the most effect on Q_{50} , followed by pWx and then IpIx.

Table 3. SAS output for multiple regression of Q_{50A} and burst modulation parameters

Variable	DF	Parameter Estimate	Standard Error	t Value	Pr > t (p-value)
Intercept	1	-3.11132	1.61212	-1.93	0.0558
Nop	1	4.51615	0.42546	10.61	<.0001
pWx	1	0.12007	0.02056	5.84	<.0001
IpIx	1	0.04587	0.00363	12.65	<.0001
R91dummy*	1	18.71064	0.87672	21.34	<.0001
R93dummy	1	15.79666	0.87055	18.15	<.0001
R94dummy	1	-2.88756	0.74810	-3.86	0.0002
R97dummy	1	1.76400	0.74810	2.36	0.0198
R101dummy	1	7.60904	0.87055	8.74	<.0001

* The dummy denotes the variables of the dummy matrix. P-value for dummy variables simply signify that activation profiles differ among the animals. Reprinted © 2015 IEEE.

Table 4. SAS output table for multiple regression of Q_{50C}

Variable	DF	Parameter Estimate	Standard Error	t Value	Pr > t (p-value)
Intercept	1	0.56723	1.06815	0.53	0.5963
Nop	1	3.42476	0.28190	12.15	<.0001
pWx	1	0.09858	0.01362	7.24	<.0001
IpIx	1	0.02722	0.00240	11.33	<.0001
R91dummy	1	6.68427	0.58089	11.51	<.0001
R93dummy	1	10.12777	0.57680	17.56	<.0001
R94dummy	1	-3.86533	0.49567	-7.80	<.0001
R97dummy	1	0.65962	0.49567	1.33	0.1856
R101dummy	1	8.46077	0.57680	14.67	<.0001

Reprinted © 2015 IEEE.

The estimated A fiber activation at Q_{50C} was used to compare fiber selectivity among various waveforms and across animals. With the recruitment curves for both A

and C fibers, it is possible to interpolate A and C fiber activation based on a chosen stimulus intensity. This intensity could be some arbitrary value, *e.g.* 20nC, or it could be more empirically chosen and based on the recruitment curves, such as Q_{50} . When stimulating the nerve at $Q_{50}C$, the expected C fiber activation would always be 50% with minor variability regardless of waveform, but the A fiber response may differ significantly with waveform. In addition, the $Q_{50}C$ value may differ with waveform due to differences in efficiency.

Using the recruitment curves derived from the parametric analysis, the level of A fiber activation at $Q_{50}C$ for all waveforms are calculated (plotted in **Figure 15**). The effects of Nop, pWx, and IpIx on the A fiber activation are then tested using, again, multiple linear regression, by using the same regression model as described in **Equation 6**, except the Q_{50} term is replaced with A fiber activation at $Q_{50}C$.

The regression results (see **Table 5**) show that, while maintaining 50% C fiber activation, only changing the IpIx has an effect on the level of A fiber activation. For all animals, increasing the IpIx is correlated with a decrease in A fiber activation ($p < 0.0001$ for IpIx; $p = 0.2019$ for Nop; and $p = 0.8176$ for pWx; residual diagnostics confirmed the regression assumptions). Though Nop and pWx do not seem to affect selectivity directly, there may be significant interaction effects.

As an example, **Figure 16** demonstrates the effect of varying only IpIx on the CNAP response. As IpIx increases, the activation levels for both A and C fibers decrease, consistent with the efficiency regression results. And interestingly, with each increase in IpIx, A fiber activation decreases more than C fiber activation, which suggests that the stimulus is becoming more selective for C fibers.

Table 5. SAS output table for multiple regression of A fiber activation at Q₅₀C.

Variable	DF	Parameter Estimate	Standard Error	t Value	Pr > t (p-value)
Intercept*	1	0.56486	0.06959	8.12	<.0001
Nop	1	-0.02355	0.01836	-1.28	0.2019
pWx	1	-0.00021	0.00089	-0.23	0.8176
IpIx	1	-0.00072	0.00016	-4.61	<.0001
R91dummy	1	-0.43002	0.03784	-11.36	<.0001
R93dummy	1	-0.29535	0.03758	-7.86	<.0001
R94dummy	1	-0.24608	0.03229	-7.62	<.0001
R97dummy	1	-0.10110	0.03229	-3.13	0.0021
R101dummy	1	0.10665	0.03758	2.84	0.0053

* The A fiber activation at Q₅₀C should be non-zero. Reprinted © 2015 IEEE.

The results from comparing different burst-modulated waveforms and rectangular pulse waveforms suggest that waveforms with short duration of charge injection (short PW or short pWx) were more charge efficient, requiring less charge to reach 50% fiber activation. This observation is consistent with modeled and empirical charge-duration relationships in literature, which all show increasing threshold charge with increasing PW in an almost linear manner (Weiss's formula)^{33,47,48,50,67}.

The results also suggest that waveforms without IpIx were more A-selective. The fiber recruitment profiles show that intervals added during a pulse, *i.e.* inter-pulson intervals, can decrease A fiber activation. This observation is also consistent with the established notions that 1) short-PW stimuli yield lower thresholds for fibers with larger diameters^{24,58,151}, and 2) sensory fibers and slow-conducting fibers have longer strength-duration time constants—longer chronaxie^{50,153,154}.

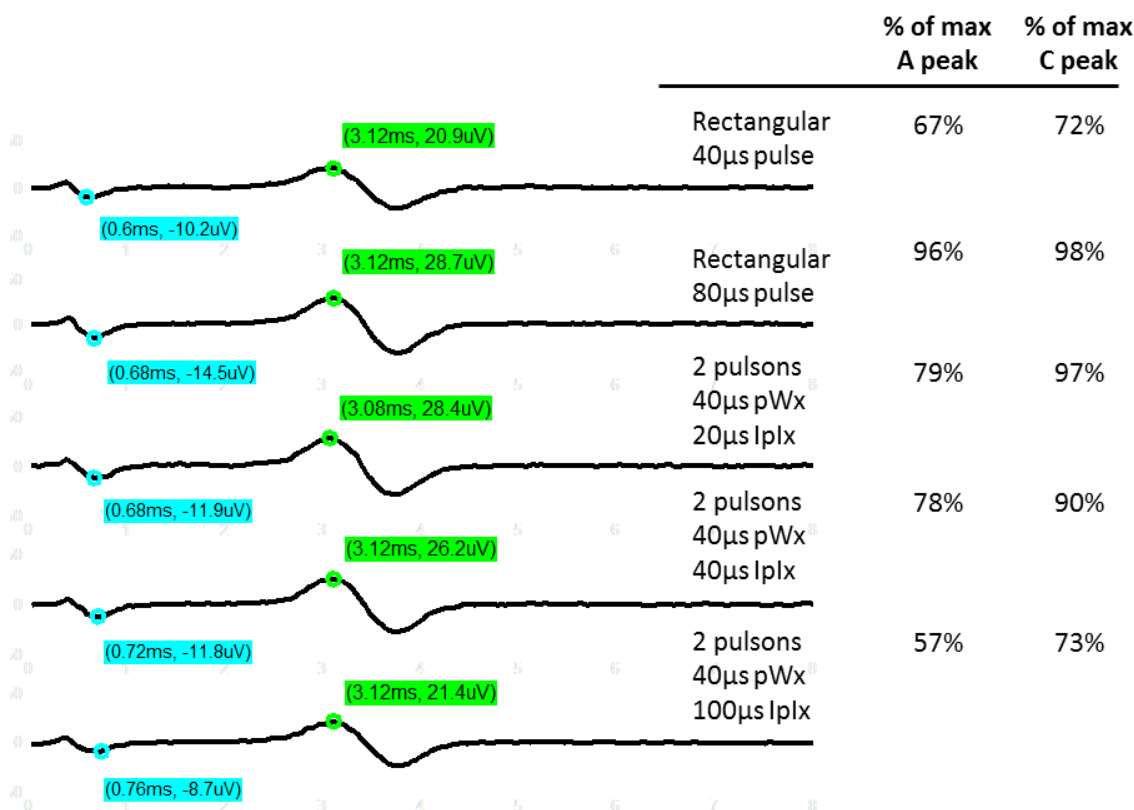


Figure 16 CNAP responses to burst-modulated waveforms. A and C fiber activation are compared for various waveforms, annotated in figure. The repetition frequency for all waveforms was 20Hz, train duration was 1 second ($n=20$ stimuli per trace), and current amplitude was 0.24mA. For simplicity, only the averaged trace is plotted. At the same amplitude, the A and C fiber response magnitudes to a single pulse of 40µs are the lowest. With 2 pulsons and $IpIx = 0$ (80µs pulse), the magnitudes are highest. As the $IpIx$ increases in duration, both A and C fiber responses decrease, and A fiber magnitude decreases more than the C fiber magnitude. Note: when the A fiber response contains a notably larger negative deflection, the case for this animal, the negative deflection was used as the peak magnitude. Reprinted © 2015 IEEE.

Regression analysis aside, the lowest Q_{50C} in the data set shown in **Figure 15** was 11.49nC (mean of $n=6$ animals), which resulted from the single 40µs pulse. This observation reiterates that short pulses are the most efficient. For this efficient, single 40µs pulse, A fiber activation was 38.7% (mean of $n = 6$) at Q_{50C} . In contrast, at Q_{50C} , the lowest A fiber activation level for burst-modulated waveforms was just 12.8% (mean of $n=4$ animals), which was from a 3-pulson waveform with pWx of 20µs and a long $IpIx$

of 200 μ s. The lowest A fiber activation when using single rectangular pulse waveforms was 35.0% (mean of $n = 6$ animals). So overall, the single rectangular pulse waveforms are not as selective for C fibers.

However, the 3-pulson waveform, though more selective for C fibers, was not as efficient, with $Q_{50C} = 19.6\text{nC}$. The most C-selective rectangular pulse waveform was the 80 μ s pulse waveform, with $Q_{50C} = 13.2\text{nC}$ and 35.0% A fiber activation. These results are all consistent with the regression analysis: a short pulse with no I_{pIx} is efficient, but a pulson-burst with long I_{pIx} tends to be more selective for C fibers.

3.8 Proposed Mechanism of Action for Burst-Modulated Waveforms

As long as the entire burst duration is shorter in duration than the refractory period, each pulson-burst can only elicit a single action potential and behaves like a single continuous pulse. This method of supra-refractory charge delivery creates a charge buildup at the axon membrane in a manner not unlike temporal summation at the synapse. With the first pulson, fibers that depolarize beyond the threshold membrane voltage will fire action potentials, and these fibers will be in the refractory period. When the next pulson is delivered, the refractory fibers cannot respond, but a portion of fibers that did not activate during the first pulson will fire. The same will be true for subsequent pulsions.

For the fibers that have not fired, because they were partially depolarized by previous pulsions, these fibers are in a state of decreased excitability. The partial depolarization causes the inactivation gates of the voltage-gated sodium channels to close, so that further depolarization results in activation of fewer fibers. Because A fibers are more readily depolarized by shorter pulses^{58,152}, the sub-threshold pulsions should affect A

fiber excitability more, which would explain the lower A activation produced by pulson-bursts. The mechanism is similar to that for the pre-pulse introduced by Grill & Mortimer^{97,150}. The major difference between pulsions and prepulses is that, unlike prepulses, pulsions do not need to be subthreshold, so each pulson can contribute to nerve activation in addition to conditioning the nerve.

The higher charge efficiency is due to the fact that the stimulus charge is delivered as narrow pulsions (microseconds to tens of microseconds). Because pulsions are generally much shorter than a rectangular pulse, at the same charge level, the pulsions are much higher in amplitude. Therefore, consistent with the principle that short PW pulses are more efficient^{33,47,48,50,67}, each pulson is highly effective at activating nerve fibers.

Though not included in the experiments presented earlier, each pulson in the burst can have different parameters (*e.g.* $pW1 \neq pW2$), creating complex patterns of charge injection that may be used to further improve efficiency and selectivity. For example, by using hyperpolarizing pulsions before depolarizing pulsions, it may even be possible to increase A fiber selectivity by similar mechanisms proposed by Grill & Mortimer^{97,150}.

3.9 Implementation of Burst-Modulated Waveforms

Burst modulation provides more control over the stimulus waveform by introducing a different set of parameters. The larger parameter space is useful for fine-tuning the tissue response, but it also makes parameter selection more difficult. For rectangular pulse waveforms, there are only two parameters—PW and AMP. In contrast, for burst-modulated waveforms, there are four—Nop, pWx, IpIx, and ampx. In the experiments so far, representative parameter sets were chosen, *e.g.* few versus many Nop,

long versus short pWx or IpIx. The parameters are then randomly combined to create various stimulus waveforms. This type of parametric sweep is a rather brute-force approach, but it does quickly yield recruitment profiles useful for comparing different waveforms. This parametric sweep process is also subject-specific and can serve as a calibration procedure.

After the parametric sweep, instead of using regression to find the relationship between the stimulus and the nerve response for a population of subjects (see *Equation 6*), analysis can be focused on the individual subject to profile the neural response for the parameters. The stimulus-response relationship then can be used to predict the individual subject's response profile for the entire parameters space. This profile can also be updated with future stimulation trials and parametric sweeps to improve its prediction accuracy and to allow it to adapt to changes over time.

In addition to improving efficiency of fiber recruitment, another advantage of burst-modulated waveforms is that the on-off nature of the waveform is easy to implement in implantable stimulators. It is more difficult, as well as more processing intensive, to generate the more complex waveforms, such as trapezoidal, step-functions, and sinusoidal pulses. For example, by using one additional switch, the processor unit of the implant would be able to generate pulson-bursts instead of standard rectangular pulses. In fact, there are existing systems capable of generating burst-modulated waveforms¹⁷⁹.

3.10 Conclusion

In the experiments described in this chapter, each animal responded differently to the same stimulus, and more generally, nerve activation profiles differed among subjects

(even after normalizing the response magnitudes, high variability is apparent in **Figure 15** and the regression results). In the clinic, patients are likely to exhibit different nerve response as well, even though the implant, the surgery, and the stimulus, in addition to other factors, are controlled carefully. The variability in the nerve response is a likely contributor to the variability of the effectiveness in patients.

By adding a set of recording electrodes, the nerve's response to the stimulus can be characterized in an objective manner. This objective response monitoring is the essence of ANC. Combining the response feedback of ANC with the systematic method of designing and analyzing burst-modulated waveforms, the nerve's response profile to different waveforms can be quickly captured. With those response profiles, the stimulus can be adjusted to create the optimal nerve response profiles.

A VNS system with ANC and burst modulation integrated can be used for studying the mechanism of VNS, pinpointing the fiber group(s) involved. At the same time, if the target fiber group(s) is known, the same system will enable optimization of stimulus selectivity and/or efficiency for each subject, boosting efficacy while reducing side effects and complications.

3.11 Notes

With permission from IEEE TNSRE, some portions of the texts and several figures in this chapter were reproduced and adapted from the manuscript Qing *et. al.*¹⁷⁴, © 2015 IEEE, which contains my original work. The manuscript contains a thorough study of burst modulation on vagus nerve activation and has been accepted for publication.

CHAPTER 4. ACTIVATION CONTROLLED VNS

4.1 Introduction to Activation Control

CHAPTER 3 presented a new method of achieving higher fiber selectivity with electrical nerve stimulation. The foundation this new method is built on a new paradigm of neurostimulation that will be referred to as activation control. Currently, neural stimulation (be it in the brain, spinal cord, or peripheral nerves) is performed in an open-loop fashion, where the neural response to stimulation (even when recorded¹⁸⁰) is usually ignored, and the physiological effects of stimulation is correlated directly to the stimulus. This standard stimulation paradigm will be referred to as stimulus control.

In contrast, activation control involves correlating the physiological effect to the neural tissue response, not the stimulus. In the brain, the response could take the form of spike activity or evoked potentials, and in nerves, the response would be CNAP. The same stimulus does not create the same response in subjects; the same stimulus may not even create the same response in the same subject at all times. Mapping the stimulus to the response will eliminate many factors that can lead to variability, such as electrode properties, discrepancies due to surgery, biological differences, and changes over time. Activation control, then, produces much stronger, reliable correlations. After all, when a neuron is stimulated, it is the resulting action potentials travelling toward the synapse that cause a specific effect, not the exact nature of the stimulus.

In CHAPTER 2, the brain response data to DBS were lacking, and so setting the parameters was arbitrary. This stimulus control paradigm is rather hit or miss. That the 200 μ A group experienced a sustained reduction in alcohol intake involved a bit of luck. The VNS experiments in CHAPTER 3 were comprised of building quantitative relationships between the stimulus and the nerve response, and this chapter will demonstrate how the nerve response affects physiology.

In the case of the vagus nerve, stimulation of the A (mostly motor efferent) and B (mostly parasympathetic) fibers causes obvious physiological effects (discussed in Chapter 1). Of all the various function of the vagus nerve, its effects on the heart are perhaps the best characterized and have the most clinical significance. The experiments summarized in this chapter involve activation-controlled stimulation of the vagus nerve. These experiments aim to demonstrate that the cardiac effect of VNS can be better correlated to the nerve response rather than the stimulus parameters. The results have important implications for the delivery of VNS in patients with epilepsy as well as patients with cardiovascular disease.

4.2 Vagus Nerve and Heart Disease

The effects of vagus nerve on the heart have been studied for a long time, dating as far back as the late 1800s¹⁸¹. And unlike the antiepileptic effects of VNS, the major autonomic functions of the vagus nerve have been well characterized. As mentioned in Section 3.3, the parasympathetic efferents of the right vagus nerve mostly decrease heart rate and contractile force, and those of the left vagus nerve mostly decrease nodal conduction^{156–158}. The left vagus nerve, when stimulated within safe limits, has less of an

impact on the heart, which is why VNS implants for epilepsy only stimulate the left vagus. However, researchers are now attempting to harness the cardiac effects of VNS and have begun experimenting with using VNS to treat cardiac disease. This time, the parasympathetic fibers of the right vagus nerve are the target.

Heart failure is a very common condition with high morbidity and mortality. In the US alone, the incidence is 550,000 patients per year, and the prevalence is 5 million. A chronic, incurable condition, heart failure requires billions of dollars to treat annually and results in high numbers of hospitalizations. More than 50,000 patients die each year from heart failure, and due to an aging population, these figures are expected to increase over time¹⁸².

Once the heart cannot adequately provide sufficient output, commonly due to myocardial infarction and scar formation, the autonomic tone of the body shifts to sympathetic overdrive. Sustained sympathetic dominance, which can manifest as increased resting heart rate, higher blood pressure, etc., increases the workload and energy demands of the heart, which is in turn damaging to the heart and leads to a downward spiral of cardiac function loss¹⁸².

The standard treatment for heart failure is using pharmaceuticals such as beta-adrenergic receptor blockers to block the sympathetic system, in addition to using inhibitors of the renin-angiotensin-aldosterone system, which help to decrease blood pressure and prevent deleterious cardiac tissue remodeling¹⁸². The standard treatment, however, has limited effectiveness, and mortality is rising even though treatments are becoming more advanced¹⁸². Since restoring autonomic balance is important, as increased

sympathetic activity and reduced vagal activity are associated with higher morbidity and mortality, VNS offers a unique potential solution for achieving that balance¹⁸³⁻¹⁸⁷.

4.3 Epilepsy, Vagus Nerve, and Heart Disease

Aside from its antiepileptic effects, VNS as of late has shown promise for treating epilepsy in a way very similar to its investigative use in heart failure. Epilepsy is a serious condition that, in addition to seizures, manifests with a wide range of systemic effects. Not as prevalent as heart failure, epilepsy nonetheless afflicts as many as 1% of the population¹⁸⁸, and mortality in patients with epilepsy is 1.3 to 9.3 times higher than the general population¹⁸⁹. Though most patients with epilepsy die of causes not directly linked to seizures, such as brain tumors, infections, and suicide, sudden unexpected death in epilepsy (SUDEP) accounts for a significant, increasing (increasing because diagnosis of SUDEP has improved) amount of deaths due to seizures^{188,190-192}. Moreover, patients with more severe and/or treatment-resistant epilepsy are more likely to encounter SUDEP, and SUDEP rates are particularly high in the younger population¹⁹¹⁻¹⁹³.

SUDEP is a fatal event, the only effective treatment being resuscitation.

Monitoring for seizures and cardiac arrest are helpful for detecting and perhaps predicting SUDEP, which can aid resuscitation efforts. The key to reducing SUDEP incidence lies in prevention. Adequate antiepileptic treatment with proper seizure control will effectively reduce the likelihood of SUDEP, as SUDEP risk increases with frequency and severity of seizures¹⁹¹⁻¹⁹³. In this manner, VNS helps to reduce SUDEP. Recently, a new potential pathway for VNS therapy to reduce the risk of SUDEP has emerged.

Evidence gathered over decades suggests that patients who died of SUDEP tend to have heart disease. Autopsy of patients who succumbed to SUDEP consistently revealed enlargement and edema of heart, lungs, and liver¹⁹⁴, all signs of congestive heart failure. In addition, autopsy results showed signs of heart disease, including atherosclerosis and most importantly, myocardial fibrosis^{195–197}. In addition, for patients <65 years of age living with epilepsy, the risk of dying from heart disease is significantly higher than the general population¹⁹⁸. Overall, in patients with epilepsy, incidence of myocardial infarction and sudden death are significantly higher as well, so is mortality from ischemic heart disease¹⁹⁸.

Considering that patients with epilepsy and patients who die from SUDEP tend to be younger than those in the general population who develop heart disease, the cardiac findings are all suggestive of repeated cardiac insults linked to epilepsy. During seizures, patients can experience various cardiorespiratory abnormalities, including tachycardia, bradycardia, even arrhythmias, signs of ischemia, even asystole and apnea^{199–203}, all of which can contribute to deterioration of cardiac function.

In fact, patients living with epilepsy do show signs of cardiac dysfunction and disease. Resting heart rate tend to be higher among patients with epilepsy, and interestingly, patients who are at higher risk of SUDEP had higher heart rate and more ECG abnormalities²⁰⁴. Much like patients suffering from heart failure, patients with epilepsy have autonomic dysfunction; more specifically, they also suffer from sympathetic dominance and decreased vagal activity^{201,205,206}.

4.4 VNS for Treating Autonomic Dysfunction

For patients with epilepsy, controlling seizures is top priority, because patients who respond to treatment and have fewer, less severe seizures tend to have lower mortality and fewer complications. For treatment-resistant patients, in the past few decades, VNS has served a relatively effective supplemental therapy. In treating epilepsy, VNS has been limited to the left vagus nerve to avoid harmful cardiac effects. With the connection between epilepsy and heart disease becoming ever stronger, particularly in the case of SUDEP, stimulation of the right vagus nerve is beginning to gather attention²⁰⁷.

Now, right-side VNS is being investigated to directly affect the heart, to protect it from heart failure and seizures. Clinical studies studying the efficacy of right-side VNS in treating patients with heart failure have produced promising results^{183,184,208}. There is also currently a large clinical study being performed to assess the direct link between restoring autonomic tone with VNS and treating heart failure²⁰⁹. In 2014, Schomer *et. al.* reported a clinical study that directly aimed to reduce interictal cardiac instability in patients with drug-resistant epilepsy by stimulating the right vagus nerve²⁰⁷. Right-side VNS in this study, in addition to reducing seizure activity, was able to improve vagal tone.

The common rationale behind VNS for heart failure and epilepsy is to restore autonomic balance by increasing parasympathetic vagal activity. In two of the heart failure studies^{183,184}, patients undergoing VNS exhibited improvements in physiological and clinical indicators, such as lower resting heart rate and higher ejection fraction, as well as in the reported quality of life. In the third, a more recent study²⁰⁸, patients reported better quality of life, though VNS did not seem to improve heart failure

progression as compared to control. Two of the heart failure studies^{184,208} reported that chronic VNS seemed to have led to improvement of parasympathetic tone.

In all these studies, the method for determining the stimulus parameters was the same as that used in standard VNS practice. That is, parameter adjustment is based on patient perception and physician's intuition. As a result, even though parameters are adjusted on an individual basis, even if the clinical response is used as a feedback, patient response is highly variable. In the 2008 Schwartz *et. al.* study¹⁸³, of the 8 total patients undergoing VNS, 4 experienced continuing heart function improvement, but 3 received temporary improvement followed by deterioration, and 1 showed no improvement and only deterioration for the 6-month study duration. In the 2011 De Ferrari *et. al.* study¹⁸⁴ and the 2015 Zannad *et. al.* study²⁰⁸, 59% and 62% of patients showed improvement, respectively. In the Schomer *et. al.* study²⁰⁷ as well, the improvement of vagal tone is highly variable.

Another important consideration in right-side VNS is that the side effects can be much more serious. The De Ferrari *et. al.* study¹⁸⁴ reported serious events that are likely linked to the stimulus, including atrial fibrillation, hypotension, and syncope. Other side effects (such as cough, dysphonia, and pain) and surgery- or device-related complications (such as infections and lead failure) are similar to left-side VNS. And again, the biggest impact of side effects is that they limit the stimulus intensity.

4.5 The Benefits of Activation Control

The key theory of activation control is that the physiological effect of neurostimulation is dependent not on the exact stimulus but rather on the neural response.

More specifically, the same stimulus can produce different neural responses in different subjects, and the same stimulus delivered at different times can even produce different responses in the same subject. Conversely, if different stimuli can elicit the exact same neural response, the activated axons will lead to the same physiological effect, regardless of stimulus pulse shape, amplitude, etc. (although, the frequency and the stimulation duration do matter^{102,141,210}).

In VNS, the activation pattern of the nerve, which manifests as a CNAP, determines the effect of stimulation. As discussed in Section 3.3, A fiber activation would lead to mostly motor contractions, and B fiber activation would lead to parasympathetic effects. Accordingly, activation of both A and B fibers will lead to a combination of motor contractions and parasympathetic effects. The effects of C fiber activation are less clear, however.

In the clinical heart failure studies^{183,184}, the experimenters reported that, when setting the stimulation parameters, a reduction in heart rate linked to the stimulation is considered therapeutic. However, the stimulus did not cause heart rate reduction in all patients; it was successful in 3 out of 8 patients¹⁸³ and only 3 out of 32 patients¹⁸⁴. The two main reasons were 1) causing intolerable side effects and 2) reaching the stimulus intensity limit, which seemed to have been set arbitrarily at pulse width of 1ms and current amplitude of 5.5mA (perhaps set by device limits).

It seemed that the investigators did not intentionally aim to activate enough B fibers to cause a heart rate reduction. And much like the mechanism for epilepsy, the exact mechanism of VNS for heart protection is yet unknown. Dosing by the stimulus

intensity is an inexact method that introduces high variability, and this way, it is difficult to determine which fiber group(s) is responsible for the therapeutic effects.

By using the level of neural activation instead of stimulus parameters as the method of dosing, the physiological response can be controlled more accurately and more precisely. The benefits of this activation-controlled over the standard stimulus-controlled stimulation are that:

1. the activation level is known, allowing accurate assessment of the strength of the stimulus and lowering the likelihood of under- or over-stimulation;
2. the nerve response can be matched to the therapeutic and side effects, to determine exact relationships;
3. the stimulation produces more consistent responses, resulting in lower variability and higher response rate; and
4. different waveforms can be used to elicit different activation patterns for targeted activation, so as to boost efficacy while reducing side effects.

4.6 Methods for Testing Activation Control

To demonstrate the benefits of activation control, similar VNS experiments as those described in Section 3.6 were conducted. The experimental setup was essentially the same as that shown in **Figure 11**, except a few differences. First, there was an additional goal of altering cardiac function, so the right vagus nerve was the target. The expected effect of right-side VNS was to decrease the heart rate, and so the decrease in heart rate served as the physiological response. To measure the heart rate, a two-lead surface ECG recording was added, in parallel to the vagus nerve recording. In fact, the

left-side VNS experiments all included an ECG recording as well, but there were no notable effects due to the stimulation, so the recordings were not analyzed in detail. See **Figure 17** for a photograph that shows the electrode cuffs wrapped around the vagus nerve and ECG electrodes attached. Settings for signal conditioning and acquisition were the same as described in Subsection 3.6.3.

The stimulus frequency remained at 20Hz, and the stimuli were still charge-balanced, cathode-leading, alternating monophasic waveforms. Unlike before, train duration was 10 seconds, because others have found that the heart rate requires several seconds to stabilize during VNS^{211,212}. Other train durations (e.g. 5 seconds, 20 seconds) were tested as well, and 10 seconds seemed to be a good balance between capturing the full effect and maximizing throughput. Some lower stimulus frequency (e.g. 10Hz, 5Hz)



Figure 17 Animal with nerve cuffs and ECG electrodes attached. Animal is under isoflurane. The electrode cuffs are wrapped around the isolated vagus nerve. The distal cuff is for stimulation, and the proximal is for recording. The ECG leads are arranged in lead II configuration, with the positive lead being near the apex of the heart. The cuffs are an earlier version of the one shown in **Figure 10**. The insulation material for these cuffs happens to be PTFE (black), not silicone. The photograph shows the left vagus cuffed.

trials were performed as well, and the only difference was that the heart rate change was smaller and took longer to manifest, simply because fewer stimuli were delivered in the same amount of time. Therefore, most of the data were collected at 20Hz. Again, different waveforms and current amplitudes were applied in random order.

4.7 ECG Data Analysis

The nerve signal and CNAP were processed in the same way as described in Section 3.6.4. The heart rate, unlike for the left-side VNS experiments, was more important, and so the ECG signal was more carefully processed to ensure that the heart rate is extracted properly. The ANC system¹³³ contains algorithm for heart rate extraction, and methods detailed in this section are modified from that existing code. **Figure 18** illustrates key steps in heart rate extraction. ECG and nerve data processing was performed using MATLAB.

First, stimulus artifacts were removed using a smooth function. Setting the number of points to smooth to 500 generally was sufficient to remove most of the artifact. This method of artifact removal is simple and fast, but it does distort the waveform and is only appropriate for determining the heart rate. Next, the smoothed ECG was normalized by the maximum voltage value, and the R peaks were extracted in the same manner as in ANC¹³³. The intervals between successive R peaks were calculated and converted to instantaneous heart rate in beats per minute (bpm). During data analysis, the R peaks were overlaid on the processed ECG signal and checked manually to ensure proper R peak identification. See **Figure 18** for the results from each step of the processing.

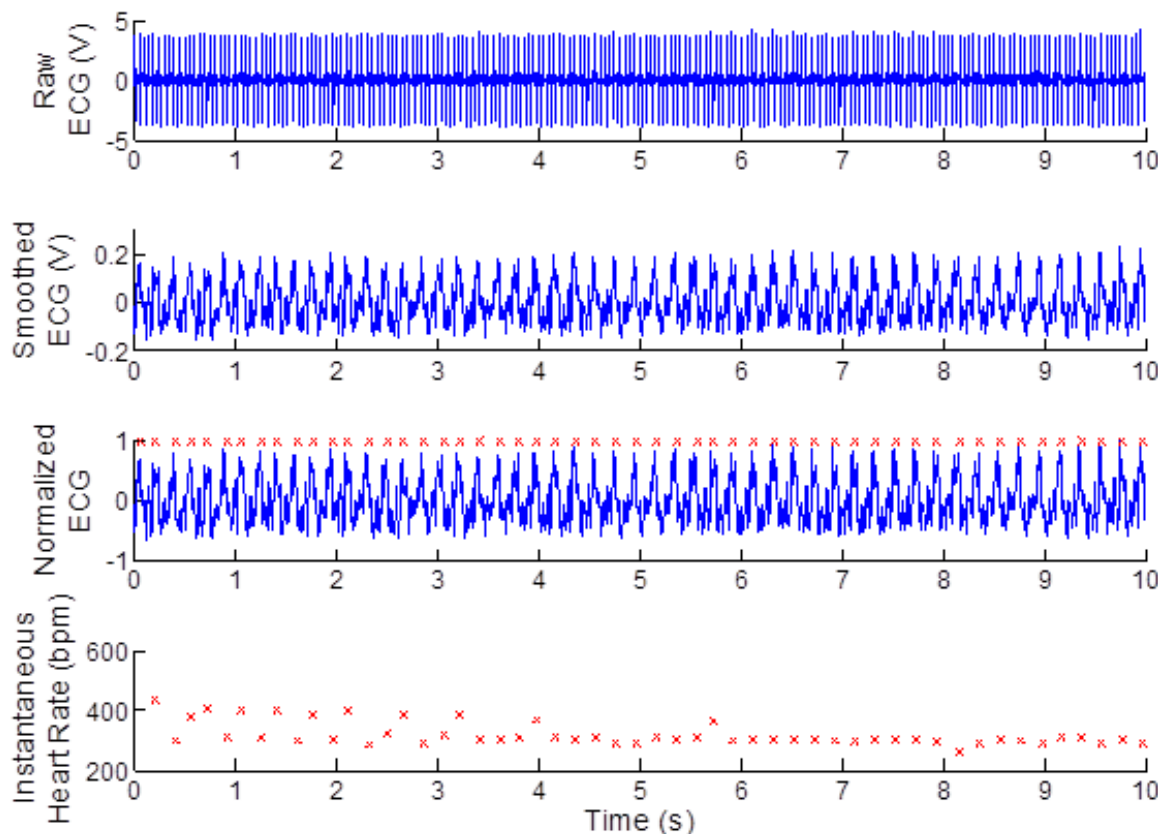


Figure 18 ECG data analysis. The 10-second raw ECG signal contains large stimulus artifacts. The artifacts are easily removed by smoothing, though the ECG waveform is deformed as well. The smoothing does not affect detection of R peaks, which remains the prominent feature in the recording (denoted by red x's above each peak). Each ECG trace and the identified R peaks are visualized and checked for accuracy. The instantaneous heart rate can be calculated from the intervals between the R peaks. In this example, there is a notable effect due to stimulation.

4.8 The Effects of Stimulus Parameters on the Vagal Response and Heart Rate

In **Figure 19** are two example series of CNAP signals resulting from one stimulus waveform at different current amplitudes. These CNAP series plots show that,

1. there are three distinguishable fiber populations with peaks occurring at different latencies;

2. even though the compound action potential complexes do interfere with each other, which again is a limitation due to the short electrode separation, peak feature extraction is still representative of fiber activation; and
3. each nerve has a distinct CNAP signal, even though the same electrodes and setup were used.

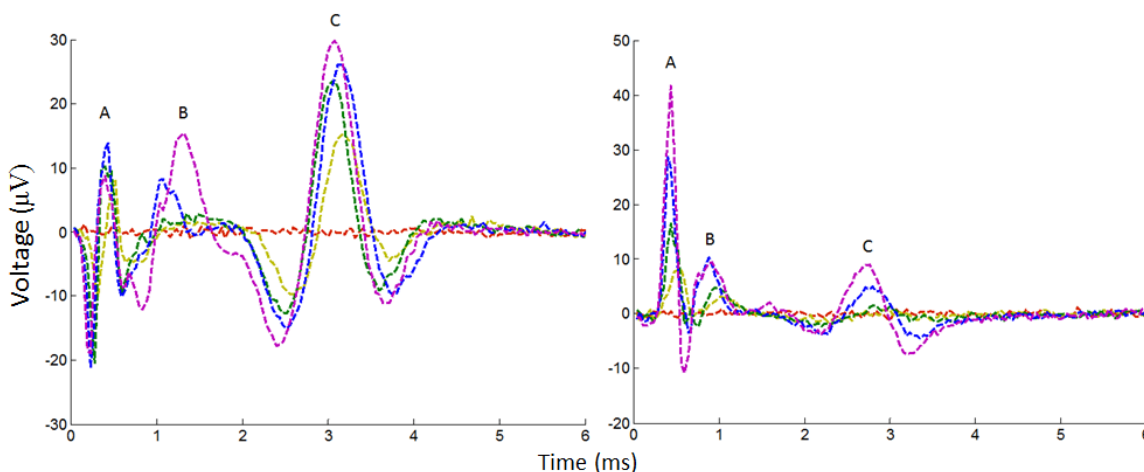


Figure 19 Example nerve responses at varying current amplitudes. The left plot contains CNAP recorded from animal R164, and the right is from R165. The overall CNAP morphology for the two subjects is different, even though the setup is the same. Each plot consists of CNAP data resulting from only a single stimulus waveform delivered at five different amplitudes (in random order). The red trace is from a zero-amplitude trial, and the trace color shifts toward violet across the spectrum as the stimulus amplitude is raised. Peak designations are marked with A, B, and C.

To compare the right vagal CNAP response profiles for the different stimulus waveforms tested, fiber recruitment profiles were constructed in a similar fashion as described in Subsection 3.6.4. A sample set of profiles is shown in **Figure 20**. The trends seen in these profiles are consistent with the results from characterizing burst-modulated waveforms (see Section 3.7, also refer to Qing *et. al.*¹⁷⁴). Namely, when two pulsons are delivered back-to-back as a single continuous pulse, the waveform is the most efficient at fiber recruitment, requiring the least amount of charge to reach a certain level of

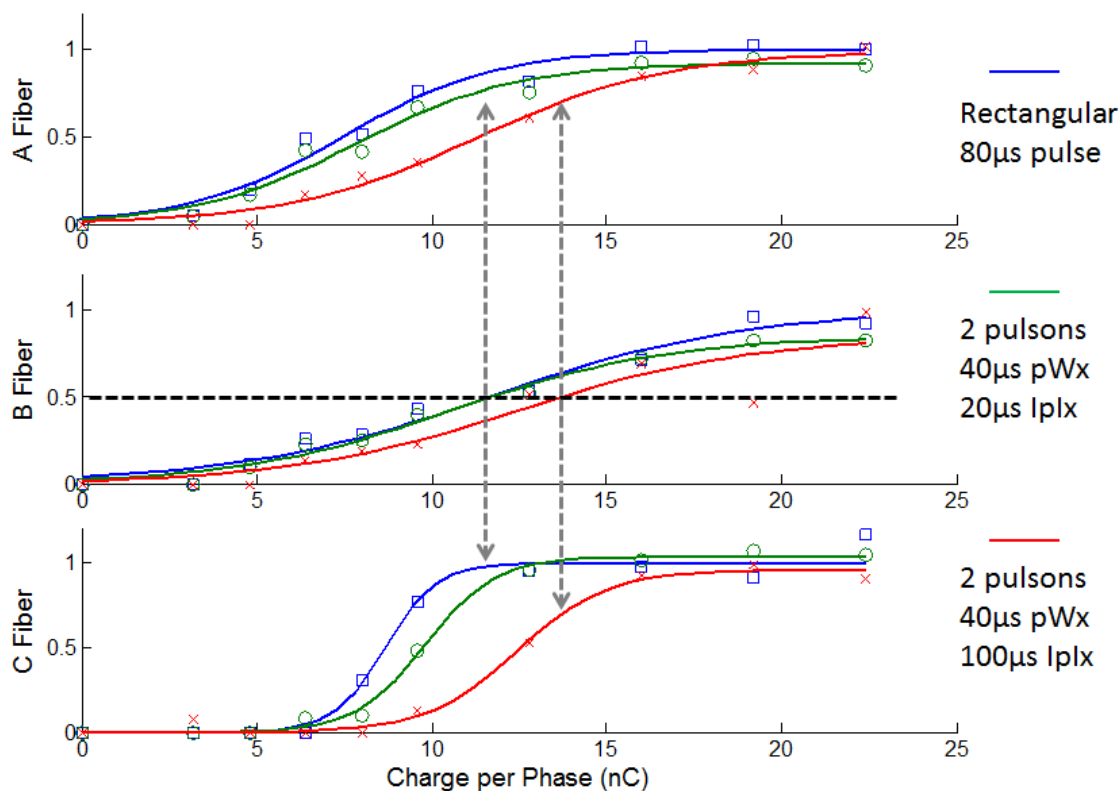


Figure 20 Fiber recruitment profiles for selected waveforms. The response peak magnitudes for A, B, and C fibers at all charge levels were converted to activation levels (see Subsection 3.6.4). The burst-modulated waveform with $100\mu\text{s}$ I_{pIx} recruits fibers differently from the other two waveforms shown. The other two waveforms are similar in shape, and their recruitment profiles are similar as well. The black dashed line marks the 50% B activation level, and the gray dashed arrows point to the estimated A and C fiber activation at 50% B activation.

activation for all fibers. When an interval is added, the efficiency decreases overall, and the change differs among the different fiber groups, leading to a change in selectivity.

The longer the interval is, the more the waveform deviates from the rectangular pulse.

Although the effects of the different waveforms on the nerve are interesting, the more important questions are how do the waveforms affect the heart rate and how does the heart rate relate to the fiber activation. In the sample **Figure 21**, the CNAP at varying amplitudes are shown with their corresponding instantaneous heart rate plots. With the

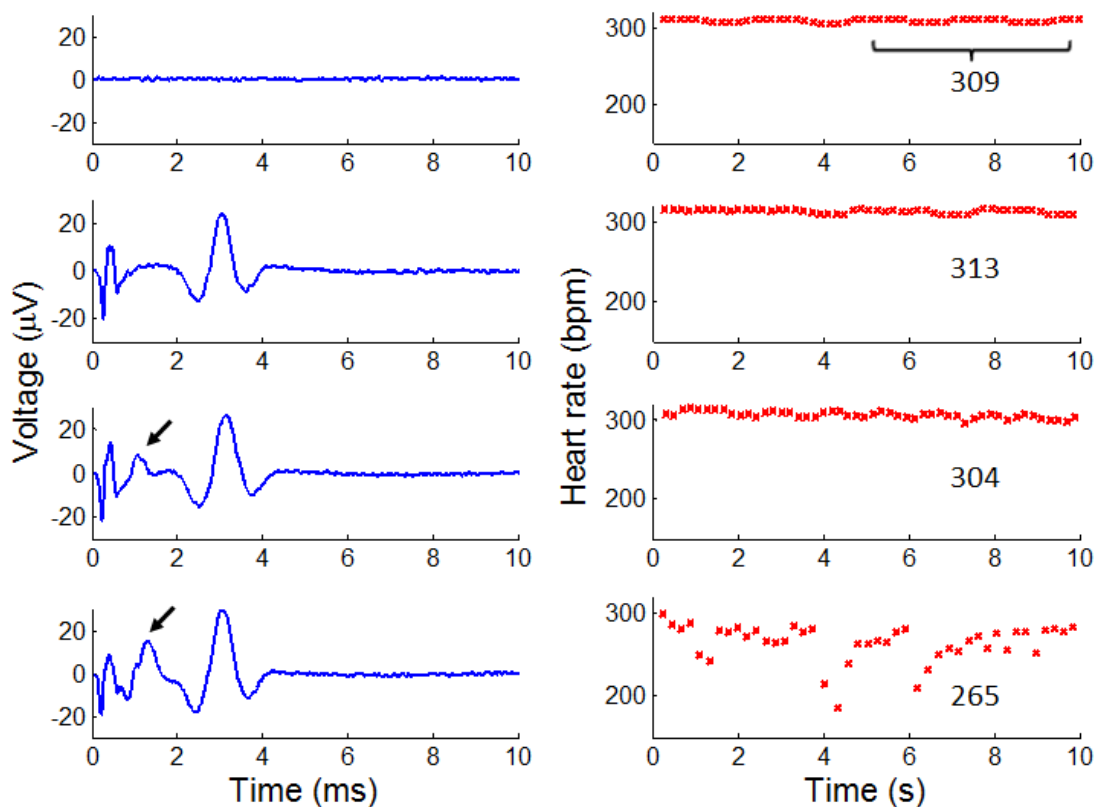


Figure 21 CNAP and corresponding heart rate. The CNAP plots show only the mean signal. The same stimulus waveform is used for all four trials shown, and the amplitude increases from top (zero-amplitude) to bottom (near maximal activation). Arrows mark B fiber peaks. The average heart rate for the final 5 seconds of the trial is annotated.

zero-amplitude trial, there was no fiber activation, and the heart rate was steady, with minor fluctuations that correspond to breathing. As the amplitude increased, fibers began to fire action potentials. However, the heart rate was not affected until B fibers were recruited, regardless of how large the A and C fiber peaks were. This observation is consistent with clinical cases where patients were implanted with vagal stimulators on the right side. These patients experienced seizure reduction without any notable cardiac effects²¹³, which suggest that other fibers were activated and B fibers were not.

To estimate the heart rate at the end of the trial, the last 5 seconds of the instantaneous heart rate data were averaged. Under isoflurane, the animal breathed once

every 1 to 2 seconds, and a duration of 5 seconds, which is longer than at least 2 cycles of breathing, was deemed long enough to provide an accurate estimate of heart rate.

Occasionally, when the stimulus was strong enough, the heart rate became very slow and irregular (see **Figure 22**). Not only is the induced arrhythmia and severe bradycardia harmful to the subject, which could affect the trials that follow, the irregular rhythm also makes analysis difficult. In these cases of arrhythmia, it seems that there is some form of conduction block, which manifests as regular P waves with some missing QRS and T waves (see **Figure 22**). Therefore, the stimulus amplitude was generally limited as to prevent arrhythmia and severe bradycardia. The rats generally have a resting heart rate of 400 bpm, which decreases and stabilizes around 350bpm under anesthesia. VNS trials that resulted in a heart rate lower than 200bpm or in overt arrhythmia were excluded from analysis.

4.9 The Vagal-Heart Rate Relationship

To study the relationship between the vagal response and heart rate, the heart rate is plotted against the magnitudes of the different fiber peaks in **Figure 23**. Data from all tested waveforms (rectangular and burst-modulated) were pooled to create each plot for each animal subject. Across all subjects, the heart rate seems to be consistently correlated to B fiber response, decreasing as the B fiber peak increases in magnitude. This correlation confirms the scientific basis of stimulating the right vagus nerve, because the right vagal B fibers are precisely the parasympathetic fibers that cause depression of cardiac function, among other effects (discussed in Sections 3.3 and 4.4).

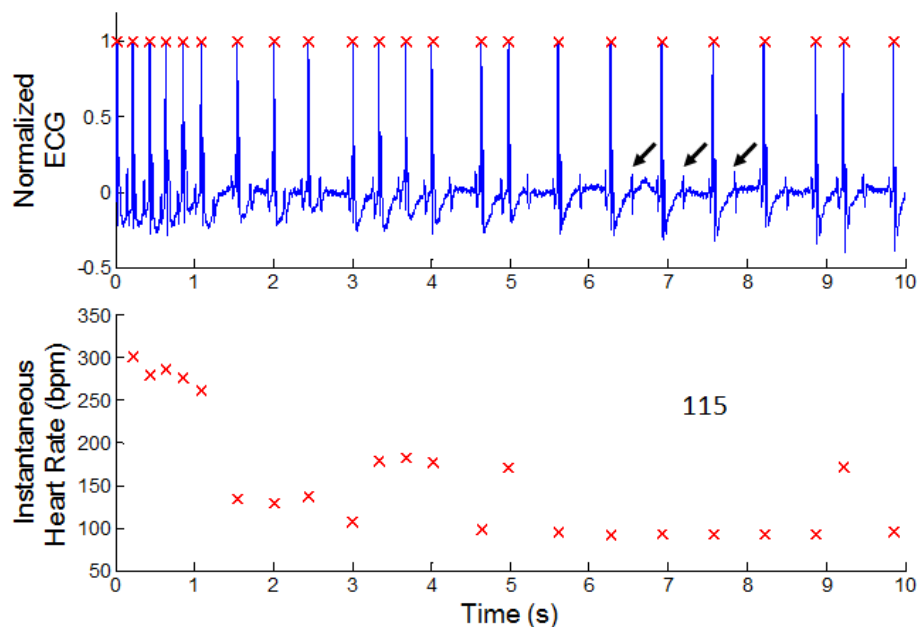


Figure 22 Example trial resulting in arrhythmia. The ECG trace is marked with x's for R peaks. Initial ECG is normal. The arrows point to several P waves without a QRS complex, a sign of failed conduction. As a result, the heart rate (estimated from R peaks) is very low. The average over the final 5 seconds (115bpm) is annotated.

In some subjects, the A and C fiber response appear to be correlated to heart rate as well. This apparent correlation is mostly due to the fact that the response magnitudes of individual fiber groups are not independent. A high-amplitude electrical stimulus of any waveform will activate more fibers in general, so that a when the B fiber response magnitude is high, C fiber magnitude is likely high as well. Another indication that A and C fiber activation are not directly related to heart rate is that, for B fibers, the heart rate decreases as soon as the peak began to appear, while for A and C fibers the heart rate is steady throughout most of the range of activation. Finally, the heart rate does not change consistently with A and C fibers across all animals, making a causal relationship unlikely.

A total of 6 animals underwent the right-side VNS experiments, starting with animals R153 and R154 and finishing with animals R162 through R165. Animals R155

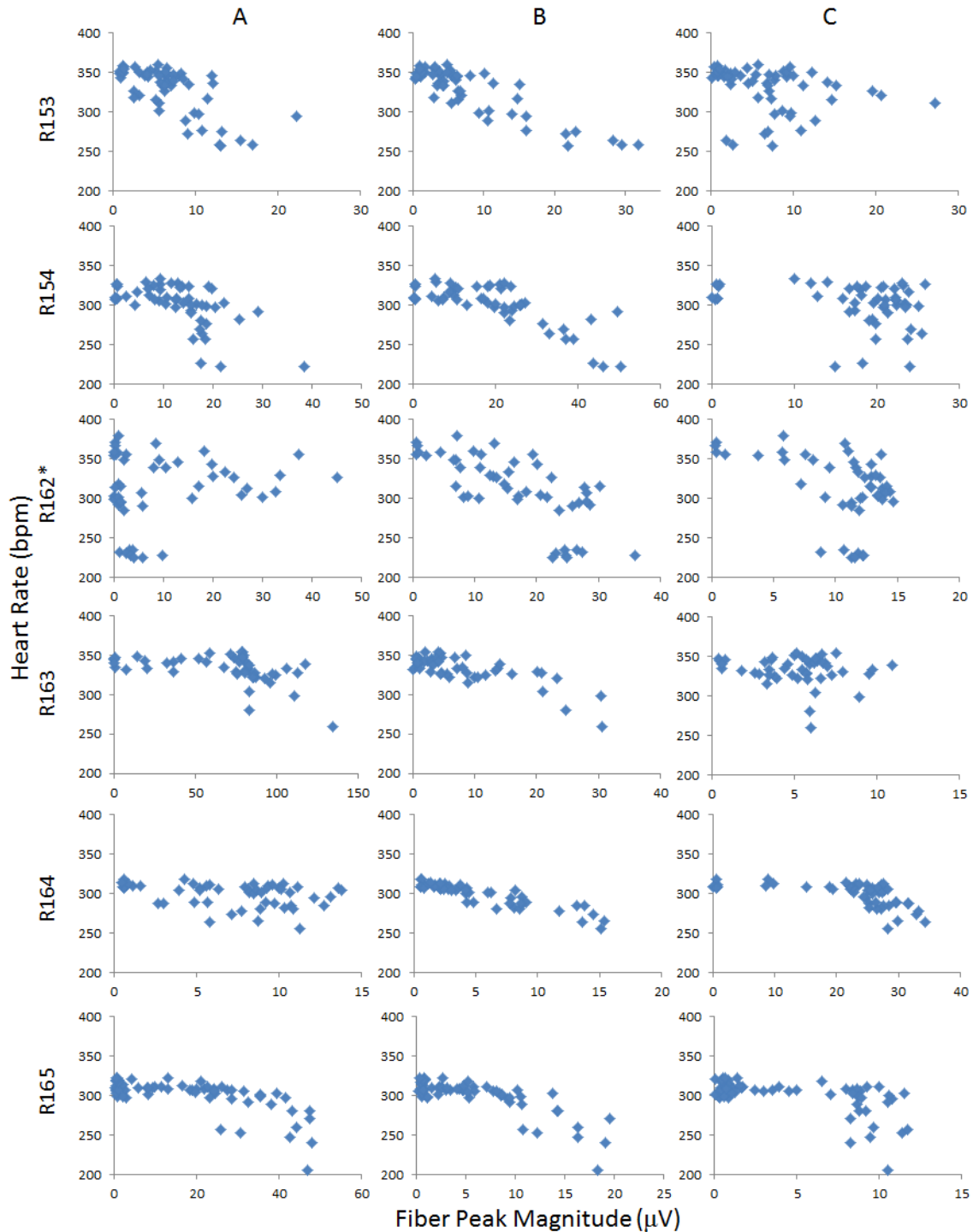


Figure 23 Right vagal CNAP and heart rate data from all animals. The columns represent the different fiber groups A, B, and C. The rows represent the different animals that underwent the experiment. * The data from R162 is more variable because the anesthesia method used was intraperitoneal ketamine/xylazine injections, whereas the others were anesthetized with isoflurane.

through R161 were used for another, unrelated project. So, for the purpose of this series of VNS experiments, these 6 animals were sequential subjects. This fact is important in showing that the results are highly reproducible, despite the variability among the subjects' CNAP responses and B fiber-heart rate relationships.

As can be seen in **Figure 23**, the range of B fiber response magnitudes and the range of heart rate vary among animals. Normalizing the fiber response and heart rate can reduce the subject-to-subject variability—normalizing the fiber response to the maximal response magnitude to produce activation levels is the same method used in the burst-modulated waveform study (see Section 3.6.4). However, because high-intensity stimuli tend to cause arrhythmia and profound bradycardia and were avoided, the maximum peak magnitudes were unknown. As a substitute for the true maximum, the highest magnitude for each fiber peak achieved during the randomized stimulation trials served as the maximum. For normalizing the heart rate, all data were simply normalized to the highest heart rate recorded. The normalized data are combined in **Figure 24**.

Normalizing the variables still does not result in a reliable profile for fiber activation and heart rate across all subjects. Aside from not having the true maximal fiber response magnitudes, there is also the challenge of accounting for variability among the fiber response-heart rate profiles for each subject. In the data shown in **Figure 23**, some of the B fiber response-heart rate trends appear linear while others are curvilinear. Therefore, even though it is technically possible to combine the normalized data and analyze all the data together, it is difficult to create a general profile that accurately represents all subjects. An individualized approach would be more appropriate.

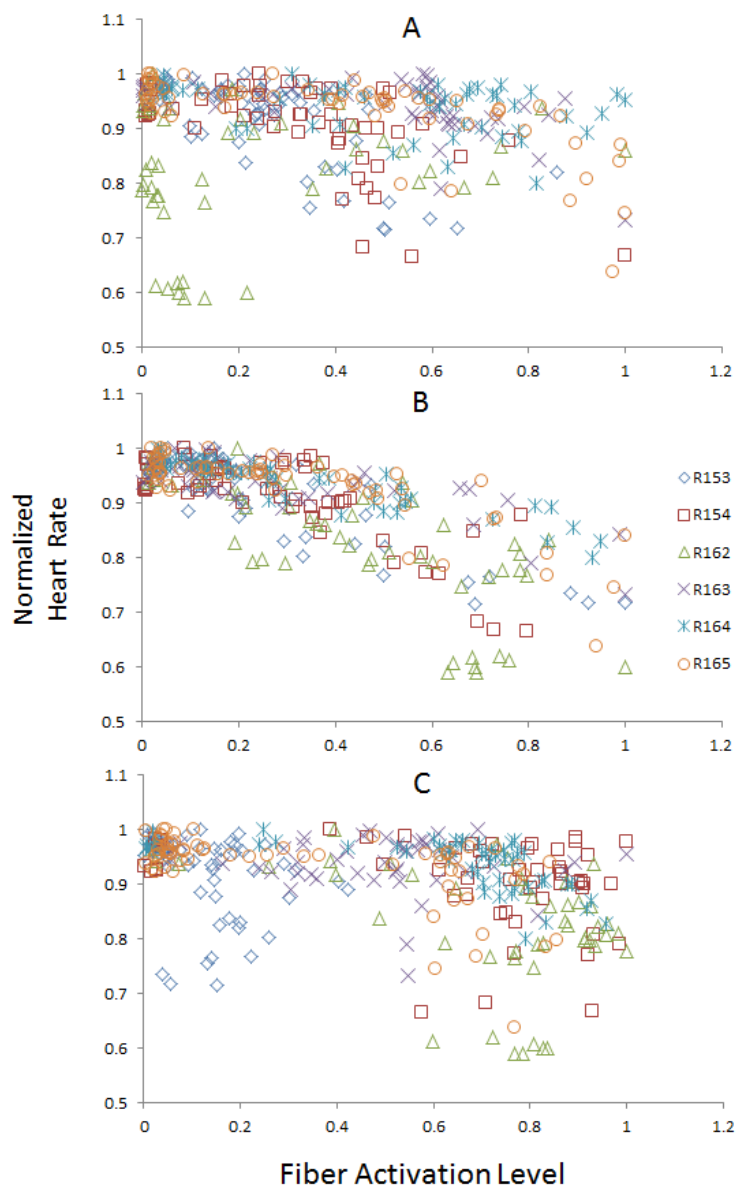


Figure 24 Combined normalized data from all animals. The heart rate and fiber response data are normalized to the highest values encountered. Data from all 6 animals and all tested waveforms are pooled.

Figure 25 shows the heart rate against B fiber magnitude for two sample subjects with the individual waveforms marked. It can be seen that as the B fiber magnitude increases, the heart rate decreases, and though different waveforms were used, the data points do not deviate from the overall trend. In more general terms, the physiological

effect is a result of neural activation and not the exact stimulus. The fact that the effect on heart rate is independent of stimulus waveform highlights the benefits of activation control. As long as the target fiber group is activated to the desired therapeutic levels, the stimulus waveforms can be altered to tune the efficiency and selectivity.

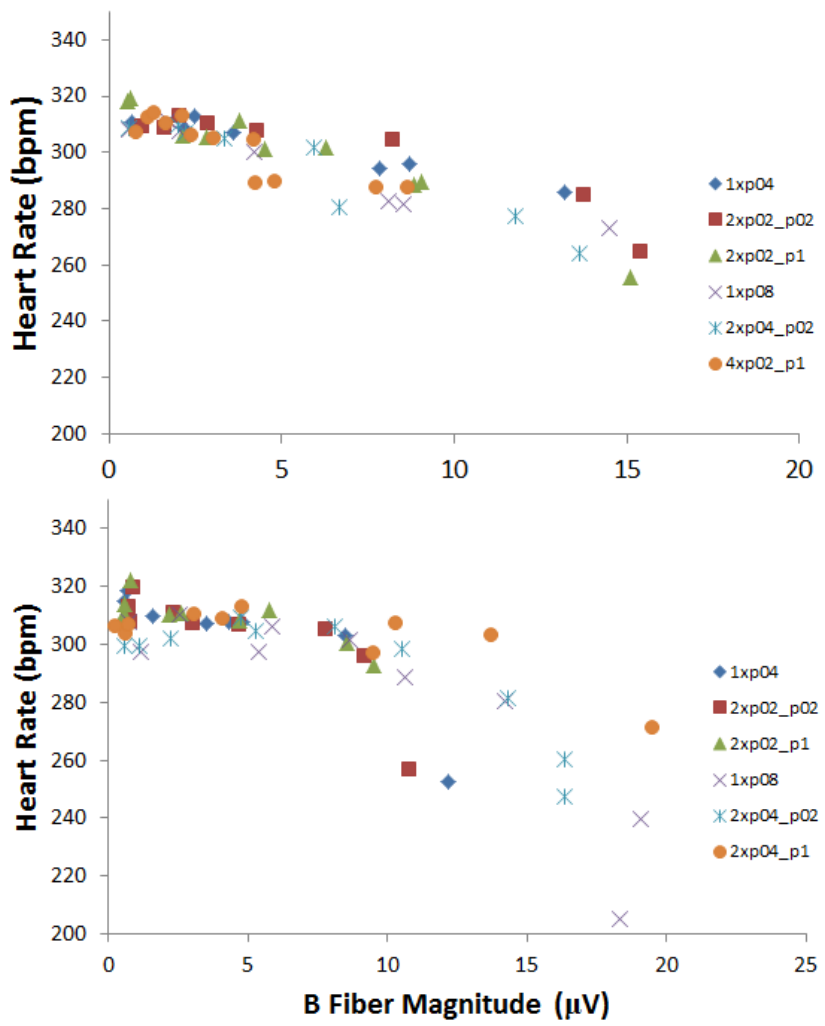


Figure 25 Example B fiber-heart rate relationships with waveforms marked. The heart rate and fiber response data are normalized to the highest values encountered. Data from all 6 animals and all tested waveforms are pooled. The figure legend for the waveforms is written as: <Nop>xp<pWx in ms>_p<IpIx in ms>. For example, “2xp02_p02” refer 2 pulsons with each having a width of 0.02ms and interval of 0.02ms.

4.10 The Effects of Right-Side VNS on Heart Function

Heart rate alone can be a strong indicator of cardiac workload and can provide a general sense of the autonomic balance. Using ultrasound imaging, which is a relatively simple procedure commonly done in the clinical setting, it is possible to determine more important measures of cardiac function. Combining the electrographical recordings of the vagus nerve and the heart and the ultrasound images can paint a complete picture of the effect of each stimulus on the heart.

As a pilot experiment, one animal (R166) underwent right-side VNS with simultaneous recordings of the vagus nerve and ECG (similar to that described in **Figure 17**) as well as ultrasound imaging. Ultrasound equipment (Vevo2100, VisualSonics) and expertise were provided by Dr. Craig Goergen's group. Image acquisition focused on the left ventricle of the heart, and image analysis yielded estimates of stroke volume, ejection fraction, and fractional shortening. Using the heart rate and stroke volume, the cardiac output can be calculated as well. See **Figure 26** for an illustration of image analysis.



Figure 26 Example ultrasound image processing. The left image shows the left ventricle in diastole with estimated chamber volume marked red; the right image shows the ventricle in systole with chamber volume marked green. Images show sagittal axis.

The relationship between vagal CNAP peak magnitudes and the heart rate for this animal is summarized in **Figure 27**. Consistent with the results in Subsection 4.8, the B fiber response is strongly linked to the heart rate. The heart rate is not correlated with A and C fibers. The baseline heart rate is also similar to those in **Figure 23**.

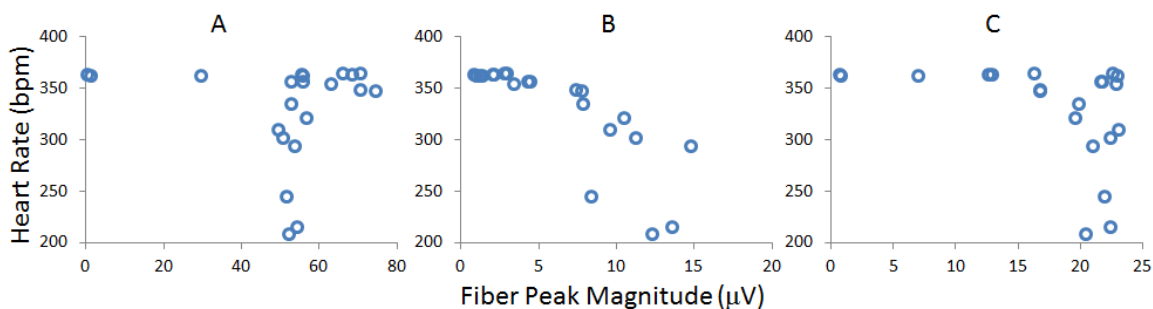


Figure 27 R166 vagal CNAP magnitudes and heart rate. The data presented here is similar to those in **Figure 23**. Only one stimulus waveform—100µs rectangular pulse waveform—was used to simplify experimentation.

The stroke volume, ejection fraction, and cardiac output data are shown in **Figure 28**. The stroke volume is not affected much by stimulation, but ejection fraction does decrease as B fiber magnitude increases. Though the stroke volume is unaffected, cardiac output decreases notably due to the lower heart rate. The baseline ejection fraction of 70% is within the normal range for rats^{214,215}. A decrease in ejection fraction suggests a decrease in ventricular contractility due to stimulation, which is also consistent with what others have reported^{216,217}.

With the heart rate data alone, one can only assume that the decreased heart rate reflects a decreased cardiac output as well. With the additional ultrasound imaging data, that assumption can be confirmed. More importantly, the availability and feasibility of performing ultrasound imaging in the clinical setting signifies that the procedure used in these experiments can be translated to patient care. When setting stimulus parameters,

vagal recording, ECG, and ultrasound can all be performed, to fully capture the effects of each stimulus. Then the appropriate stimulus parameters to generate the optimal neural activation pattern can be determined.

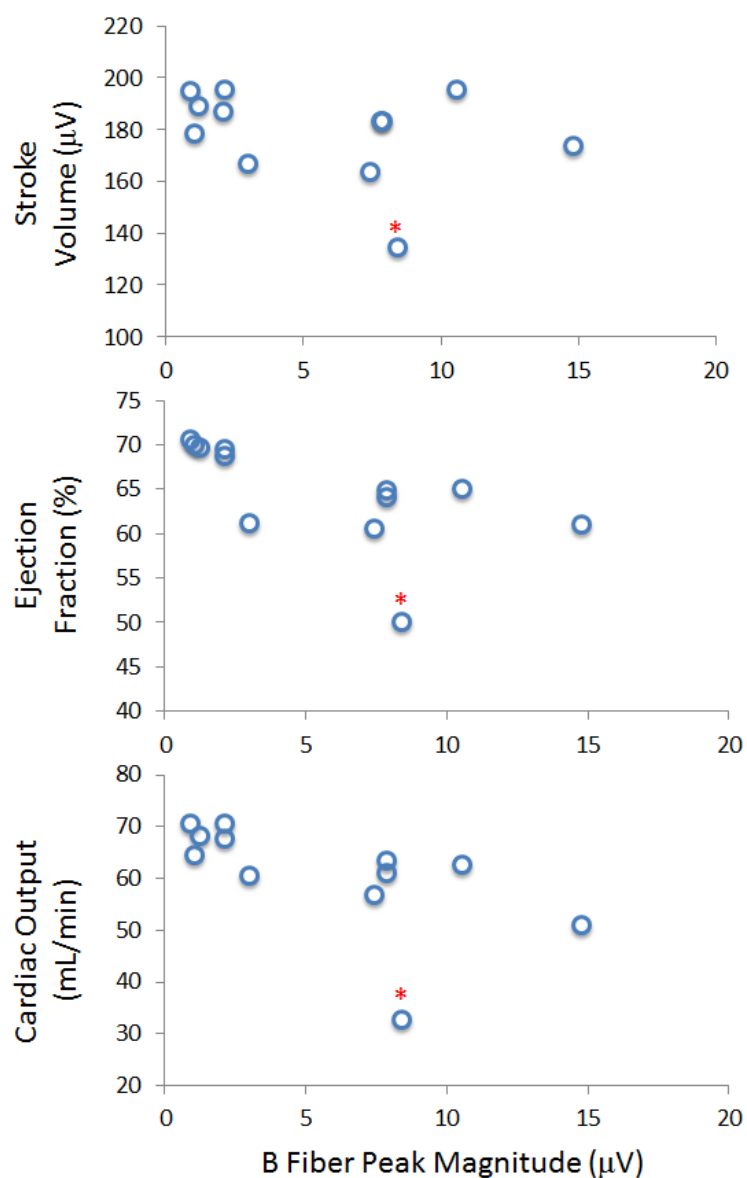


Figure 28 R166 B fiber-left ventricle function relationship. Left ventricle data was made available by Dr. Goergen's group. The red asterisk marks an outlier trial, where a fairly low B fiber activation led to bradycardia and arrhythmia. The data point is included for completeness.

4.11 Notes

The contents of this chapter are being prepared for submission for publication. Likely, the VNS experiment with ultrasound imaging will be repeated a few more times to collect additional data. The tentative title is “Controlling the vagal effects on the heart by B fiber activation”. I will be the first author on this article.

CHAPTER 5. CONCLUSION

5.1 Objective, Individualized Stimulation Dosing

The differences in the B fiber-heart rate profile among the subjects serve as a strong argument for the implementation of a more objective and individualized approach to VNS, and neurostimulation in general. The objective aspect can be achieved by 1) recording the nerve response to the stimulus; 2) creating a profile for the nerve response to the stimulus; and 3) finding the ultimate effect of the nerve activation on physiology. If VNS is used for seizure suppression, the physiological effect would be changes in seizure frequency and severity. For heart protection, in epilepsy or heart failure, the physiological effect would be resting heart rate and heart rate dynamics, among other indicators. In spinal cord stimulation, compound action potential analysis is still a valid method for measuring the neural response. In brain stimulation, the response would be in the form of evoked potentials or spike activity. This objective approach forms the foundation of activation control, which allows stimulation dosing based on the subject's response, and can reduce subject-to-subject variability.

The stimulus parameters are still important, but they simply are not the major factor in determining how the body responds. For example, if the stimulator can only provide a certain amount of voltage, or if the electrodes can only safely pass a certain amount of current, it is necessary to limit the stimulus amplitude. Also, the efficiency of

stimulation (charge per phase to achieve target activation) needs to be monitored as well, because the most selective waveform is usually not the most efficient. Draining the batteries too quickly will require more replacement procedures and increases the risk of complications. However, just for the purpose of creating a physiological effect, the neural response is more important than the stimulus. This fact is true at least in the case of stimulating the right vagus nerve to lower the heart rate. And in this case, the stimulus is just a means to an end—two different stimuli that can elicit a similar vagal response will lead to a similar drop in heart rate.

The individualized aspect can be achieved by creating response profiles for each individual rather than trying to group subjects together for analysis. The group approach will yield a certain group response rate, because the same neural activation likely does not produce the same change for everyone in the group. Again using the right-side VNS as an example, the same level of B fiber activation in different subjects does not produce the same amount of heart rate decrease (see **Figure 24**). Dosing each individual subject based on the unique profile of the subject ensures that each will achieve the optimal balance of therapeutic effects and side effects.

Implanting more sensors to record more physiological data is not always feasible, nor desirable. Without constant physiological data feedback, it would not be possible to perform activation-controlled stimulation. However, during patients' clinic visits it would still be better to dose by the patient's individual neural response rather than just the stimulus parameters.

The objective, individualized method of neurostimulation used in conjunction with the described method for optimization for efficiency and selectivity of stimulus

waveforms, discussed in detail in CHAPTER 1, creates a unique stimulus dosing system. This dosing system first allows researchers to determine which fiber group(s) is important for therapy and which fiber group(s) leads to side effects. It also allows clinicians to determine how to activate the target group(s) in order to maximize efficacy and minimize side effects. Ultimately, patients should respond in a more consistent manner, and the overall response rate should increase.

5.2 Refining DBS Parameters

Like for VNS, DBS parameters are also set to produce the maximal clinical effect without causing intolerable side effects^{16,89,218,219}. Unlike for VNS, due to its more invasive nature, DBS causes side effects that can be quite severe. Stimulation can adversely affect 1) cognition, such as causing memory and attention deficits, 2) mental health, such as inducing anxiety and depression, 3) speech, and 4) functions of certain cranial nerves^{218,220,221}. In the study by Koller *et. al.*, out of 25 patients, as high as 21 reported paresthesia, and 15 reported headaches²¹⁸.

Also unlike VNS, the therapeutic and side effects of DBS are more due to lack of spatial-, rather than fiber-, selectivity. In other words, enough volume of the target tissue must be activated to produce therapeutic effect, but activating too much volume will affect neighboring regions and cause side effects. For example, to reduce parkinsonian symptoms, the subthalamic nucleus is a common target. By modeling the electric field from DBS electrodes, Cameron McIntyre *et. al.* demonstrated the relationship between distance from electrode and threshold voltage for activation (recall that DBS operates under voltage-control)⁶⁰. The results show that stimulation of the subthalamic nucleus

also activates nearby fibers in the internal capsule, leading to the commonly observed side effects^{60,222}.

Therefore, increasing spatial-selectivity would increase efficacy and decrease side effects. Reducing electrode size can improve spatial-selectivity, but a smaller electrode will have a smaller potential volume of activation. The best way to achieve better spatial-selectivity is to improve the accuracy of electrode placement, which is dependent on surgical and electrode advances.

Nonetheless, activation control and stimulus optimization can still be applied to DBS. Recording evoked potentials in the region being stimulated and other associated regions in the brain can yield valuable data on the effects of the stimulus. Simultaneous stimulation and recording using a standard commercial DBS electrode has been demonstrated already²²³. Other methods of recording are also available^{94,224,225}.

Specifically, in stimulating the nucleus accumbens shell for treating alcohol use and other addiction disorders, the accumbens itself and the prefrontal cortex are major targets for recording the effect of nucleus accumbens stimulation^{132,224,226–228}. Central and peripheral side effects can also be monitored. The desired level of neural response, once determined, can be monitored and maintained, while the stimulus waveform can be adjusted to fine-tune efficiency and selectivity. Similar systems can be applied to other applications of DBS as well, such as for treating Parkinson's disease. Once again, even if this neural response feedback-driven process can only be implemented during patient visits, the objective, individualized dosing system still has advantages over the current standard dosing system.

5.3 Ideas for Future VNS Work

So far, the VNS experiments aimed to improve stimulus design and dosing system have shown that the fiber selectivity, as well as efficiency, of the stimulus can be adjusted. The only major modification required is a set of recording electrodes. Ideally, skin surface electrodes would suffice, allowing clinicians to record the vagal response without adding more implantable components. The feasibility and reliability of recording human vagal responses from surface electrodes will need to be tested.

To fully utilize the benefits of action-controlled stimulation, the stimulator would need to be able to generate different waveforms. Burst-modulated waveforms can be rectangular in shape and were specifically designed to allow easy implementation using microcontroller-based stimulus generators. Incorporation into commercial implants should be simple but still require testing. A provisional patent²²⁹ (the order of inventors was mistakenly submitted; Kurt Y Qing should be the first inventor) has been filed based on my work with burst-modulated waveforms, and there is a full U.S. patent in progress of being filed.

The experiments in CHAPTER 4 characterized the effect of right vagal B fibers on heart rate. The next step is to characterize the physiological effect of the other major fiber groups. A fibers should lead to activation of laryngeal muscles. In the rat experiments or in future clinical studies, laryngeal electromyography would provide physiological data due to A fiber activation, on either the left or right side. In the rat, it may be difficult due to limited space. C fiber activation are more difficult to study, since their effect tend to be slow, prolonged. However, since the subdiaphragmatic vagus nerve

is mostly composed of C fibers^{142,143,149}, characterizing changes in gut motility may offer an objective method to measure the physiological effects of C fiber activation.

Finally, the biggest question to answer is whether the different vagus nerve activation patterns can produce differences in antiepileptic effects (or heart failure, or other applications). I have conducted some preliminary VNS experiments attempting to compare the effect of different nerve activation patterns on seizure frequency and severity. The tetanus toxin rat model of epilepsy^{230,231} was used. Rats treated with an intra-hippocampal injection of tetanus toxin develop frequent spontaneous seizures, which is similar to the epilepsy syndrome in human patients.

In my experiments, animals treated with tetanus all experienced seizures, one even died shortly after a seizure. Seizures were detected via a differential recording across two cranial bone screws and confirmed via video recording (the electrographic and video recording system used was the Pinnacle 8200). Seizure behavior matched that described in literature^{230,231}. However, the VNS produced inconsistent results, and so it was difficult to determine how VNS affected seizures.

The tetanus-treated rats were implanted with two vagal cuffs (same as shown in **Figure 10**). Immediately after implantation, it is possible to stimulate the nerve and record a convincing CNAP response. The impedance across the two leads of the cuffs increase over time, as measured by electrochemical impedance spectroscopy (same methods used as described in Subsection 3.6.2). The increase is expected due to natural tissue scarring, and the electrodes stay viable even months after implant. The longest implant period is 68 days, and in this animal, the recording cuff impedance at 1kHz increased from 1.2 before implantation to a maximum of 6.4k Ω *in vivo*, and the

stimulation cuff increased from 1.7 to a maximum of 13.7k Ω . However, the vagal signal deteriorates over time, and a few days after surgery, it is no longer possible to elicit a CNAP response.

The problem likely lies in the physical properties of the nerve cuffs. Unlike the commercial ones, which are self-sizing, the custom cuffs are rather stiff and do not self-size. It could be that over the course of days, due to continued movements of the animal and scar tissue formation, the electrode leads lost close contact with the nerve. It is even possible that tissue swelling and scarring from healing, along with irritation from the cuff due to movement, led to nerve degeneration. A more sophisticated, sizing cuff electrode is required to preserve vagus function and excitability. Only then can chronic VNS experiments be conducted properly.

REFERENCES

REFERENCES

1. Goetz, C. G., Poewe, W., Rascol, O. & Sampaio, C. Evidence-based medical review update: pharmacological and surgical treatments of Parkinson's disease: 2001 to 2004. *Mov. Disord.* **20**, 523–39 (2005).
2. Fahn, S. A new look at levodopa based on the ELLDOPA study. *J. Neural Transm. Suppl.* 419–26 (2006). at <<http://www.ncbi.nlm.nih.gov/pubmed/17017562>>
3. Katzenschlager, R. *et al.* Fourteen-year final report of the randomized PDRG-UK trial comparing three initial treatments in PD. *Neurology* **71**, 474–80 (2008).
4. Kwan, P., Schachter, S. C. & Brodie, M. J. Drug-resistant epilepsy. *N. Engl. J. Med.* **365**, 919–26 (2011).
5. Berg, A. T. & Kelly, M. M. Defining intractability: comparisons among published definitions. *Epilepsia* **47**, 431–6 (2006).
6. Sindrup, S. H. & Jensen, T. S. Efficacy of pharmacological treatments of neuropathic pain: an update and effect related to mechanism of drug action. *Pain* **83**, 389–400 (1999).
7. Pinto, R. Z. *et al.* Drugs for relief of pain in patients with sciatica: systematic review and meta-analysis. *Bmj* **344**, e497–e497 (2012).
12. Mulrow, C. D. *et al.* Efficacy of newer medications for treating depression in primary care patients. *Am. J. Med.* **108**, 54–64 (2000).
13. WHO. *Neurological disorders: public health challenges. Health (San Francisco)* (2006).
14. WHO. *The global burden of disease: 2004 update. Update* (2008).
15. Groves, D. A. & Brown, V. J. Vagal nerve stimulation: a review of its applications and potential mechanisms that mediate its clinical effects. *Neurosci. Biobehav. Rev.* **29**, 493–500 (2005).

16. Kringelbach, M. L., Jenkinson, N., Owen, S. L. F. & Aziz, T. Z. Translational principles of deep brain stimulation. *Nat. Rev. Neurosci.* **8**, 623–35 (2007).
17. Ben-Menachem, E. Vagus-nerve stimulation for the treatment of epilepsy. *Lancet Neurol.* **1**, 477–482 (2002).
18. Smyth, M. D., Tubbs, R. S., Bebin, E. M., Grabb, P. A. & Blount, J. P. Complications of chronic vagus nerve stimulation for epilepsy in children. *J. Neurosurg.* **99**, 500–3 (2003).
19. Oh, M. Y., Abosch, A., Kim, S. H., Lang, A. E. & Lozano, A. M. Long-term hardware-related complications of deep brain stimulation. *Neurosurgery* **50**, 1268–74; discussion 1274–6 (2002).
20. Duchenne, G. B. & Tibbits, H. *A Treatise on Localized Electrization, and its applications to pathology and therapeutics (translation)*. (Hardwicke, 1971).
21. Piccolino, M. Animal electricity and the birth of electrophysiology: the legacy of Luigi Galvani. *Brain Res. Bull.* **46**, 381–407 (1998).
22. Jones, H. B. (editor) & Cantar (editor), F. R. S. *On Animal Electricity: being an abstract of the discoveries of Emil du Bois-Reymond. Search* (John Churchill, Princes Street, SOHO, 1852).
23. Lapique, L. Quantitative investigations of electrical nerve excitation treated as polarization. 1907. (translation). *Biol. Cybern.* **97**, 341–9 (2007).
24. Gorman, P. H. & Mortimer, J. T. The effect of stimulus parameters on the recruitment characteristics of direct nerve stimulation. *IEEE Trans. Biomed. Eng.* **30**, 407–14 (1983).
25. Shepherd, R. K. & Javel, E. Electrical stimulation of the auditory nerve: II. Effect of stimulus waveshape on single fibre response properties. *Hear. Res.* **130**, 171–88 (1999).
26. Van den Honert, C. & Mortimer, J. T. The response of the myelinated nerve fiber to short duration biphasic stimulating currents. *Ann. Biomed. Eng.* **7**, 117–25 (1979).
27. Berry, G. A. & Rutherford. Note on Pflüger's Law of Contraction. *J. Anat. Physiol.* **10**, 604–8 (1876).

28. Hodgkin, A. L. & Huxley, A. F. A quantitative description of membrane current and its application to conduction and excitation in nerve. *J. Physiol.* **117**, 500–44 (1952).
29. Hill, A. V. Excitation and accommodation in nerve. *Proc. R. Soc. London. Ser. B, Biol. Sci.* **119**, 305–355 (1936).
30. Fang, Z. P. & Mortimer, J. T. Selective activation of small motor axons by quasi-trapezoidal current pulses. *IEEE Trans. Biomed. Eng.* **38**, 168–74 (1991).
31. Van den Honert, C. & Mortimer, J. T. Generation of unidirectionally propagated action potentials in a peripheral nerve by brief stimuli. *Science* **206**, 1311–2 (1979).
32. Merrill, D. R., Bikson, M. & Jefferys, J. G. R. Electrical stimulation of excitable tissue: design of efficacious and safe protocols. *J. Neurosci. Methods* **141**, 171–98 (2005).
33. Weiss, G. Sur la possibilité de rendre comparable entre eux les appareils servant à l'excitation électrique. *Arch. Ital. Biol.* **35**, 413–446 (1901).
34. Irnich, W. Georges Weiss' fundamental law of electrostimulation is 100 years old. *Pacing Clin. Electrophysiol.* **25**, 245–8 (2002).
35. Lapique, L. Définition expérimentale de l'excitabilité. *Comptes rendus Hebd. des séances mémoires la Société Biol.* **67**, 280–283 (1909).
36. Lilly, J. C., Hughes, J. R., Alvord, E. C. & Galkin, T. W. Brief, noninjurious electric waveform for stimulation of the brain. *Science* **121**, 468–9 (1955).
37. Bard, A. J. & Faulkner, L. R. *Electrochemical Methods: Fundamentals and Applications*. (John Wiley & Sons Inc., 2001).
38. Cogan, S. F. Neural stimulation and recording electrodes. *Annu. Rev. Biomed. Eng.* **10**, 275–309 (2008).
39. Randles, J. E. B. Kinetics of rapid electrode reactions. *Discuss. Faraday Soc.* **1**, 11 (1947).
40. Grill, W. M. & Mortimer, J. T. Electrical properties of implant encapsulation tissue. *Ann. Biomed. Eng.* **22**, 23–33 (1994).
41. Williams, J. C., Hippensteel, J. A., Dilgen, J., Shain, W. & Kipke, D. R. Complex impedance spectroscopy for monitoring tissue responses to inserted neural implants. *J. Neural Eng.* **4**, 410–23 (2007).

42. Polikov, V. S., Tresco, P. A. & Reichert, W. M. Response of brain tissue to chronically implanted neural electrodes. *J. Neurosci. Methods* **148**, 1–18 (2005).
43. Biran, R., Martin, D. C. & Tresco, P. A. Neuronal cell loss accompanies the brain tissue response to chronically implanted silicon microelectrode arrays. *Exp. Neurol.* **195**, 115–26 (2005).
44. Wei, X. F. & Grill, W. M. Impedance characteristics of deep brain stimulation electrodes in vitro and in vivo. *J. Neural Eng.* **6**, 046008 (2009).
45. Lempka, S. F., Miocinovic, S., Johnson, M. D., Vitek, J. L. & McIntyre, C. C. In vivo impedance spectroscopy of deep brain stimulation electrodes. *J. Neural Eng.* **6**, 046001 (2009).
46. Lasia, A. in *Modern Aspects of Electrochemistry* (eds. Conway, B. E., Bockris, J. & White, R. E.) **32**, 143–248 (Kluwer Academic/Plenum Publishers, 1999).
47. Geddes, L. A. & Bourland, J. D. The strength-duration curve. *IEEE Trans. Biomed. Eng.* **32**, 458–9 (1985).
48. Bostock, H. The strength-duration relationship for excitation of myelinated nerve: computed dependence on membrane parameters. *J. Physiol.* **341**, 59–74 (1983).
49. Nowak, L. G. & Bullier, J. Axons, but not cell bodies, are activated by electrical stimulation in cortical gray matter. *Exp. Brain Res.* **118**, 477–488 (1998).
50. Mogyoros, I., Kiernan, M. C. & Burke, D. Strength-duration properties of human peripheral nerve. *Brain* **119** (Pt 2, 439–47 (1996).
51. Gallistel, C. R. Self-stimulation in the rat: quantitative characteristics of the reward pathway. *J. Comp. Physiol. Psychol.* **92**, 977–98 (1978).
52. Gallistel, C. R. Note on temporal summation in the reward system. *J. Comp. Physiol. Psychol.* **87**, 870–5 (1974).
53. Barry, F. E., Walter, M. S. & Gallistel, C. R. On the optimal pulse duration in electrical stimulation of the brain. *Physiol. Behav.* **12**, 749–54 (1974).
54. Matthews, G. Neural substrate for brain stimulation reward in the rat: cathodal and anodal strength-duration properties. *J. Comp. Physiol. Psychol.* **91**, 858–74 (1977).
55. Koivuniemi, A. S. & Otto, K. J. Asymmetric versus symmetric pulses for cortical microstimulation. *IEEE Trans. Neural Syst. Rehabil. Eng.* **19**, 468–76 (2011).

56. Holsheimer, J., Demeulemeester, H., Nuttin, B. & de Sutter, P. Identification of the target neuronal elements in electrical deep brain stimulation. *Eur. J. Neurosci.* **12**, 4573–7 (2000).
57. Rizzone, M. *et al.* Deep brain stimulation of the subthalamic nucleus in Parkinson's disease: effects of variation in stimulation parameters. *J. Neurol. Neurosurg. Psychiatry* **71**, 215–9 (2001).
58. Rattay, F. Analysis of models for extracellular fiber stimulation. *IEEE Trans. Biomed. Eng.* **36**, 676–82 (1989).
59. McIntyre, C. C. & Grill, W. M. Finite Element Analysis of the Current-Density and Electric Field Generated by Metal Microelectrodes. *Ann. Biomed. Eng.* **29**, 227–235 (2001).
60. McIntyre, C. C., Mori, S., Sherman, D. L., Thakor, N. V & Vitek, J. L. Electric field and stimulating influence generated by deep brain stimulation of the subthalamic nucleus. *Clin. Neurophysiol.* **115**, 589–95 (2004).
61. Wei, X. F. & Grill, W. M. Current density distributions, field distributions and impedance analysis of segmented deep brain stimulation electrodes. *J. Neural Eng.* **2**, 139–47 (2005).
62. Stoney, S. D., Thompson, W. D. & Asanuma, H. Excitation of pyramidal tract cells by intracortical microstimulation: effective extent of stimulating current. *J. Neurophysiol.* **31**, 659–69 (1968).
63. Tehovnik, E. J. Electrical stimulation of neural tissue to evoke behavioral responses. *J. Neurosci. Methods* **65**, 1–17 (1996).
64. Goldman, D. E. Potential, impedance, and rectification in membranes. *J. Gen. Physiol.* **27**, 37–60 (1943).
65. McNeal, D. R. Analysis of a model for excitation of myelinated nerve. *IEEE Trans. Biomed. Eng.* **23**, 329–37 (1976).
66. McIntyre, C. C. & Grill, W. M. Excitation of central nervous system neurons by nonuniform electric fields. *Biophys. J.* **76**, 878–88 (1999).
67. Warman, E. N., Grill, W. M. & Durand, D. Modeling the effects of electric fields on nerve fibers: determination of excitation thresholds. *IEEE Trans. Biomed. Eng.* **39**, 1244–54 (1992).

68. McIntyre, C. C. & Grill, W. M. Extracellular stimulation of central neurons: influence of stimulus waveform and frequency on neuronal output. *J. Neurophysiol.* **88**, 1592–604 (2002).
69. McIntyre, C. C., Grill, W. M., Sherman, D. L. & Thakor, N. V. Cellular effects of deep brain stimulation: model-based analysis of activation and inhibition. *J. Neurophysiol.* **91**, 1457–69 (2004).
70. Rattay, F. The basic mechanism for the electrical stimulation of the nervous system. *Neuroscience* **89**, 335–46 (1999).
71. Durand, D. M. in *The Biomedical Engineering Handbook: Second Edition* (ed. Bronzino, J. D.) (CRC Press LLC, 2000). doi:10.1201/9781420049510
72. Rattay, F. Analysis of models for external stimulation of axons. *IEEE Trans. Biomed. Eng.* **33**, 974–7 (1986).
73. BeMent, S. L. & Ranck, J. B. A model for electrical stimulation of central myelinated fibers with monopolar electrodes. *Exp. Neurol.* **24**, 171–86 (1969).
74. Armstrong, D. M., Harvey, R. J. & Schild, R. F. The spatial organisation of climbing fibre branching in the cat cerebellum. *Exp. Brain Res.* **18**, 40–58 (1973).
75. Ranck, J. B. Which elements are excited in electrical stimulation of mammalian central nervous system: a review. *Brain Res.* **98**, 417–40 (1975).
76. Benabid, A. L. *et al.* Chronic electrical stimulation of the ventralis intermedius nucleus of the thalamus as a treatment of movement disorders. *J. Neurosurg.* **84**, 203–14 (1996).
77. Porter, R. Focal stimulation of hypoglossal neurones in the cat. *J. Physiol.* **169**, 630–40 (1963).
78. Koivuniemi, A. S., Regele, O. B., Brenner, J. H. & Otto, K. J. Rat behavioral model for high-throughput parametric studies of intracortical microstimulation. *Conf. Proc. IEEE Eng. Med. Biol. Soc.* **2011**, 7541–4 (2011).
79. Gorman, A. L. Differential patterns of activation of the pyramidal system elicited by surface anodal and cathodal cortical stimulation. *J. Neurophysiol.* **29**, 547–64 (1966).
80. Hern, J. E., Landgren, S., Phillips, C. G. & Porter, R. Selective excitation of corticofugal neurones by surface-anodal stimulation of the baboon's motor cortex. *J. Physiol.* **161**, 73–90 (1962).

81. Donaldson, N. D. & Donaldson, P. E. When are actively balanced biphasic ('Lilly') stimulating pulses necessary in a neurological prosthesis? I. Historical background; Pt resting potential; Q studies. *Med. Biol. Eng. Comput.* **24**, 41–9 (1986).
82. Donaldson, N. D. & Donaldson, P. E. When are actively balanced biphasic ('Lilly') stimulating pulses necessary in a neurological prosthesis? II. pH changes; noxious products; electrode corrosion; discussion. *Med. Biol. Eng. Comput.* **24**, 50–6 (1986).
83. Brummer, S. B. & Turner, M. J. Electrical stimulation of the nervous system: The principle of safe charge injection with noble metal electrodes. *Bioelectrochemistry Bioenerg.* **2**, 13–25 (1975).
84. Mortimer, J. T., Shealy, C. N. & Wheeler, C. Experimental nondestructive electrical stimulation of the brain and spinal cord. *J. Neurosurg.* **32**, 553–9 (1970).
85. Schmitt, O. H. & Schmitt, F. O. A universal precision stimulator. *Science* **76**, 328–30 (1932).
86. Penfield, W. & Boldrey, E. Somatic motor and sensory representation in the cerebral cortex of man as studies by electrical stimulation. *Brain* **60**, 389–443 (1937).
87. Butson, C. R. & McIntyre, C. C. Tissue and electrode capacitance reduce neural activation volumes during deep brain stimulation. *Clin. Neurophysiol.* **116**, 2490–500 (2005).
88. Lempka, S. F., Johnson, M. D., Miocinovic, S., Vitek, J. L. & McIntyre, C. C. Current-controlled deep brain stimulation reduces in vivo voltage fluctuations observed during voltage-controlled stimulation. *Clin. Neurophysiol.* **121**, 2128–33 (2010).
89. Mayberg, H. S. *et al.* Deep brain stimulation for treatment-resistant depression. *Neuron* **45**, 651–60 (2005).
90. Krauss, J. K. Pallidal deep brain stimulation in patients with cervical dystonia and severe cervical dyskinesias with cervical myelopathy. *J. Neurol. Neurosurg. Psychiatry* **72**, 249–256 (2002).
91. Greenberg, B. D. *et al.* Three-year outcomes in deep brain stimulation for highly resistant obsessive-compulsive disorder. *Neuropsychopharmacology* **31**, 2384–93 (2006).
92. Schuurman, P. R. *et al.* A comparison of continuous thalamic stimulation and thalamotomy for suppression of severe tremor. *N. Engl. J. Med.* **342**, 461–8 (2000).

93. Cheung, T. & Tagliati, M. Deep brain stimulation: can we do it better? *Clin. Neurophysiol.* **121**, 1979–80 (2010).
94. Agnesi, F., Blaha, C. D., Lin, J. & Lee, K. H. Local glutamate release in the rat ventral lateral thalamus evoked by high-frequency stimulation. *J. Neural Eng.* **7**, 26009 (2010).
95. Okun, M. S. *et al.* Subthalamic deep brain stimulation with a constant-current device in Parkinson's disease: an open-label randomised controlled trial. *Lancet Neurol.* **11**, 140–9 (2012).
96. Foutz, T. J. & McIntyre, C. C. Evaluation of novel stimulus waveforms for deep brain stimulation. *J. Neural Eng.* **7**, 066008 (2010).
97. Grill, W. M. & Mortimer, J. T. Stimulus waveforms for selective neural stimulation. *IEEE Eng. Med. Biol. Mag.* **14**, 375–385 (1995).
98. Millar, J. & Barnett, T. G. The zeta pulse: a new stimulus waveform for use in electrical stimulation of the nervous system. *J. Neurosci. Methods* **77**, 1–8 (1997).
99. Sahin, M. & Tie, Y. Non-rectangular waveforms for neural stimulation with practical electrodes. *J. Neural Eng.* **4**, 227–33 (2007).
100. Wilson, B. S. *et al.* Better speech recognition with cochlear implants. *Nature* **352**, 236–8 (1991).
101. Nie, K., Stickney, G. & Zeng, F.-G. Encoding frequency modulation to improve cochlear implant performance in noise. *IEEE Trans. Biomed. Eng.* **52**, 64–73 (2005).
102. Birdno, M. J. *et al.* Stimulus features underlying reduced tremor suppression with temporally patterned deep brain stimulation. *J. Neurophysiol.* **107**, 364–83 (2012).
103. Wyckhuys, T. *et al.* Suppression of hippocampal epileptic seizures in the kainate rat by Poisson distributed stimulation. *Epilepsia* **51**, 2297–304 (2010).
104. Henderson, M. B. *et al.* Deep brain stimulation of the nucleus accumbens reduces alcohol intake in alcohol-preferring rats. *Neurosurg. Focus* **29**, E12 (2010).
105. Knapp, C. M., Tozier, L., Pak, A., Ciraulo, D. a & Kornetsky, C. Deep brain stimulation of the nucleus accumbens reduces ethanol consumption in rats. *Pharmacol. Biochem. Behav.* **92**, 474–9 (2009).

106. Hasin, D. S., Stinson, F. S., Ogburn, E. & Grant, B. F. Prevalence, correlates, disability, and comorbidity of DSM-IV alcohol abuse and dependence in the United States: results from the National Epidemiologic Survey on Alcohol and Related Conditions. *Arch. Gen. Psychiatry* **64**, 830–42 (2007).
107. WHO. *Global status report on alcohol and health*. (2011).
108. Finney, J. W. & Moos, R. H. The long-term course of treated alcoholism: I. Mortality, relapse and remission rates and comparisons with community controls. *J. Stud. Alcohol* **52**, 44–54 (1991).
109. Kennedy, B. P., Isaac, N. E. & Graham, J. D. The role of heavy drinking in the risk of traffic fatalities. *Risk Anal.* **16**, 565–569 (1996).
110. John, U. *et al.* Excess Mortality of Alcohol-Dependent Individuals After 14 Years and Mortality Predictors Based on Treatment Participation and Severity of Alcohol Dependence. *Alcohol. Clin. Exp. Res.* **37**, 156–163 (2013).
111. Bouza, C., Angeles, M., Magro, A., Muñoz, A. & Amate, J. M. Efficacy and safety of naltrexone and acamprosate in the treatment of alcohol dependence: a systematic review. *Addiction* **99**, 811–28 (2004).
112. Anton, R. F. *et al.* Naltrexone and cognitive behavioral therapy for the treatment of outpatient alcoholics: results of a placebo-controlled trial. *Am. J. Psychiatry* **156**, 1758–64 (1999).
113. Anton, R. F. *et al.* Combined pharmacotherapies and behavioral interventions for alcohol dependence: the COMBINE study: a randomized controlled trial. *JAMA* **295**, 2003–17 (2006).
114. Kuhn, J. *et al.* Remission of alcohol dependency following deep brain stimulation of the nucleus accumbens: valuable therapeutic implications? *J. Neurol. Neurosurg. Psychiatry* **78**, 1152–3 (2007).
115. Heinze, H.-J. *et al.* Counteracting incentive sensitization in severe alcohol dependence using deep brain stimulation of the nucleus accumbens: clinical and basic science aspects. *Front. Hum. Neurosci.* **3**, 22 (2009).
116. Müller, U. J. *et al.* Successful treatment of chronic resistant alcoholism by deep brain stimulation of nucleus accumbens: first experience with three cases. *Pharmacopsychiatry* **42**, 288–91 (2009).
117. Kuhn, J. *et al.* Observations on unaided smoking cessation after deep brain stimulation of the nucleus accumbens. *Eur. Addict. Res.* **15**, 196–201 (2009).

118. Witjas, T. *et al.* Addiction in Parkinson's disease: impact of subthalamic nucleus deep brain stimulation. *Mov. Disord.* **20**, 1052–5 (2005).
119. Mantione, M., van de Brink, W., Schuurman, P. R. & Denys, D. Smoking cessation and weight loss after chronic deep brain stimulation of the nucleus accumbens: therapeutic and research implications: case report. *Neurosurgery* **66**, E218; discussion E218 (2010).
120. Rouaud, T. *et al.* Reducing the desire for cocaine with subthalamic nucleus deep brain stimulation. *Proc. Natl. Acad. Sci. U. S. A.* **107**, 1196–200 (2010).
121. Liu, H.-Y. *et al.* Chronic deep brain stimulation in the rat nucleus accumbens and its effect on morphine reinforcement. *Addict. Biol.* **13**, 40–6 (2008).
122. Vassoler, F. M. *et al.* Deep brain stimulation of the nucleus accumbens shell attenuates cocaine priming-induced reinstatement of drug seeking in rats. *J. Neurosci.* **28**, 8735–9 (2008).
123. Taghva, A., Corrigan, J. D. & Rezai, A. R. Obesity and Brain Addiction Circuitry: Implications for Deep Brain Stimulation. *Neurosurgery* **71**, 224–238 (2012).
124. Vorspan, F., Mallet, L., Corvol, J.-C., Pelissolo, A. & Lépine, J.-P. Treating addictions with deep brain stimulation is premature but well-controlled clinical trials should be performed. *Addiction* **106**, 1535–6; author reply 1537–8 (2011).
125. Carter, A., Bell, E., Racine, E. & Hall, W. Ethical Issues Raised by Proposals to Treat Addiction Using Deep Brain Stimulation. *Neuroethics* **4**, 129–142 (2010).
126. Carter, A. & Hall, W. Proposals to trial deep brain stimulation to treat addiction are premature. *Addiction* **106**, 235–7 (2011).
127. Hall, W. & Carter, A. Is deep brain stimulation a prospective “cure” for addiction? *F1000 Med. Rep.* **3**, 4 (2011).
128. Bell, R. L., Rodd, Z. A., Lumeng, L., Murphy, J. M. & McBride, W. J. The alcohol-preferring P rat and animal models of excessive alcohol drinking. *Addict. Biol.* **11**, 270–88 (2006).
129. Penn, P. E., McBride, W. J., Lumeng, L., Gaff, T. M. & Li, T. K. Neurochemical and operant behavioral studies of a strain of alcohol-preferring rats. *Pharmacol. Biochem. Behav.* **8**, 475–481 (1978).
130. Cicero, T. J., Snider, S. R., Perez, V. J. & Swanson, L. W. Physical dependence on and tolerance to alcohol in the rat. *Physiol. Behav.* **6**, 191–198 (1971).

131. Di Chiara, G. *et al.* Dopamine and drug addiction: the nucleus accumbens shell connection. *Neuropharmacology* **47 Suppl 1**, 227–41 (2004).
132. Di Chiara, G. Nucleus accumbens shell and core dopamine: differential role in behavior and addiction. *Behav. Brain Res.* **137**, 75–114 (2002).
133. Ward, M. P. Cranial Nerve Modulation for Treatment-Resistant Major Depressive Disorder and Temporal Lobe Epilepsy. (Purdue University, 2012).
134. Wilden, J. A. *et al.* Reduced ethanol consumption by alcohol-preferring (P) rats following pharmacological silencing and deep brain stimulation of the nucleus accumbens shell. *J. Neurosurg.* **120**, 997–1005 (2014).
135. Crown, W. H. *et al.* The impact of treatment-resistant depression on health care utilization and costs. *J. Clin. Psychiatry* **63**, 963–71 (2002).
136. Sackeim, H. a *et al.* Vagus nerve stimulation (VNS) for treatment-resistant depression: efficacy, side effects, and predictors of outcome. *Neuropsychopharmacology* **25**, 713–28 (2001).
137. DeGiorgio, C. M. *et al.* Prospective long-term study of vagus nerve stimulation for the treatment of refractory seizures. *Epilepsia* **41**, 1195–1200 (2000).
138. Labar, D. Vagus nerve stimulation for 1 year in 269 patients on unchanged antiepileptic drugs. *Seizure* **13**, 392–398 (2004).
139. Schachter, S. C. Vagus nerve stimulation therapy summary: five years after FDA approval. *Neurology* **59**, S15–S20 (2002).
140. Ben-Menachem, E. Vagus nerve stimulation, side effects, and long-term safety. *J. Clin. Neurophysiol.* **18**, 415–8 (2001).
141. Labiner, D. M. & Ahern, G. L. Vagus nerve stimulation therapy in depression and epilepsy: therapeutic parameter settings. *Acta Neurol. Scand.* **115**, 23–33 (2007).
142. Mei, N., Condamin, M. & Boyer, A. The composition of the vagus nerve of the cat. *Cell Tissue Res.* **209**, (1980).
143. Foley, J. O. & DuBois, F. S. Quantitative studies of the vagus nerve in the cat. I. The ratio of sensory to motor fibers. *J. Comp. Neurol.* **67**, 49–67 (1937).
144. Friede, R. L. & Samorajski, T. Relation between the number of myelin lamellae and axon circumference in fibers of vagus and sciatic nerves of mice. *J. Comp. Neurol.* **130**, 223–31 (1967).

145. Gasser, H. The classification of nerve fibers. *Ohio J. Sci. Ohio J. Sci.* **41**, 145–159 (1941).
146. Erlanger, J. & Gasser, H. The action potential in fibers of slow conduction in spinal roots and somatic nerves. *Am. J. Physiol.* **92**, 43–82 (1930).
147. Hursh, J. Conduction velocity and diameter of nerve fibers. *Am. J. Physiol.* **127**, 131–139 (1939).
148. Woodbury, D. M. & Woodbury, J. W. Effects of vagal stimulation on experimentally induced seizures in rats. *Epilepsia* **31 Suppl 2**, S7–19 (1990).
149. Evans, D. H. & Murray, J. G. Histological and functional studies on the fibre composition of the vagus nerve of the rabbit. *J. Anat.* **88**, 320–37 (1954).
150. Grill, W. M. & Mortimer, J. T. Inversion of the current-distance relationship by transient depolarization. *IEEE Trans. Biomed. Eng.* **44**, 1–9 (1997).
151. Szlavik, R. B. & de Bruin, H. The effect of stimulus current pulse width on nerve fiber size recruitment patterns. *Med. Eng. Phys.* **21**, 507–515 (1999).
152. Blair, E. & Erlanger, J. A comparison of the characteristics of axons through their individual electrical responses. *Am. J. Physiol.* **106**, 524–564 (1933).
153. Mogyoros, I. Strength-duration properties of sensory and motor axons in amyotrophic lateral sclerosis. *Brain* **121**, 851–859 (1998).
154. West, D. C. & Wolstencroft, J. H. Strength-duration characteristics of myelinated and non-myelinated bulbospinal axons in the cat spinal cord. *J. Physiol.* **337**, 37–50 (1983).
155. Tewfik, T. L. Vagus Nerve Anatomy. *Medscape* (2013). at <<http://emedicine.medscape.com/article/1875813-overview>>
156. Cohn, A. E. On the differences in the effects of stimulation of the two vagus nerves on rate and conduction of the dog's heart. *J. Exp. Med.* **16**, 732–757 (1912).
157. Randall, W. C. & Armour, J. A. Regional vagosympathetic control of the heart. *Am. J. Physiol.* **227**, 444–52 (1974).
158. Ardell, J. L. & Randall, W. C. Selective vagal innervation of sinoatrial and atrioventricular nodes in canine heart. *Am. J. Physiol.* **251**, H764–73 (1986).
159. Ramsay, R. E. *et al.* Vagus Nerve Stimulation for Treatment of Partial Seizures: 2. Safety, Side Effects, and Tolerability. *Epilepsia* **35**, 627–636 (1994).

160. Handforth, A. *et al.* Vagus nerve stimulation therapy for partial-onset seizures: A randomized active-control trial. *Neurology* **51**, 48–55 (1998).
161. Rutecki, P. Anatomical, physiological, and theoretical basis for the antiepileptic effect of vagus nerve stimulation. *Epilepsia* **31 Suppl 2**, S1–6 (1990).
162. Zabara, J. Inhibition of Experimental Seizures in Canines by Repetitive Vagal Stimulation. *Epilepsia* **33**, 1005–1012 (1992).
163. Koo, B., Ham, S. D., Sood, S. & Tarver, B. Human vagus nerve electrophysiology: a guide to vagus nerve stimulation parameters. *J. Clin. Neurophysiol.* **18**, 429–33 (2001).
164. Krahl, S. E., Senanayake, S. S. & Handforth, a. Destruction of peripheral C-fibers does not alter subsequent vagus nerve stimulation-induced seizure suppression in rats. *Epilepsia* **42**, 586–9 (2001).
165. Krahl, S. E. Vagus nerve stimulation for epilepsy: A review of the peripheral mechanisms. *Surg. Neurol. Int.* **3**, S47–52 (2012).
166. Bhadra, N. & Kilgore, K. L. Direct current electrical conduction block of peripheral nerve. *IEEE Trans. Neural Syst. Rehabil. Eng.* **12**, 313–24 (2004).
167. Kilgore, K. L. & Bhadra, N. Nerve conduction block utilising high-frequency alternating current. *Med. Biol. Eng. Comput.* **42**, 394–406 (2004).
168. Tanner, J. A. Reversible blocking of nerve conduction by alternating-current excitation. *Nature* **195**, 712–3 (1962).
169. Branner, A, Stein, R. B. & Normann, R. a. Selective stimulation of cat sciatic nerve using an array of varying-length microelectrodes. *J. Neurophysiol.* **85**, 1585–94 (2001).
170. Tyler, D. J. & Durand, D. M. Functionally selective peripheral nerve stimulation with a flat interface nerve electrode. *IEEE Trans. Neural Syst. Rehabil. Eng.* **10**, 294–303 (2002).
171. Accornero, N., Bini, G., Lenzi, G. L. & Manfredi, M. Selective Activation of peripheral nerve fibre groups of different diameter by triangular shaped stimulus pulses. *J. Physiol.* **273**, 539–60 (1977).
172. Tosato, M., Yoshida, K., Toft, E. & Struijk, J. J. Quasi-trapezoidal pulses to selectively block the activation of intrinsic laryngeal muscles during vagal nerve stimulation. *J. Neural Eng.* **4**, 205–12 (2007).

173. Vuckovic, A., Tosato, M. & Struijk, J. J. A comparative study of three techniques for diameter selective fiber activation in the vagal nerve: anodal block, depolarizing prepulses and slowly rising pulses. *J. Neural Eng.* **5**, 275–86 (2008).
174. Qing, K. Y., Ward, M. P. & Irazoqui, P. P. Burst-modulated waveforms optimize electrical stimuli for charge efficiency and fibre selectivity. *IEEE Trans. Neural Syst. Rehabil. Eng.* (Accepted). (2015).
175. Ward, M. P., Rajdev, P., Ellison, C. & Irazoqui, P. P. Toward a comparison of microelectrodes for acute and chronic recordings. *Brain Res.* **1282**, 183–200 (2009).
176. Ben-Menachem, E., Revesz, D., Simon, B. J. & Silberstein, S. Surgically implanted and non-invasive vagus nerve stimulation: a review of efficacy, safety and tolerability. *Eur. J. Neurol.* n/a–n/a (2015). doi:10.1111/ene.12629
177. Ward, M. P. *et al.* A flexible platform for biofeedback-driven control and personalization of electrical nerve stimulation therapy. *IEEE Trans. Neural Syst. Rehabil. Eng.* (In Press). (2015).
178. Mollet, L. *et al.* Electrophysiological responses from vagus nerve stimulation in rats. *Int. J. Neural Syst.* **23**, 1350027 (2013).
179. McDermott, H. An advanced multiple channel cochlear implant. *IEEE Trans. Biomed. Eng.* **36**, 789–797 (1989).
180. Tosato, M., Yoshida, K., Toft, E., Nekrasas, V. & Struijk, J. J. Closed-loop control of the heart rate by electrical stimulation of the vagus nerve. *Med. Biol. Eng. Comput.* **44**, 161–169 (2006).
181. Gaskell, W. H. The Croonian Lecture: On the Rhythm of the Heart of the Frog, and on the Nature of the Action of the Vagus Nerve. *Philos. Trans. R. Soc. London* **173**, 993–1033 (1882).
182. Hunt, S. A. *et al.* 2009 Focused Update Incorporated Into the ACC/AHA 2005 Guidelines for the Diagnosis and Management of Heart Failure in Adults. A Report of the American College of Cardiology Foundation/American Heart Association Task Force on Practice Guidelines Developed. *J. Am. Coll. Cardiol.* **53**, e1–e90 (2009).
183. Schwartz, P. J. *et al.* Long term vagal stimulation in patients with advanced heart failure. First experience in man. *Eur. J. Heart Fail.* **10**, 884–891 (2008).
184. De Ferrari, G. M. *et al.* Chronic vagus nerve stimulation: A new and promising therapeutic approach for chronic heart failure. *Eur. Heart J.* **32**, 847–855 (2011).

185. Mortara, A. *et al.* Arterial baroreflex modulation of heart rate in chronic heart failure: clinical and hemodynamic correlates and prognostic implications. *Circulation* **96**, 3450–3458 (1997).
186. Adamson, P. B. *et al.* Continuous autonomic assessment in patients with symptomatic heart failure: Prognostic value of heart rate variability measured by an implanted cardiac resynchronization device. *Circulation* **110**, 2389–2394 (2004).
187. Thayer, J. F., Yamamoto, S. S. & Brosschot, J. F. The relationship of autonomic imbalance, heart rate variability and cardiovascular disease risk factors. *Int. J. Cardiol.* **141**, 122–131 (2010).
188. Sander, J. W. The epidemiology of epilepsy revisited. [Curr Opin Neurol. 2003] - PubMed result. *Curr. Opin. Neurol.* **16**, 165–70 (2003).
189. Shackleton, D. P., Westendorp, R. G. J., Kasteleijn-Nolst Trenité, D. G. a, de Craen, A. J. M. & Vandenbroucke, J. P. Survival of patients with epilepsy: an estimate of the mortality risk. *Epilepsia* **43**, 445–450 (2002).
190. Zieliński, J. J. Epilepsy and mortality rate and cause of death. *Epilepsia* **15**, 191–201 (1974).
191. Annegers, J. F. & Coan, S. P. SUDEP: Overview of definitions and review of incidence data. *Seizure* **8**, 347–352 (1999).
192. Walczak, T. S. *et al.* Incidence and risk factors in sudden unexpected death in epilepsy: a prospective cohort study. *Neurology* **56**, 519–525 (2001).
193. Tomson, T., Nashef, L. & Ryvlin, P. Sudden unexpected death in epilepsy: current knowledge and future directions. *Lancet Neurol.* **7**, 1021–1031 (2008).
194. Leestma, J. E., Walczak, T., Hughes, J. R., Kalelkar, M. B. & Teas, S. S. A prospective study on sudden unexpected death in epilepsy. *Ann. Neurol.* **26**, 195–203 (1989).
195. P-Codrea, S., Dalager-pedersen, S., Dam, M. & Vesterby-charles, A. Sudden Unexpected Death in Epilepsy. *Am. J. Forensic Med. Pathol.* **26**, 99–105 (2005).
196. Falconer, B. & Rajs, J. Post-mortem findings of cardiac lesions in epileptics: a preliminary report. *Forensic Sci.* **8**, 63–71 (1976).
197. Natelson, B. H., Suarez, R. V, Terrence, C. F. & Turizo, R. Patients with epilepsy who die suddenly have cardiac disease. *Arch. Neurol.* **55**, 857–860 (1998).

198. Annegers, J. F., Hauser, W. A. & Shirts, S. B. Heart disease mortality and morbidity in patients with epilepsy. *Epilepsia* **25**, 699–704 (1984).
199. Nei, M., Ho, R. T. & Sperling, M. R. EKG abnormalities during partial seizures in refractory epilepsy. *Epilepsia* **41**, 542–548 (2000).
200. Zijlmans, M., Flanagan, D. & Gotman, J. Heart rate changes and ECG abnormalities during epileptic seizures: Prevalence and definition of an objective clinical sign. *Epilepsia* **43**, 847–854 (2002).
201. Sevcencu, C. & Struijk, J. J. Autonomic alterations and cardiac changes in epilepsy. *Epilepsia* **51**, 725–737 (2010).
202. Nashef, L. *et al.* Apnoea and bradycardia during epileptic seizures: relation to sudden death in epilepsy. *J. Neurol. Neurosurg. Psychiatry* **60**, 297–300 (1996).
203. Eggleston, K. S., Olin, B. D. & Fisher, R. S. Ictal tachycardia: The head-heart connection. *Seizure* **23**, 496–505 (2014).
204. Drake, M. E., Reider, C. R. & Kay, a. Electrocardiography in epilepsy patients without cardiac symptoms. *Seizure* **2**, 63–65 (1993).
205. Lotufo, P. A., Valiengo, L., Benseñor, I. M. & Brunoni, A. R. A systematic review and meta-analysis of heart rate variability in epilepsy and antiepileptic drugs. *Epilepsia* **53**, 272–282 (2012).
206. Stöllberger, C. & Finsterer, J. Cardiorespiratory findings in sudden unexplained/unexpected death in epilepsy (SUDEP). *Epilepsy Res.* **59**, 51–60 (2004).
207. Schomer, A. C., Nearing, B. D., Schachter, S. C. & Verrier, R. L. Vagus nerve stimulation reduces cardiac electrical instability assessed by quantitative T-wave alternans analysis in patients with drug-resistant focal epilepsy. *Epilepsia* **55**, 1996–2002 (2014).
208. Zannad, F. *et al.* Chronic vagal stimulation for the treatment of low ejection fraction heart failure: results of the NEural Cardiac TherApy foR Heart Failure (NECTAR-HF) randomized controlled trial. *Eur. Heart J.* **36**, 425–433 (2015).
209. Hauptman, P. J. *et al.* Rationale and study design of the INcrease of Vagal TonE in Heart Failure study: INOVATE-HF. *Am. Heart J.* **163**, 954–962.e1 (2012).
210. Grill, W. M., Snyder, C. A. A. N. & Miocinovic, S. Deep brain stimulation creates an informational lesion of the stimulated nucleus. *Neurol. Res.* **15**, 19–22 (2004).

211. Warner, H. R. & Cox, a. A mathematical model of heart rate control by sympathetic and vagus efferent information. *J. Appl. Physiol.* **17**, 349–355 (1962).
212. Warner, H. R. & Russell, R. O. Effect of combined sympathetic and vagal stimulation on heart rate in the dog. *Circ. Res.* **24**, 567–573 (1969).
213. Navas, M. *et al.* Treatment of refractory epilepsy in adult patients with right-sided vagus nerve stimulation. *Epilepsy Res.* **90**, 1–7 (2010).
214. Pfeffer, J., Pfeffer, M., Fletcher, P. & Braunwald, E. Alterations of cardiac performance in rats with established spontaneous hypertension. *Am. J. Cardiol.* **44**, 994–998 (1979).
215. Fletcher, P. J., Pfeffer, J. M., Pfeffer, M. A. & Braunwald, E. Left ventricular diastolic pressure-volume relations in rats with healed myocardial infarction. Effects on systolic function. *Circ. Res.* **49**, 618–626 (1981).
216. DeGeest, H., Levy, M. N., Zieske, H. & Lipman, R. I. Depression of ventricular contractility by stimulation of the vagus nerves. *Circ. Res.* **17**, 222–235 (1965).
217. Matsuura, W. *et al.* Vagal stimulation decreases left ventricular contractility mainly through negative chronotropic effect. *Am. J. Physiol.* **273**, H534–H539 (1997).
218. Koller, W. C., Lyons, K. E., Wilkinson, S. B., Troster, a I. & Pahwa, R. Long-term safety and efficacy of unilateral deep brain stimulation of the thalamus in essential tremor. *Mov. Disord.* **16**, 464–8 (2001).
219. Burchiel, K. J., Anderson, V. C., Favre, J. & Hammerstad, J. P. Comparison of pallidal and subthalamic nucleus deep brain stimulation for advanced Parkinson's disease: results of a randomized, blinded pilot study. *Neurosurgery* **45**, 1375–82; discussion 1382–4 (1999).
220. Rodriguez-Oroz, M. C. *et al.* Bilateral deep brain stimulation in Parkinson's disease: a multicentre study with 4 years follow-up. *Brain* **128**, 2240–9 (2005).
221. Kleiner-Fisman, G. *et al.* Subthalamic nucleus deep brain stimulation: summary and meta-analysis of outcomes. *Mov. Disord.* **21 Suppl 1**, S290–304 (2006).
222. Tamma, F. *et al.* Anatomico-clinical correlation of intraoperative stimulation-induced side-effects during HF-DBS of the subthalamic nucleus. *Neurol. Sci.* **23 Suppl 2**, S109–10 (2002).
223. Kent, A. R. & Grill, W. M. Instrumentation to record evoked potentials for closed-loop control of deep brain stimulation. in *Proceedings of the Annual International*

Conference of the IEEE Engineering in Medicine and Biology Society, EMBS 6777–6780 (2011). doi:10.1109/IEMBS.2011.6091671

224. McCracken, C. B. & Grace, A. a. Nucleus accumbens deep brain stimulation produces region-specific alterations in local field potential oscillations and evoked responses in vivo. *J. Neurosci.* **29**, 5354–5363 (2009).
225. Behrend, C. E. *et al.* Toward feedback controlled deep brain stimulation: Dynamics of glutamate release in the subthalamic nucleus in rats. *J. Neurosci. Methods* **180**, 278–289 (2009).
226. Luigjes, J. *et al.* Deep brain stimulation in addiction: a review of potential brain targets. *Mol. Psychiatry* **17**, 572–83 (2012).
227. Vassoler, F. M. *et al.* Deep brain stimulation of the nucleus accumbens shell attenuates cocaine reinstatement through local and antidromic activation. *J. Neurosci.* **33**, 14446–54 (2013).
228. Wise, R. A. Drug-activation of brain reward pathways. *Drug Alcohol Depend.* **51**, 13–22 (1998).
229. Irazoqui, P. P., Ward, M. P. & Qing, K. Y. Burst pulse tissue stimulation method and apparatus. (2014).
230. Mellanby, J., George, G., Robinson, a & Thompson, P. Epileptiform syndrome in rats produced by injecting tetanus toxin into the hippocampus. *J. Neurol. Neurosurg. Psychiatry* **40**, 404–14 (1977).
231. Jefferys, J. G. & Williams, S. F. Physiological and behavioural consequences of seizures induced in the rat by intrahippocampal tetanus toxin. *Brain* **110** (Pt 2, 517–32 (1987).

VITA

VITA

KURT Y. QING

EDUCATION

Purdue University, West Lafayette, IN Doctor of Philosophy in Engineering Biomedical Engineering	August 2011 – May 2015 (projected)
Indiana University School of Medicine, Indianapolis, IN Doctor of Medicine (combined with PhD)	August 2009 – May 2017 (projected)
Northwestern University, Evanston, IL Bachelors in Science Biomedical Engineering Minor in Global Health	August 2005 – December 2008

AWARDS

Dean's Council Scholarship, Indiana University School of Medicine	2009 – 2011
Creativity Foundation Legacy Prize (http://creativity-found.org/legacy-prize/entry/kurt-y-qing/)	2010
CIMIT Prize finalist, CIMIT (http://www.cimit.org/news/cimit-prize-09-winners.html)	2009
Advanced E-Team Funded Project, NCIIA (now VentureWell) (http://nciia.org/sites/default/files/newsletter_spring_2009.pdf)	2008 – 2009
Margaret and Muir Frey Memorial Prize 2 nd place, Northwestern (http://www.northwestern.edu/bme/pdf/BMEnews9-19-08.pdf)	2008

BMEidea national competition 2nd place, NCIIA 2008
 (<http://www.nciia.org/RESOURCES/application/pdf/fall2008.pdf>)

RESEARCH EXPERIENCE

Biomedical Engineering, Purdue University

Advisor: Pedro Irazoqui

Graduate research assistant August 2011 – May 2015

- Fabrication and characterization of nerve and brain microelectrodes
- Design, fabrication, and characterization of printed circuit boards for stimulation and recording in animals
- Design and testing of application-specific integrated circuits
- Developing and conducting animal surgery and experimentation
- Developing and studying rat model of chronic epilepsy
- Biomedical instrumentation
- Custom graphical user interface and complex routines in MATLAB
- Closed-loop neurostimulation, deep brain stimulation, vagus nerve stimulation
- Statistical analysis

KMC ApneAlert, Northwestern University

Advisor: Matthew Glucksberg

Design team leader January 2008 – August 2009

- Led circuitry design and modification.
- Led device prototyping and bench top testing.
- Obtained IRB approval and led device testing on human subjects at Prentice Women's Hospital in Chicago and Karl Bremer Hospital in Western Cape, South Africa.
- Wrote grants and secured funding for the project.
- Coordinated research and design efforts with nurses, doctors, and a device manufacturer in South Africa.

Biomedical Engineering, Northwestern University

Advisor: Robert Linsenmeier

Independent student researcher September 2007 – August 2009

- Designed and experimented with a real-time recording system for measuring the pH of cultured human tissue for Children's Memorial Research Center

Biomedical Engineering, Northwestern University

Advisor: Robert Linsenmeier

Undergraduate research assistant June 2007 – August 2007

- Supported real-time, *in vivo* oxygen measurements in rat retina by fabricating recording electrodes and assisting surgical preparations.
- Developed algorithm for data analysis.

PUBLICATIONS

PUBLICATIONS

Journal Articles

Qing, K. Y., Ward, M. P. & Irazoqui, P. P. Controlling the vagal effects on the heart by B fiber activation (tentative title). (*In Preparation*). (2015).

Qing, K. Y., Ward, M. P. & Irazoqui, P. P. Burst-modulated waveforms optimize electrical stimuli for charge efficiency and fibre selectivity. *IEEE Trans. Neural Syst. Rehabil. Eng.* (*Accepted*). (2015).

Wilden, J. A., **Qing, K. Y.**, *et al.* Reduced ethanol consumption by alcohol-preferring (P) rats following pharmacological silencing and deep brain stimulation of the nucleus accumbens shell. *J. Neurosurg.* **120**, 997–1005 (2014).

Ward, M. P., **Qing, K. Y.**, *et al.* A flexible platform for biofeedback-driven control and personalization of electrical nerve stimulation therapy. *IEEE Trans. Neural Syst. Rehabil. Eng.* (*In Press*). (2015).

Dryg, I. D., Ward, M. P., **Qing, K. Y.**, *et al.* Magnetically inserted neural electrodes: tissue response and functional lifetime. *IEEE Trans. Neural Syst. Rehabil. Eng.* (*Accepted*). (2015).

Patents

Irazoqui, P. P., Ward, M. P. & Qing, K. Y. Burst pulse tissue stimulation method and apparatus. (2014, provisional).*

* Qing, K. Y. should be first inventor. A full patent is currently being prepared.